UCLouvain
Institute of Mechanics,
Materials and Civil Engineering

UMONS
University of Mons

Impact of Hydrogen on Power System Adequacy

Application to the Belgian System in 2030.

Doctoral dissertation presented by

Aurélia Hernandez

in partial fulfillment of the requirements for
the degree of Doctor in Engineering Sciences

October 2024

Thesis committee

Pr. Emmanuel De Jaeger (UCLouvain, co-supervisor)
Pr. François Vallée (UMons, co-supervisor)
Pr. Sandra Soares-Frazao (UCLouvain, jury president)
Pr. Hervé Jeanmart (UCLouvain, jury secretary)
Pr. Jacques Lobry (UMons)
Pr. Sylvain Quoilin (ULiège)
Pr. Pierre Henneaux (ULB)

Remerciements

C'est avec beaucoup d'émotions que mon séjour à l'UCLouvain s'achève après 4 ans de recherche. Faire une thèse n'a jamais fait partie des plans puisque j'ai plus ou moins découvert en quoi cela consistait en lisant l'offre d'emploi si on peut la nommer ainsi. Un drôle de métier dont la représentation par l'entourage peut varier : étudiant-chercheur bénévole, rat de laboratoire en blouse blanche qui fait des découvertes incroyables, et j'en passe. Au terme de ce séjour, et de l'écriture de ce manuscrit que vous vous apprêtez à lire, j'aimerais remercier celles et ceux qui ont contribué au projet.

Un immense merci à mes promoteurs de thèse Pr. Emmanuel De Jaeger et Pr. François Vallée. Merci Emmanuel pour la confiance que tu m'as accordée en me proposant de rejoindre le projet BEST en tant que doctorante. Merci pour ton accompagnement sain et bienveillant, mais aussi pour ta gentillesse et ta bonne compagnie. C'est une chance d'avoir pu travailler avec quelqu'un qui a une expérience comme la tienne dans le domaine des réseaux électriques, et tout ça dans un cadre paisible et rassurant. Merci François de m'avoir accompagnée en tant que co-promoteur durant cette thèse, de m'avoir accueillie dans ton équipe de recherche à Mons, mais aussi pour ton enthousiasme, ton dynamisme, et ta bonne humeur constante. C'est réellement inspirant d'avoir pu travailler avec quelqu'un doté d'une clairvoyance remarquable et d'une énergie contagieuse.

Un grand merci aux membres du jury Pr. Hervé Jeanmart, Pr. Jacques Lobry, Pr. Sylvain Quoilin, Pr. Pierre Henneaux, et Pr. Sandra Soares Frazao d'avoir relu avec beaucoup d'attention ce manuscrit. Merci pour vos commentaires constructifs, et les discussions lors de la défense privée qui ont permis d'améliorer la qualité du travail.

Merci au SPF Economie qui a financé cette thèse au travers du projet BEST. Merci aussi à Hervé Jeanmart et Véronique Dias d'avoir assuré la bonne coordination du projet.

Merci aux collègues de MEED qui ont rendu chaque journée au bureau tellement agréable, au point de me donner envie de venir sur place tous les jours, même en sachant que je raterais la correspondance à Ottignies (RIP). Une mention spéciale à Raül et Olivier, mes chers acolytes du bureau B-138, qui ont fait de ce bureau un endroit spécial. Merci Raül pour les debriefs entre deux écrans et Olivier pour ton essui, tes chaussettes et pour WholeTrack. Une attention particulière à ceux qui ont ensoleillé mes journées depuis un autre bureau : Merci à Paul pour ta bonne humeur légendaire, à Eduardo pour la découverte des pupusas, à Guigui pour ton enthousiasme dans le Bonjour canaille de chaque matin, à Emilio pour les runs à midi, et à Jeanno mon coup de foudre pour les tours du bloc et les rigolades.

Merci aux collègues du TFL qui m'ont très souvent accueillie pour une petite pause café-eau pétillante. Un merci spécial à Paolo pour avoir perdu son calme dans un Airbnb, mais surtout pour avoir été mon acolyte depuis le J1 de notre mémoire, à Martin pour avoir volé toute la nourriture de R.s.l (mes pensées vont aux autres victimes), à Xav pour la contrebande d'eau pétillante en tous lieux et les trajets FlixBus (bravo pour le nouveau badge), à Sara pour les escapades de grimpe et la vibe, au trinôme Hervé-Véronique-Francesco pour votre amitié, votre enthousiasme, et votre bonne compagnie, et enfin à Denix pour la collaboration Larvae Observations in Vortical Environments et les pizzas à Beez.

Merci aux collègues montois de la GELE Team à Mons qui m'ont toujours accueillie chaleureusement. C'était un réel plaisir de venir travailler à Mons. Mention spéciale à Thuy-hai mon binôme adequacy, merci pour nos conversations interminables, les remboursements natures en collations, et d'avoir partagé avec moi certains casse-têtes.

Merci à celles et ceux qui nous rendent la vie facile : Nathalie, Isabelle, et Astrid à l'UCLouvain, et Manu à l'UMons. Petite dédicace spéciale à Nathalie pour les partages-tips vestimentaires et à Manu pour son partage de savoir et d'expérience dans le domaine de l'électricité en général.

Après avoir remercié les personnes que j'ai croisées au quotidien dans les couloirs au travail, il est temps de remercier celles et ceux qui font partie de ma vie, et qui m'ont suivie aussi pendant ces quatre années.

Merci à ma famille pour leur soutien depuis toujours. Un immense merci à mes parents d'être aux petits soins, chacun à votre façon, de m'encourager, de me guider quand c'est nécessaire, et de m'inspirer. Merci à mes frères et sœurs : Tetard, Juju, et Mimi for the jokes, and the english.

Merci à mes ami.e.s, mes frères et sœurs de cœur. Ceux et celles qui ensoleillent mon quotidien depuis longtemps, et qui font partie de la famille. Merci aux filles du buisson Alice, Harmo, Anneso, Bl, Eva pour la cohabitation, la sororité, le fun, et le soutien surtout durant cette dernière année haute en couleur ; aux mégères Annick et Soso pour les rires et l'amitié ; à Thibault pour avoir été mon co-équipier, mon appui, ma force, et mon supporter n°1 pendant longtemps ; à la team des boys Joan, Brimz, Maloul, Mathieu, Simahr, Yan et Bazar pour votre folie ; au sang Bl, Choussi et Gorfou pour les wist, les rigolades et le scoutisme^^ ; à toutes les Pep's pour le fun, la niak, le love, et les verres post-entrainement chez Maria; à Lélé pour ta folie, mais aussi pour le réconfort et la force que tu m'as apportés, à Margo et Diego pour les projets partagés, le FireBot, et les rires ; à mon petit filleul la Miloche pour la mignonerie ; aux anciens résidents et squatteuses de la coloc Général Henry pour les marchés de Noël, et les repas joyeux. Merci aussi à ceux et celles que je n'ai pas cités ici, mais avec qui on a partagé de beaux moments, vous vous reconnaitrez. Merci. Vous rendez la vie plus belle.

Bonne lecture.
Aurel.

Abstract

Hydrogen is foreseen to be part of our future energy systems as Europe has the ambition to be a carbon-neutral continent by 2050. Given that the energy sector is responsible for a significant portion of European GHG emissions, its transition is key. Green hydrogen – produced through electrolyzers powered by low-carbon electricity – is under the spotlight as various studies claim that it can be used as a feedstock for the industry, and as an alternative fuel for heavy transportation and future back-up generation units which are hard-to-electrify sectors. These studies also state that hydrogen deployment will consist in the development of a future hydrogen network.

As the grid undergoes significant changes, such as shifting to intermittent renewable energy production and increasing the electrification of various end-use demands, probabilistic adequacy studies that assess whether a power system can meet consumers' demand at all times and in all locations becomes essential. Integrating electrolyzers into the power system introduces an unconventional and variable electrical demand. Indeed, to produce green hydrogen, electrolyzers will primarily consume when renewable energy sources are producing. Furthermore, the hydrogen system comprising a pipeline network, storage facilities, import points, and hydrogen-to-power units may influence electrolyzer consumption.

The primary objective of this work is to quantify the impact of this unconventional demand on power system adequacy. Specifically, we aim to answer the question: What is the impact of e-hydrogen on the adequacy of the Belgian power system?

To address this, we developed a probabilistic adequacy tool capable of analyzing large and complex systems, such as a country, while considering the coupled operation of electricity and hydrogen systems. This tool includes an economic dispatch model that minimizes load shedding and operational costs of the system. It incorporates network constraints via DC-OPF formulation, and integrates the interdependencies between the electricity and hydrogen systems. The hydrogen system encompasses electrolyzers, storage units, pipelines, hydrogen-to-power units, import points, and an annual hydrogen demand. From this model, key adequacy indicators such as Energy-not-served (ENS) and Loss-of-load (LOL) are derived. This model is integrated into a sequential Monte Carlo process to obtain expected values for these indicators (EENS and LOLE). The process also accounts for yearly uncertainties, including renewable energy production variability and technology unplanned outages.

After testing the tool on smaller systems, it is applied to a coupled electricity-hydrogen system representative of Belgium in 2030. Various scenarios reflecting current uncertainties, such as grid and offshore wind farm expansions, and different flexibility means were analyzed.

Key findings for the Belgian system in 2030 include the crucial role of flexibility, which significantly enhances adequacy indicators across all scenarios, highlighting its importance in such studies. Given the model's assumption of unlimited hydrogen imports, the system does not experience energy deficits due to hydrogen demand. Therefore, hydrogen integration, under these conditions, does not negatively impact power system adequacy. Assessing the impact of constraining hydrogen demand requires setting limits on local production. In the scenario considering offshore wind farm and grid extension, as well as all flexibility means, constraining electrolyzers up to a 90% annual load factor does not compromise Belgium's adequacy with 447 MW of electrolyzers. This suggests that local hydrogen production, if managed flexibly, will not affect system adequacy. Despite incorporating flexibility and 447 MW of electrolyzers, curtailment peaks remain high, reaching values of 6-7 GW, indicating the system's limited capacity to absorb very high renewable energy peaks.

In conclusion, this study demonstrates that while the integration of green hydrogen into the Belgian power system introduces new challenges, particularly with respect to managing the variable demand from electrolyzers, it does not inherently compromise system adequacy when flexibility measures are in place.

Keywords: electrolyzers, hydrogen, multi-period DC optimal power flow, probabilistic adequacy tool, sequential Monte Carlo simulations.

Résumé

L'hydrogène devrait faire partie de nos futurs systèmes énergétiques, l'Europe ayant l'ambition de devenir un continent neutre en carbone d'ici à 2050. Étant donné que le secteur de l'énergie est responsable d'une part importante des émissions européennes de gaz à effet de serre, sa transition est essentielle. L'hydrogène vert - produit par des électrolyseurs alimentés par de l'électricité à faible teneur en carbone – suscite beaucoup d'intérêt, car plusieurs études affirment qu'il peut être utilisé comme matière première pour l'industrie et comme carburant alternatif pour les transports lourds et les futures unités de production d'appoint, qui sont des secteurs difficiles à électrifier. Ces études indiquent également que le déploiement de l'hydrogène consistera en la mise en place d'un futur réseau d'hydrogène.

Alors que le réseau électrique subit des changements importants, tels que le passage à une production intermittente d'énergie renouvelable et l'augmentation de l'électrification de diverses demandes d'utilisation finale, les études probabilistes d'adéquation qui évaluent si un système électrique peut répondre à la demande des consommateurs à tout moment et en tout lieu deviennent essentielles. L'intégration des électrolyseurs dans le système électrique introduit une demande électrique non conventionnelle et variable. En effet, pour produire de l'hydrogène vert, les électrolyseurs consommeront principalement lorsque les sources d'énergie renouvelables produisent. En outre, le système d'hydrogène comprenant un réseau de pipelines, des installations de stockage, des points d'importation et des unités de conversion de l'hydrogène en électricité peut influencer la consommation de l'électrolyseur.

L'objectif principal de ce travail est de quantifier l'impact de cette demande non conventionnelle sur l'adéquation du système électrique. Plus précisément, nous visons à répondre à la question suivante : Quel est l'impact de l'e-hydrogène sur l'adéquation du système électrique belge ? Pour ce faire, nous avons développé un outil probabiliste d'adéquation capable d'analyser des systèmes vastes et complexes, tels qu'un pays, tout en considérant le fonctionnement couplé des systèmes d'électricité et d'hydrogène. Cet outil comprend un modèle de dispatching économique qui minimise le délestage de charge et les coûts opérationnels du système. Il incorpore les contraintes du réseau via la formulation DC-OPF et intègre les interdépendances entre les systèmes d'électricité et d'hydrogène. Le système hydrogène comprend des électrolyseurs, des unités de stockage, des pipelines, des unités de récupération, des points d'importation et une demande annuelle d'hydrogène. Ce modèle permet d'obtenir des indicateurs clés d'adéquation tels que l'énergie non distribuée (ENS) et la perte de charge (LOL). Ce modèle est intégré dans un processus séquentiel de Monte Carlo afin d'obtenir une estimation de ces indicateur (EENS et LOLE). Le processus considère aussi des incertitudes annuelles, y compris la variabilité de la production d'énergie renouvelable et les pannes non-planifiées des différentes technologies.

Après avoir testé l'outil sur des systèmes de plus petite taille, il a été appliqué à un système couplé électricité-hydrogène représentatif de la Belgique en 2030. Différents scénarios reflétant les incertitudes actuelles, tels que l'expansion du réseau et des parcs éoliens offshore, et différents moyens de flexibilité ont été analysés.

Les principales conclusions pour le système belge en 2030 incluent le rôle crucial de la flexibilité, qui améliore considérablement les indicateurs d'adéquation dans tous les scénarios, soulignant son importance dans de telles études. Compte tenu de l'hypothèse du modèle selon laquelle les importations d'hydrogène sont illimitées, le système ne connaît pas de déficits énergétiques dus à la demande d'hydrogène. Par conséquent, l'intégration de l'hydrogène, dans ces conditions, n'a pas d'impact négatif sur l'adéquation du système électrique. Pour évaluer l'impact de l'integration de la demande d'hydrogène, il faut fixer des contraintes sur la production locale. Dans le scénario prenant en compte l'extension du parc éolien offshore et du réseau, ainsi que tous les moyens de flexibilité, le fait de contraindre les électrolyseurs à un facteur de charge annuel de 90 % ne compromet pas l'adéquation du système belge avec 447 MW d'électrolyseurs. Cela suggère que la production locale d'hydrogène, si elle est gérée de manière flexible, n'affectera pas l'adéquation du système. Malgré l'intégration de la flexibilité et 447 MW d'électrolyseurs, les pics d'excès de production restent élevés, atteignant des valeurs de 6-7 GW, ce qui illustre la capacité limitée du système à absorber des pics d'énergie renouvelable très élevés.

En conclusion, cette étude démontre que si l'intégration de l'hydrogène vert dans le système électrique belge introduit de nouveaux défis, notamment en ce qui concerne la gestion de la demande variable des électrolyseurs, elle ne compromet pas intrinsèquement l'adéquation du système lorsque des mesures de flexibilité sont en place.

Contents

Nomenclature

Indices

b	Index of battery storage system $\in [1,n_b]$
d	Index of day $\in [1,n_d]$
e	Index of electrolyzer $\in [1,n_e]$
g	Index of conventional generator $\in [1,n_g]$
h	Index of hydrogen-to-power unit $\in [1,n_h]$
i	Index of abroad electrical interconnection $\in [1,n_i]$
j	Index of abroad hydrogen interconnection $\in [1,n_j]$
k	Index of H_2 pipeline $\in [1,n_k]$
l	Index of transmission line $\in [1,n_l]$
n	Index of bus node $\in [1,n_n]$
$n_{from}(l)$	Index of *from node* of line l
n_{ref}	Index of reference node
$n_{to}(l)$	Index of *to node* of line l
p	Index of pumped-hydro storage system $\in [1,n_p]$
q	Index of hydrogen storage unit $\in [1,n_q]$
r	Index of renewable plant connected to the transmission grid $\in [1,n_r]$
t	Index of time slot $\in [1,n_t]$

Sets

B_n	Set of battery groups located at node n
E_n	Set of electrolyzers located at node n
G_n	Set of generators located at node n
H_n	Set of hydrogen-to-power units located at node n
I_n	Set of abroad electrical interconnections connected to node n
J_n	Set of abroad hydrogen interconnections connected to node n
$K_{from,n}$	Set of H_2 pipelines whose sign flow is defined to exit node n
$K_{to,n}$	Set of H_2 pipelines whose sign flow is defined to enter node n
$L_{from,n}$	Set of lines whose sign flow is defined to exit node n
$L_{to,n}$	Set of lines whose sign flow is defined to enter node n
P_n	Set of PHS systems located at node n
Q_n	Set of hydrogen storage units located at node n
R_n	Set of renewable power plants located at node n

Stochastic Parameters

$\alpha_{el}(e,t)$	Hourly availability of electrolyzer $e \in \{0,1\}$
$\alpha_{gen}(g,t)$	Hourly availability of generator $g \in \{0,1\}$
$\alpha_{H2P}(h,t)$	Hourly availability of H2P unit $h \in \{0,1\}$
$\alpha_{imp}(i,t)$	Hourly availability of abroad electrical interconnection $i \in \{0,1\}$

$\alpha_l(l,t)$ Hourly availability of transmission line l $\in \{0,1\}$

$\mathrm{res}(r,t)$ Hourly power production of renewable power plant r [MWh/h]

Fixed Parameters

α_{v1m} Share of electric vehicles with a flexible charging behavior connected to a charging station [-]

$\Delta\Theta_{max}$ Phase angle difference of two adjacent nodes [rad]

$\eta_{batt,in/out}$ In/out-flow efficiency of battery b [-]

η_c H_2 compression factor [-]

η_{el} Electrolyzer efficiency [-]

η_{H2P} Hydrogen-to-power plant efficiency [-]

$\eta_{phs,in}(p)$ Pump efficiency of PHS p [-]

$\eta_{phs,out}(p)$ Turbine efficiency of PHS p [-]

$b_{pu}(l)$ Susceptance of line l [pu]

$c_{gen}(g)$ Operational cost of conventional generator g [€/MWh]

c_{H_2} Cost of imported hydrogen [€/$\mathrm{MWh_{H_2}}$]

$c_{imp}(i)$ Cost of imported electricity at interconnection i [€/MWh]

c_{shift} Cost of load shifting [€/MWh]

c_{v-shed} Cost of voluntary load shedding [€/MWh]

$d_{dist-gen}(n)$ Share of distributed conventional generation associated to node n [-]

$d_{ev}(n)$ Share of electric vehicle fleet associated to node n [-]

$d_{H_2}(n)$ Share of hydrogen demand associated to node n [-]

$d_{hp}(n)$ Share of heat-pumps associated to node n [-]

$d_{hydro}(n)$ Share of hydroelectric run-of-the-river units associated to node n [-]

$d_l(n)$ Share of traditional electrical demand associated to node n [-]

$d_{onsh}(n)$ Share of onshore wind turbines associated to node n [-]

$d_{pv}(n)$ Share of PV installations associated to node n [-]

$d_{sh}(n)$ Share of shedable demand associated to node n [-]

$d_s(n)$ Share of shiftable demand associated to node n [-]

$e_{imp,max,year}(i)$ Maximum yearly imported energy at interconnection i [MWh/year]

$e_{shift,max,day}$ Maximum daily shiftable energy [MWh/day]

$e_{v-shed,max,day}$ Maximum daily voluntary shedding [MWh/day]

$f_{H_2,max}(k)$ Maximum hydrogen flow that can transit through pipeline k [$\mathrm{MWh_{H_2}}$/h]

$f_{max}(l)$ Maximum power that can transit through line l) [MW]

$l(t)$ Hourly traditional electrical demand [MWh/h]

$l_{H_2,fixed}(t)$ Hourly fixed H_2 demand [MWh_{H_2}/h]

$l_{H_2,flex,day}$ Daily flexible H_2 demand [MWh_{H_2}/day]

$l_{heat,fixed}(t)$ Hourly fixed electrical demand for heat [MWh/h]

$l_{heat,flex,day}$ Daily flexible electrical demand for heat [MWh/day]

$l_{mob,fixed}(t)$ Hourly fixed electrical demand for electrical moblity [MWh/h]

$l_{mob,flex,day}$ Daily flexible electrical demand for electrical moblity [MWh/day]

$l_{resi}(t)$ Hourly residual electrical demand [MWh/h]

$lf_{dist-gen}(t)$ Hourly load factor of distributed conventional generation [-]

$lf_{hydro}(t)$ Hourly load factor of hydroelectric run-of-the-river units [-]

$lf_{onsh}(t)$ Hourly load factor of onshore wind turbines [-]

$lf_{pv}(t)$ Hourly load factor of PV [-]

M Big value used for Big-M method

n_{ev} Number of electric vehicles [-]

n_{hp} Number of heat-pumps [-]

$p_{batt,in/out,max}(b)$ Maximum input/output power of the battery group b [MWh]

$p_{charger}$ Power of the electric vehicle charging station [MW]

$p_{dist-gen,max}$ Installed capacity of distributed conventional generating units [MW]

$p_{el,max}(e)$ Installed capacity of electrolyzer e) [MW]

$p_{gen,max}(g)$ Installed capacity of generator g [MW]

$p_{gen,min}(g)$ Minimum operating power of generator g [MW]

$p_{H2P,max}(h)$ Installed capacity of H2P plant h [MW]

$p_{hp,individual}$ Electrical capacity of an individual heat-pump [MW]

$p_{hp,max}$ Installed capacity of heat pumps [MW]

$p_{hydro,max}$ Capacity of installed hydroelectric run-of-the-river units [MW]

$p_{imp,max,tot}$ Maximum aggregated imports [MW]

$p_{imp,max}(i)$ Maximum import capacity at interconnection i [MW]

$p_{onsh,max}$ Capacity of installed onshore wind turbines [MW]

$p_{phs,in/out,max}(p)$ Maximum input/output power of the pumped-hydro storage p [MWh]

$p_{pv,max}$ Capacity of installed PV [MW]

$p_{shift,max}$ Maximum load that can be shifted (removed) [MWh/h]

$p_{v-shed,max}$ Maximum voluntary shed power [MWh]

$q_{H_2,fixed}(t)$ Hourly H_2 demand [MWh_{H_2}/h]

$q_{H_2,imp,max}(j)$ Maximum hourly hydrogen import at interconnection j [MWh_{H_2}/h]

s_{base} Base power of the per-unit system [MVA]

$soc_{batt,max}(b)$ Maximum capacity of the battery group b [MWh]

$soc_{H_2,sto,max}(q)$ Maximum capacity of the hydrogen storage q [MWh_{H_2}]

$soc_{phs,max}(p)$ Maximum capacity of the pumped-hydro storage p [MWh]

$voll$ Value of loss-load [€/MWh]

$voll_{H_2}$ Value of loss-load for hydrogen [€/MWh_{H_2}]

w_{hp1m} Share of heat-pumps with a flexible charging behavior [-]

w_{v1m} Share of electric vehicles with a flexible charging behavior [-]

Variables

$\Theta(n,t)$ Hourly phase angle of node n [rad]

$C(n,t)$ Hourly curtailed electrical power at node n) [MWh/h]

$E_{v-shed}(n,t)$ Hourly voluntary load shedding at node n [MWh/h]

$Ens(n,t)$ Hourly electrical energy-not-served at node n [MWh/h]

$Ens_{H_2}(n,t)$ Hourly hydrogen energy-not-served at node n [MWh_{H_2} /h]

$F(k,t)$ Hourly flowing electricity through line k [MWh/h]

$F_{H_2}(k,t)$ Hourly flowing hydrogen through pipeline k [MWh/h]

$P_{batt,in}(b,t)$ Hourly electrical power feeding the battery group b [MWh/h]

$P_{batt,out}(b,t)$ Hourly electrical power produced by the battery group b [MWh/h]

$P_{el}(n,t)$ Hourly power consumed by electrolyzers at node n [MWh/h]

$P_{gen}(g,t)$ Hourly production of conventional generator g [MWh/h]

$P_{H2P}(h,t)$ Hourly power produced by H2P plant h [MWh/h]

$P_{heat,flex}(n,t)$ Hourly power dedicated to heat production at node n [MWh/h]

$P_{imp}(i,t)$ Hourly imported electricity from interconnection i [MWh/h]

$P_{mob,flex}(n,t)$ Hourly power dedicated to electric mobility charging at node n [MWh/h]

$P_{phs,in}(p,t)$ Hourly electrical power feeding the pumps of PHS p [MWh/h]

$P_{phs,out}(p,t)$ Hourly electrical power produced by the turbines of PHS p [MWh/h]

$Q_{H_2,flex}(n,t)$ Hourly flexible hydrogen consumed at node n [MWh_{H_2}/h]

$Q_{H_2,imp}(n,t)$ Hourly H_2 imported from node n [MWh_{H_2}/h]

$Q_{H_2,sto,in/out}(q,t)$ Hourly H_2 flowing in/out of the H_2 storage unit q [MWh_{H_2}/h]

$S_{add}(n,t)$ Hourly shiftable electrical demand added at node n [MWh/h]

$S_{rem}(n,t)$ Hourly shiftable electrical demand removed at node n [MWh/h]

$Soc_{batt}(b,t)$ Hourly state-of-charge of the battery group b [MWh]

$Soc_{H_2,sto}(q,t)$ Hourly state-of-charge of the H_2 storage unit q [MWh_{H_2}]

$Soc_{phs}(p,t)$ Hourly state-of-charge of the pumped hydro storage (PHS) p [MWh]

CHAPTER 1

Introduction

Chapter overview

- Context
- Objective of the thesis
- State-of-the-art: research gap and contributions
- Outline of the manuscript

The European Green Deal aims to make Europe the first carbon neutral continent by 2050. An intermediate step objective is the reduction of 55% of greenhouse gas (GHG) emissions by 2030 compared to 1990 levels, as outlined in the Fit-for-55 Package. Since the energy sector accounts for more than 75% of the European GHG emissions [1], decarbonizing this sector is essential to reach the aforementioned targets. In Belgium, this intermediate objective has been divided into three regional targets for 2030: the Walloon Region aims for a 55% reduction in emissions, the Flemish Region targets a 35 % reduction, and Brussels-Capital seeks a 32 % reduction. In this context, green hydrogen – produced through water electrolysis powered by low carbon energy sources – could play a crucial role in decarbonizing the mobility and industry sectors, which are hard-to-decarbonize sectors as part of their applications cannot be electrified, and the power sector. Indeed, hydrogen is a potential fuel for heavy transportation, a feedstock for the industrial sector, and an alernative fuel for generation units. For these reasons, many studies assert that hydrogen will be part of future energy systems. Also, hydrogen has been the subject of numerous studies. However, its impact on the power system adequacy has not yet been fully explored.

In this Chapter, we explore the different future energy system projections for Belgium and the pivotal role that hydrogen plays in the latter. Then the objective of this work is clearly outlined, followed by a review of the state-of-the-art highlighting current research, and gaps in the domain. Finally we present the outline of the manuscript.

> The Chapter is structured according to the following sections: Section 1.1 explores the role of hydrogen in the future Belgian energy system. Section 1.3 presents the objective of this thesis, and Section 1.4 exposes the state-of-the-art in the domain, the research gap, and the contributions brought by this thesis. Finally, Section 1.5 outlines the structure of this manuscript.

1.1 Pathways for the Belgian energy transition

When focusing on Belgium, different pathways are proposed to reach climate neutrality in the energy sector, usually relying on electrification and/or molecules. Hereunder, are listed the results/future plans of several studies conducted by: Bureau Fédéral du Plan (Oct. 2020) [2] , Elia (Nov. 2021) [3], Service Public Fédéral (Dec. 2021 and updated in Oct. 2022) [4], EnergyVille (Oct. 2022) [5], and Sustainable Energy Group from UCLouvain [6, 7] (Sep. 2024).

Even though the works summarized hereunder study the same national neutral-carbon scenario for 2050, they all use different modeling tools and different hypotheses. For this reason, not all solutions converge, and fortunately! This offers a panel of material to be discussed. However, they all seem to agree that molecules will play an important role in our future energy system, that a big share of this hydrogen will be produced by electrolyzers (locally or abroad), and that hydrogen is a promising energy carrier that could help decarbonize our energy system.

Bureau Fédéral du Plan - Fuel for Future - October 2020

The EU-Commission shared their hydrogen strategy which consists in installing 40 GW of renewable hydrogen electrolyzers by 2030 in order to launch the hydrogen economy as recovery plan in a context of energy transition. Following that announcement, the Bureau Fédéral du Plan has released a report named "Fuel for Future". In this report, they try to identify the place that hydrogen could take in the future Belgian energy system by 2050 [2]. They consider in this study two scenarios leading to a net-zero GHG emissions energy system by 2050 : 1) Deep electrification: *a* *far-reaching electrification of the final energy consumption* vs. 2) Diversified Energy Supply: *considering a sustained and increased used of gas for transport, industrial heating, and power generation*.

The total demand in 2050 more than triples compared to 2018. In both scenarios, the future electricity mix is composed of ∼2/3 of renewables, and ∼1/3 of gas-fired units (e-gas, biogas, fossil gas) with carbon capture and storage (CCS). However, the results in terms of flexibility are different:

- Deep Electrification scenario: will *rely primarily on direct electrification (e.g. heat pumps or electric vehicles)* – Electric vehicles, and electricity imports (14.4 GW) will be the daily, and weekly flexibilities even though electrolyzers (10.6 GW) provide still half of the flexibility – Domestic production of hydrogen reaches 80 TWh (with 7547 FLH [1] or 86.15 % load factor for electrolyzers).
- Diversified Energy Supply scenario: will *integrate more indirect electrification (e.g. conversion to hydrogen, or ammonia)* – Gas-fired power plants (11 GW) and electrolyzers (19.1 GW) will be the main daily, weekly, and annual flexibility providers – Domestic production of hydrogen reaches 99 TWh (with 5183 FLH or 59.17 % load factor for electrolyzers).

When pre-setting exogenously hydrogen imports to 3.6 €/kg_{H_2}(90 €/MWh_{H_2}), the results claim that in both scenarios, no hydrogen will be imported except when considering a higher marginal cost for electricity production. In that case, import of hydrogen appears: 18 TWh in the Deep Electrification scenario, and 11 TWh in the Diversed Energy Supply scenario. Furthermore, if in addition to that, a lower price for hydrogen imports of 2 €/kg_{H_2}(50 €/MWh_{H_2}) is considered, imports drastically increase even more, up to 69 TWh for the Deep Electrification scenario.

Elia - Roadmap to net-zero - November 2021

Elia also published a report, "Roadmap to net zero" which details the group's vision on building a climate-neutral European energy system by 2050 [3]. They consider two different transformation pathways for Europe: 1) ELEC pathway: most sectors are electrified vs. 2) MOL pathway: *characterised by high levels of indirect electricity demand needed to produce green molecules* (i.e. certain energy sectors are supposed to be fed by those molecules). And the following conclusions are stated:

[1] FLH for Full Load Hours.

- The ELEC-pathway: For Belgium, the solution leads to an energy demand of 305 TWh, and an electricity demand of 245 TWh (x3 compared to 2018) due to a strong electrification (mainly direct electricity 69% which is very efficient).
- The MOL-pathway: For Belgium, the solution leads to an energy demand of 360 TWh, and to an electricity demand of 325 TWh (x4 compared to 2018) due to the production of green molecules (mainly indirect electricity 65% which has high conversion losses).

The study claims that Europe will only be able to satisfy its direct electrification with domestic renewables and will have to import green molecules from other continents to satisfy its indirect electrification demand. However, the renewable potentials are *unevenly distributed across Europe*, thus Belgium will require an intensified cooperation from European countries to satisfy its direct electrification. Indeed, the study shows that Belgium will only be able to satisfy 28% of its direct electrification in the MOL-pathway, and 37% in the ELEC-pathway.

Furthermore, if it is considered that indirect electricity is imported under the form of green molecules from abroad EU and that these are under the form of hydrogen, and have been produced by electrolysers having an efficiency of 70%, the ELEC-pathway which requires 75 TWh of indirect electrification would import 52 TWh of hydrogen, and the MOL-pathway which requires 210 TWh would import 147 TWh of hydrogen [2].

SPF - Stratégie fédérale pour l'hydrogène - December 2021 (updated in Oct. 2022)

The Service Public Federal (SPF) also released a report, "Stratégie fédérale pour l'hydrogène" [4] which details the Belgian ambition for green molecules, and of being a hub for Europe. In this report, the SPF identifies the sectors that will require green molecules to decarbonize by 2050: industry, heavy transportation, flexibility and back-up units for the power sector, and the construction sector. This sums up to a yearly demand of 125 to 200 TWh of hydrogen molecules and its derivatives in Belgium by 2050.

Even though Europe has ambitions to install 6 GW of electrolyzers by 2024, and 40 GW by 2030, the installed capacity in Belgium will be limited due to weak domestic

[2] This interpretation is not from Elia, and is a personal extrapolation in order to have an order of magnitude to be compared with other studies.

renewable potential. Indeed, Belgium has the ambition to install 150 MW of electrolyzers by 2026 in a *strategic interest to gain expertise in the operation of these units and support technological development of Belgian companies*. However, following the "Declaration d'Esbjerg" (May 2022), Belgium, with Denmark, Germany, and Netherlands committed in installing 65 GW of offshore wind turbines and 20 GW of electrolyzers by 2030 and 150 GW of offshore wind turbines by 2050.

Today, an existing hydrogen pipeline exists and was developed by a private actor (Air Liquide) in order to supply industrial clients. This network links Zeebrugge, Gent, Antwerpen, and Charleroi. However, still today some industrial clusters are not connected to the network and the government would like to pursue its development. The federal government has as an objective i) the commissioning of 100-160 km of pipelines, among others thanks to the reuse of unused pipelines in the country (e.g. low calorific value gas pipelines) by 2026, and ii) the interconnection with neighbouring hydrogen networks (Germany, France, Netherlands) by 2028 in line with the ambition to represent a hub for imports and transits of hydrogen molecules.

EnergyVille - The Power of Perspetcive: 2050 Paths - October 2022

In the project 'Perspective 2050' [5], EnergyVille tries to give insights on possible pathways to reach a carbon neutral Belgium by 2050. Three scenarios are considered: 1) the Central scenario permits electrification, molecules imports, and domestic molecule production, vs. 2) the Electrification scenario considers more offshore wind power capacity – thanks to the "Declaration d'Esbjerg", Belgium will have access to 16 GW outside of the Belgian territorial waters –, and the option to invest in new nuclear technology – focusing research on small modular reactors (SMR), with an average size of 300 MW, operational from 2045, and of generation IV – are also considered, vs. 3) the Molecules scenario allows synthetic molecules imports at lower costs (30% cost reduction compared to Central scenario, i.e. 1.7 €/kg_{H_2} by 2050) and access to cross-border CO_2 storage in Norway and Netherlands (by 5 Mton/year).

These scenarios are optimized for 2050 and quite surprisingly, their results do not differ that much:

- Central scenario: Demand in electricity doubles compared to 2020 and the role of clean molecules grows but is limited to 11% (15.3 TWh) of final energy consumption (FEC). The installed capacity of electrolyzers is 13.2 GW : 5GW installed centrally producing 12.5 TWh of hydrogen (2500 FLH or 28.5% load factor), and 8.2 GW installed at industry (steel and chemical sectors) producing 10.6 TWh (1292 FLH or 14.75% load factor). Imports of hydrogen reach 36 TWh.

- Electrification scenario: Demand in electricity more than doubles (x2.3) compared to 2020 and clean molecules represent 16.3 TWh of FEC. The installed capacity is 8.2 GW producing 28 TWh (3414 FLH or 38.9% load factor) because of a more constant access to electricity at lower cost. Imports of hydrogen reaches 5 TWh.
- Clean molecules scenario: Demand in electricity is the same as electrification scenario and clean molecules represent 14% of FEC (27.3 TWh). The installed capcaity of electrolyzers is 10.4 GW installed, producing 13.7 TWh (1000 FLH or 11.4% load factor). Imports of hydrogen reaches 91 TWh at a lower price (scenario assumption).

Sustainable Energy Group from UCLouvain – project BEST – September 2024

Within the ETF[3] Project BEST (Belgian Energy System), two studies give interesting results. The first one conducted by X. Rixhon [6] focuses on Belgium and studies the energy transition pathways to reach a neutral-carbon system by 2050, and the second one conducted by P. Thiran [7], extends to Europe, and explores different options to reach a fossil-free European energy system by 2050.

- The European study allows imports of renewable fuels (derived from renewable electricity or biomass) from outside of Europe at a certain cost. However, no imports are noticed. Countries importing renewable fuels do it from other European countries. In this work, three scenarios are derived: i) reference study case: where nuclear power is not considered ii) nuclear scenario: nuclear is considered available, iii) sufficiency scenario: a lower demand is considered, and no nuclear power. The results show that:
  - In the reference scenario, Belgium imports a total of 154 TWh of renewable fuels: 49.7 TWh of e-FT[4] fuels, 9.2 TWh of e-methane, 61.9 TWh of e-hydrogen, and 33 TWh of e-methanol.

[3] ETF: Energy Transition Fund

[4] Fischer Tropsch (FT) fuels represent synthetic fuels replacing typical fossil fuels, i.e. light fuel oil, diesel, gasoline, and jet fuel.

- In the nuclear scenario, Belgium imports a total of 149.3 TWh of renewable fuels: 75.6 TWh of e-FT fuels, 29.5 TWh of e-hydrogen, and 44.2 TWh of e-methanol. In this scenario, Belgium does not import, but exports e-methane (5.4 TWh).
- In the sufficiency scenario, Belgium imports a total of 82.4 TWh of renewable fuels: 6.5 TWh of e-FT fuels, 2.2 TWh of e-methane, 34.7 TWh of e-hydrogen, and 38.9 TWh of e-methanol.

Belgium does not install electrolyzers in any scenario.

- The Belgian study optimizes the pathway to a neutral-carbon system in 2050, starting from 2020 with a myopic formulation approach, and steps of 5 years. Two scenarios are studied for Belgium: i) REF: the reference scenario, and the ii) SMR: a scenario where the SMR technology is available from 2040 up to 6 GW. The results show that:
  - In the REF scenario, Belgium imports e-fuels: 39 TWh of e-methane, 16 TWh of e-hydrogen, 44 TWh f e-ammonia, and 55 TWh of e-methanol.
  - In the SMR scenario, Belgium imports e-fuels: 7 TWh of e-methane, 16 TWh of e-hydrogen, 11 TWh f e-ammonia, and 55 TWh of e-methanol. The main difference is that it imports way less e-methane, and less e-ammonia.

  Belgium does not install electrolyzers in any scenario.

In both of these studies, electrolyzers are not foreseen to be installed in Belgium. These results differ from the statements of other studies but are justified. However, they both claim that renewable fuels will be part of our future energy systems, and that Belgium will be a big importer.

1.2 Hydrogen in a World context

1.2.1 Consumption of hydrogen in the world

The consumption of hydrogen is depicted in Fig. 1.1 , reaching a value of 94.8 Mt in 2022. In the fast and until today, refining and ammonia represent the majority of the use.

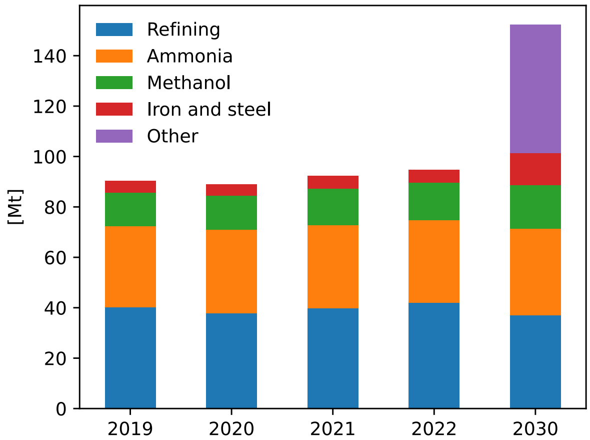

Figure 1.1: Hydrogen consumption in the world from 2019 to 2022, and hydrogen consumption forecast for 2030 - Source: IEA 2023 [8].

The use of hydrogen in these different sectors are listed below:

- Oil and gas refineries: hydrocracking consists in breaking down hydrocarbons in the presence of hydrogen into lighter, and more valuable products (gasoline, diesel), and hydrotreating consists in removing sulfur and other impurities from petroleum fuels.

- Nitrogen and phosphorus-based fertilizers require ammonia which is produced through the Haber-Bosch Process. The Haber-Bosch Process converts nitrogen and hydrogen into ammonia.

- To produce chemicals such as formaldehyde, acetic acid, and plastics, methanol is necessary. Methanol can be produced by the reaction of carbon monoxide or dioxide carbon and hydrogen.

- Hydrogenation reactions in chemical synthesis require hydrogen as well. This occurs in the food (e.g. produce margarine from vegetable oil) and chemical industry.

- To allow a protective atmosphere, hydrogen is used to prevent oxidation and as a reducing agent. This is done in the glass industry and in electronics manufactures.

- While hydrogen is indispensable in the uses described above, different technologies and processes are trying to shift to hydrogen to lighten their impact in terms of emissions. Steel production is trying to replace the coal by hydrogen in the iron-reduction step. Glass production is also trying to use hydrogen combustion for high temperatures. Fuel cells are used to retribute electricity back from hydrogen, and could be used in the transport sector, or power sector. Also, hydrogen will serve as a basis for synthetic fuels.

1.2.2 Production of hydrogen in the world

To serve this hydrogen consumption, different production process coexist: coal gasification, steam methane reforming, water electrolysis, and methane pyrolysis, and are listed below. Depending on the used process, hydrogen is assigned a color.

- Coal gasification consists in the oxidation of coal by air, oxygen, or steam. This process produces a synthetic gas consisting in a mix of carbon monoxide, hydrogen, carbon dioxide, methane, and steam. Carbon monoxide will react with the water molecules to produce carbon dioxide and hydrogen. The hydrogen produced in this process is referred as black hydrogen if using lignite or brown hydrogen if using bituminous.

- During the steam methane reforming process, methane reacts under high temperatures with steam water which produces hydrogen and carbon monoxide. The produced carbon monoxide then reacts with the steam as well, and converts to carbon dioxide. The resulting by-product of this process, i.e. carbon dioxide can either be released in the atmosphere (grey hydrogen), or captured and stored (blue hydrogen).

- Water electrolysis uses electricity to separate the oxygen and hydrogen atoms of water molecules. If using electricity produced by renewable energies, it is green hydrogen; if using electricity produced by solar energy, it is yellow hydrogen; and if using electricity produced by nuclear energy, it is pink hydrogen. Hydrogen produced through electrolysis with a diversified mix depending on what is available is sometimes referred to yellow as well.

- Methane pyrolysis transforms methane into solid carbon, and hydrogen. This hydrogen is referred as turquoise.

In 2022, 62% of the hydrogen is grey, 21% is black, and 16% is by-product hydrogen that takes places in refineries and petrochemical industries. Blue and green hydrogen represent 0.6 and 0.1% respectively [9].

1.2.3 Oxygen: a by-product

Oxygen is the by-product of the water electrolysis process. For every gram of hydrogen produced, 8 grams of oxygen is produced. One could ask if this production could be valued or should it just be released in the atmosphere.

Oxygen is used in the industrial, medical, food and health sectors for many reasons [10]. Below are listed its principal uses:

- Combustion enhancement and efficiency: oxygen is used to enrich the air within the combustion process to increase its efficiency, and lower NOx emissions. Examples: steel, glass, and metal manufacturing, oil refining.
- Chemical and petrochemical industry : oxygen allows oxidation reactions which can produce chemicals, and syngas.
- Medical and life-support purposes.
- Water treatment applications: oxygen is used to produce ozone and aeration.

To produce this oxygen, several technologies and process exist [11]: i) cryogenic separation where the different boiling temperatures of nitrogen and oxygen are used to separate them, ii) pressure swing adsorption (PSA) where zeolites under pressure collect nitrogen, and allows oxygen to pass, iii) membrane technology which filters slow gases like nitrogen, and allows fast gases like oxygen to pass, iii) by-product which are processes that aim to produce nitrogen or hydrogen for example, and where oxygen is a by-product. Depending on the oxygen purity, daily volume, and pressure required, a choice can be made on the used technology to produce it. One of the biggest oxygen exporter in the world is Belgium. In 2021 Belgium is the second worldwide exporter and exported 536 kt of oxygen after the USA (1252 kt) [10].

1.3 This Thesis

As mentioned above, part of this hydrogen production might occur locally through the water electrolysis process. The integration of electrolyzers into the power system will create an additional electrical demand, but this demand is not common. Producing green hydrogen only makes sense when powered by renewable energy sources (RES), otherwise, traditional methods like steam methane reforming (gray hydrogen) would emit less CO_2. Consequently, the consumption profile of electrolyzers is highly variable as it follows RES production. Moreover, in some of the referenced studies, electrolyzers are also utilized as flexibility. Due to these factors, the additional electrical demand from electrolyzers is unconventional and requires thorough analysis. Specifically, we need to determine if we have sufficient transmission and generation capacities to meet this new demand. This requirement is the essence of adequacy: the system's ability to satisfy consumers' demand at all times and in all locations.

As proposed by the reports detailed above, electrolyzers will not come along alone, and will be integrated into a whole hydrogen system with a pipeline network, storage facilities, import points, and hydrogen-to-power units. Therefore, it is essential to consider the entire hydrogen system to fully understand the impact of hydrogen production via water electrolysis on our power system. This leads to the following central question:

What is the impact of e-hydrogen and e-fuels on the Belgian power system adequacy?

To address this question, we will model the interactions between the hydrogen and power systems and use computational methods to quantify the impact on system adequacy.

1.4 State-of-the-Art

Numerous studies in the literature have explored the integration of hydrogen and electrolyzers into power systems. However, none of these studies fully answer our research question: *What is the impact of hydrogen on power system adequacy?*. To assess the existing literature, the studies have been categorized based on three key characteristics (necessary to answer the question): i) conducting an adequacy or reliability study, ii) considering coupled systems (such as power-gas or power-hydrogen systems), and iii) integrating a hydrogen demand.

Although no study ticks all three characteristics, they at least tick two of them. The Venn diagram in Figure 1.2 illustrates the possible relationships and overlaps between these characteristics. Many studies fall into the two following categories:

- System operation studies of coupled systems, integrating a hydrogen demand (green zone).
- Adequacy studies of coupled systems (red zone).

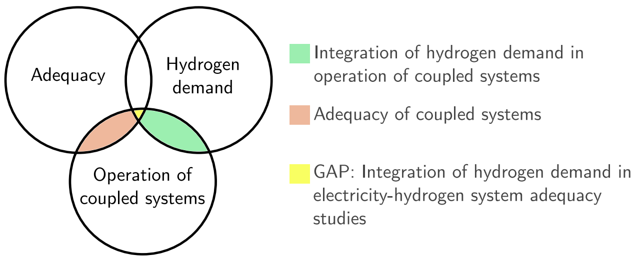

Figure 1.2: Categories of the reviewed studies in the domain of hydrogen integration in power system adequacy studies.

In the first category, the studies incorporate hydrogen demand into power systems by adding electrolyzers, but focus on system operation, and overlook the adequacy aspect. In the second category, coupled systems (power-gas and power-hydrogen) are analyzed from an adequacy perspective but hydrogen is never considered as a demand per se. Additionally, in this second category, most of these studies concentrate on power-gas systems, treating hydrogen only as an intermediate energy carrier between the power and gas systems. Although these studies do no address fully our research question, they do approach it from different angles.

To the author's knowledge, no studies have thoroughly examined the effect of hydrogen demand on power system adequacy while considering the entire hydrogen system, rather than focusing solely on electrolyzers. It is the full overlap of all three characteristics (yellow zone) that is identified as the research gap in this domain. To comprehensively answer our research question, what is needed are adequacy studies considering coupled hydrogen-electricity systems while explicitly accounting for hydrogen demand.

In conclusion, while several studies partially address the question *What is the impact of hydrogen demand on power system adequacy?*, each of them lacks certain critical elements required for a complete analysis. This gap highlights the need to develop a tool that fully integrates all necessary components (adequacy study - power-hydrogen system representation - hydrogen demand) to comprehensively study the impact of hydrogen demand on power system adequacy.

The two next sections (1.4.1, 1.4.2) will focus on an analysis of the existing studies in the literature, identifying which aspects of the research question they address and which elements differentiates one from another. Following this, an exploration of existing tools and models that have been developed by the research community is presented (Section 1.4.3), evaluating their potential for adaptation or extension in building the desired tool, even though the decision will be made to develop a new model from scratch rather than relying on existing frameworks. Finally, the contributions of this work are highlighted.

1.4.1 Integration of hydrogen demand in power system operation studies

Hydrogen has been considered in power system operation by several authors already. The dynamic and reactive power behavior of electrolyzers is integrated into a security-constrained multi-period[5] AC optimal power flow (SC-MP-AC-OPF) in [12] which considers line outages. Energy hubs consisting in electrolyzers, hydrogen storage, and hydrogen-to-power units, are integrated into a three stage robust security-constrained multi-period unit commitment DC power flow (SC-MP-UC-DC-PF) in [13]. The first stage optimises the UC, the second checks the DC-PF, and the last tests the robustness of the solution with the variability of the wind power forecast. Hydrogen storage is considered in a stochastic SC-UC-DC-OPF in [14] which considers price-based demand response as well. The stochasticity considers 5 typical wind power scenarios (clustered from Monte Carlo sampling) with a certain probability. An integrated power-heat-hydrogen system is studied in [15] to explore flexibility enhancement through sector coupling, and the impact on wind power curtailment. All these studies optimize the operational costs on a daily basis. Hydrogen is also integrated into a multi-energy UC-DC-OPF model which optimizes both the annuitized investment and operation costs in [16]. In this case, hydrogen production through water electrolysis and steam methane reforming with carbon capture and storage are considered. Hydrogen is integrated into a multi-energy model framework REMix in [17] which optimizes both operational and investment costs and focuses on the hydrogen infrastructure expansion. And finally, in [18], the hydrogen supply chain is integrated into a planning model tool which optimizes the investment, and operation of the electrical system while integrating a certain hydrogen demand for export purposes.

[5]The multi-period criteria refers to the consideration of multiple time periods, and interlinks them with one another. This criteria is essential to optimize storage and flexibility capacities.

Table 1.1: Integration of hydrogen in operation of power systems: state-of-the-art and comparison. Abbreviations: security-constrained (SC), multi-period (MP), alternative/direct current (AC/DC), Optimal Power Flow (OPF), Power Flow (PF), Unit-Commitment & Economic Dispatch (UCED), Investment (Inv.).)

Ref.	Hourly resolution	Multi node	Time horizon	H2 demand	H2 storage	H2-to Power	Inv. model	Formulation
[12]	✓	✓	Day	✓	✓	✓	✗	SC-MP-AC-OPF
[13]	✓	✓	Day	✓	✓	✓	✗	SC-MP-UCED-DC-PF
[14]	✓	✓	Day	✓	✓	✓	✗	SC-UCED-DC-OPF
[16]	✓	✓	Year	✓	✓	✗	✓	UCED-DC-OPF
[17]	✓	✓	Year	✓	✓	✓	✓	-
[19]	✓	✗	Day/Year	✓	✓	✗	✗	H2 supply chain model
[18]	✓[a]	✗[b]	Multiple years	✓	✓	✗	✓	UCED + H2 supply chain
[15]	✓	-	Day	✓	✓	✗	✗	UCED

[a] using typical days.
[b] multi-regional with transmissin lines between them but internal grid not considered.

1.4.2 Adequacy of coupled systems

Power-gas integrated systems

Also, many studies have assessed the reliability of integrated gas-power systems. Their reliability is assessed in an event-based non-sequential sampling in [20, 21], in a 2 hours time horizon in [22], in a daily time horizon in [23–26], in a weekly time horizon in [27], in a yearly time horizon in [28–30], and on a several year time horizon considering investment costs in [31]. Usually, the main objective is to model precisely the availability of gas-fired units which play a major and growing role in power systems. Although, all studies consider gas-fired units as the technologies that link both systems, few studies [28, 20, 23, 31] also considered power-to-gas technologies allowing bi-directional flows between both systems.

Table 1.2: Reliability of integrated gas-power systems: state-of-the-art and comparison. Abbreviations: Gas-fired power plants (GFPP) - Power-to-gas (P2G), electrical compressors (EC), Non-sequential (Non-seq.).

Ref.	Hourly resolution	Multi node	Time horizon	Elec/Gas Link	Bi-directional	Elec/Gas coupling
[22]	✓	✓	2 hours	GFPP	✗	✓
[28]	✓	✓	1 year	P2G, CHP	✓	✓+ heat
[20]	✓	✓	Non-seq.	P2G, GFPP	✓	✓
[23]	✓	✓	1 day	GFPP, P2G	✓	✓
[24]	✓	✓	1 day	GFPP	✗	✓
[25]	✓	-	1 day	GFPP, P2G	✗	✓
[29]	✓	✗	1 year	GFPP	✗	✗only elec
[21]	✓	✓	Non-seq.	GFPP, EC	✗	✓
[31]	✗	✓	10 years	GFPP, EC, P2G	✓	✓
[30]	✓	✓	1 year	GFPP	✗	✓
[26]	✓	✓	1 day	GFPP, EC	✗	✓
[27]	✓	✓	1 week	GFPP	✗	✓

Power-hydrogen integrated systems

Literature on the impact of hydrogen on power system adequacy has only been studied by three authors. A first study analyzed the impact of producing hydrogen and storing it to manage over-production of wind power sources from a market-based point of view within a sequential Monte Carlo adequacy framework in [32]. This study does not consider network constraints. Another study considered the fraction of blended hydrogen in gas flow equations and studied the effects on integrated gas-power systems reliability in [33]. The third study quantifies the impact of a hydrogen storage system - including an electrolyzer, a hydrogen storage tank, and a fuel cell - on the adequacy of a power system in [34]. Hydrogen demand is considered in none of the studies, hydrogen production takes place to benefit from excess production, or to store energy and convert it back to electricity. These studies do not quantify the impact that a hydrogen demand has on the power system as such.

Table 1.3: Integration of hydrogen in adeqaucy: state-of-the-art and comparison.

Ref.	Hourly resolution	Multi node	Time horizon	H2 demand	H2 storage	H2-to Power	AC/DC Power Flow	Inv. model
[32]	✓	✗	1 year	✗[a]	✓	✗	✗	✓
[33]	✓	✓	1 week	✗[b]	✓	✗	DC OPF	✗
[34]	✓	✓	1 year	✗	✓	✓	DC OPF	✗

[a] No fixed hydrogen demand: hydrogen production with surplus of renewable electricity production and sold.
[b] No fixed hydrogen demand: surplus of renewable electricity production produces hydrogen - which is transformed into methane or not - and blended into natural gas pipelines.

1.4.3 Existing power and energy system models

Evaluating the impact of hydrogen demand on power system adequacy requires a model that i) permits adequacy assessments, ii) represents both electricity and hydrogen systems, iii) considers the transmission grid and its network constraints through load flow, and iv) has a multi-period formulation to be able to integrate time-dependent technologies like storage and flexibility. This would be a hydrogen-integrated power system model with a multi-period DC-OPF formulation. Ready-made models for this purpose do not currently exist. However, many existing power and energy system tools used by small or big communities exist in the literature. Although they do not have all four features listed above, they are close to it. Among them, the ones that permit multi-period studies, consider network constraints (through the DC-OPF formulation), and that have an hourly resolution are listed in Table 1.4. They are compared based on whether they support unit commitment modeling, include an adequacy assessment feature, handle multi-energy carriers, are open-source, and the programming languages they use.

Table 1.4: Power and energy system modeling tools that allow the DC-OPF formulation, have a multi-period modeling, and that have an hourly resolution.

Model Name	**Unit-commitment**	**Adequacy integrated**	**Multi-energy**	**Open-source**	**Programming Language**
Antares-Simulator	✓	✓	✓	✓	C++
AnyMOD.jl	✗	✗	✓	✓	Julia
DIgSILENT PowerFactory	✓	✓	✗	✗	-
MOST[a]	✓	✗	✗	✓	MATLAB
NEPLAN	✓	✓	✗	✗	-
oemof	✓	✗	✓	✓	Python
PLEXOS	✓	✓	✓	✗	-
POMATO	✗	✗	✗	✓	Python & Julia
PowerSimulations.jl	✓	✗	✗	✓	Julia
PSS/E	✓	✓	✗	✗	-
PSS/SINCAL	✗	✓	✓	✗	-
PyPSA	✓	✗	✓	✓	Python
St(ELMOD)	✓	✗	✗	✓	GAMS
TransiEnt	✗	✗	✓	✓	Modelica

[a] Matpower Optimal Scheduling Tool.

As previously said, none of these models are ready-made for our study-case. Two possibilities appear: start from scratch and develop the desired model, or starting with existing open-source model, and add/replace/modify parts (e.g. equations). For example, in the second option, models that do not have integrated adequacy assessments could be customized by an external Monte Carlo framework to include the probabilistic feature, and models that do not have the multi-energy carrier formulation could be extended as well with additional equations to consider sector coupling. Both options have benefits and disadvantages, but they mainly imply a different way of working. While the first option will imply a mastering of the model structure, and equations, it will take a lot of time, especially for ensuring robustness and validation. The second option will imply to break into someone else's code which is a relevant skill, and due to time savings, it will allow to get further into the research. In this work it has been chosen to start a model from scratch.

1.4.4 Research gap and contributions

To the author's knowledge, no study proposes a probabilistic adequacy tool able to study the impact of hydrogen in terms of demand, storage and imports on power system adequacy studies. This work therefore aims at fulfilling this gap. The main contributions of this work are:

i) The integration of the hydrogen energy vector in a probabilistic adequacy tool with its conversion and storage technologies (electrolyzers, hydrogen-to-power units, hydrogen storage units), as well as its transport network (hydrogen pipeline network). This probabilistic adequacy tool is a novel sequential Monte Carlo tool based on a multi-period DC optimal power flow (MP-DC-OPF) with an hourly resolution and specifically tailored for yearly horizons (8760 hours).

ii) The study of the impact of hydrogen on Roy Billinton Test System slightly modified.

iii) The study of the impact of hydrogen on adequacy and on the operation of a complex and realistic power system representative of the future Belgian transmission (220 and 380 kV) grid in 2030.

1.5 Outline of the manuscript

The work presented in this manuscript is structured according to the following chapters:

- **Chapter 2: Theoretical Foundations and Legal Framework of Reliability.** This Chapter presents the theoretical foundations around the concept of adequacy. The Chapter also extends to the development of the loss-of-load expectation (LOLE) threshold concept, as well as the legal framework and standards for Europe, and Belgium.

- **Chapter 3: Power-to-Hydrogen models in Adequacy Studies.** This Chapter focuses on modeling electrolyzers for adequacy studies. We develop and integrate two power-to-hydrogen models - non-linear and linear - that describe the steady-state behavior of electrolyzers into an adequacy study.

- **Chapter 4: Adequacy Assessment Tool with the integration of the hydrogen energy vector.** This Chapter describes the developed probabilistic adequacy tool integrating the hydrogen energy vector, details the equations of the model, and finally verifies the model with benchmark test systems.

- **Chapter 3: Analysis on a test system.** This Chapter illustrates the probabilistic adequacy tool's functionality with an application on a modified Roy Bilinton Test System (RBTS). This simple case study demonstrates the impact of hydrogen integration in terms of demand, storage, production, and imports.

- **Chapter 4: Analysis on the Belgian 2030 case.** This Chapter applies the probabilistic adequacy tool to the Belgium 2030 study, evaluating various scenarios. We examine the effects of grid extensions, offshore wind farm deployments, flexibility measures, and hydrogen production on adequacy indicators and overall system operation..

CHAPTER 2

Theoretical Foundations and Legal Framework of Reliability

Chapter overview

- Theoretical introduction to reliability and risk assessments.
- Derivation of the loss-of-load-expectation (LOLE) threshold formulation with the value-of-lost-load (VOLL), and the cost-of-new-entry (CONE).
- Reliability standards and legal framework in Belgium.

In this Chapter, we explore the theoretical foundations of reliability and risk assessments. We contrast deterministic and probabilistic approaches, as well as adequacy and security studies highlighting their respective methodologies and applications. The chapter also extends to the development of the loss-of-load expectation (LOLE) threshold concept defined by the ACER (Agency for the Cooperation of Energy Regulators) in the European context to provide a comprehensive understanding of its meaning, as well as the legal framework and standards for Europe, and Belgium.

> The Chapter is structured according to the following sections: Section 2.1 introduces the concepts of reliability and adequacy. Section 2.2 develops the LOLE formulation within the European context, and Section 2.3 details the legal framework and reliability standards in Belgium.

2.1 Introduction to reliability

Although this thesis is focused on adequacy assessments, let's take a step back and look at the general theory of reliability. The reliability of power systems is paramount for ensuring uninterrupted supply of electricity to consumers, industries, and critical infrastructure. Assuring high reliability is just the same as assuring a low risk level for a power system. Indeed, reliability and risk are just two equivalent concepts. The concept of risk incorporates the likelihood of an event, and its impact.

2.1.1 Deterministic vs. probabilistic approach

In the past, deterministic methods like percentage reserve in generation capacity planning or single contingency principle in transmission planning (N-1 criteria) [1] were used to assess the reliability of power systems. However, several changes have occurred since back then: the electrical demand has increased, interconnections have been multiplied, conventional energy sources have been replaced by RES, the energy market was liberalized leading to more trading, markets are coupled, demand-side participation has began, the aging of power system component is a reality, etc. These changes increase stress on the electrical grid [36]. At the same time, the power system is required to be as economical as possible, so the generating units run closer to their maximum capacities. Deterministic methods to assess reliability may not be sufficient nor up to date anymore, as they do not consider the probabilistic behavior which is much stronger today than before.

To make this possible, i.e. reduce costs while maximizing the power generated by the units, without increasing the risk of blackout, probabilistic reliability analysis are more than needed [36]. Unlike deterministic studies, probabilistic studies take into account the likelihood, and not only the impact of the different events.

2.1.2 Risk/Reliability evaluation method

Power system risk evaluation consists in four main steps [37]:

i) Define outage models for components of the system
ii) Select system states and their probability of occurrence
iii) Analyze system states and evaluate the potential consequences

[1] remaining elements in operation after the outage of a component in the system are capable of accommodating a new operational situation without violating operational security limits [35]

iv) Quantify the risk indices

Different functional zones, such as generation, transmission, and distribution systems are concerned by these risk assessment studies. Hierarchical level one (HL1) focuses on generation systems only, HL2 on both generation and transmission systems, and HL3 concerns all the functional zones. However, assessing the risk with HL3 is not feasible, because of computational time issues, and the minimum accuracy required. Usually, the HL3 indices are obtained by evaluating the risk of distribution systems separately and taking into account the HL2 indices [37].

2.1.3 Adequacy and Security

Depending on the type of system analysis (iii), risk assessments are divided in two categories: adequacy and security studies. Adequacy can be referred as the « existence of sufficient facilities (i.e. generation units, transmission and distribution systems), within the system to satisfy the consumers demand » [38]. These studies are usually conducted under steady-state conditions. Security is referred as the « ability of the system to respond to disturbances (events and faults) which can cause the loss of equipment and to the dynamic process occurring when the system transits from one state to another » [38]. These studies are performed under transient conditions.

When assessing the adequacy of a system over a period of time, each state is considered individually, and is determined adequate or inadequate. If an inadequate state occurs, i.e. load unsatisfied, violation of power system constraints on voltage/reactive power/-line loading, a remedial action is undertaken, such as a load shedding, or a re-dispatch. However, if this inadequate state generates a dynamic process which takes place faster than the remedial action, the system might find itself in an insecure situation. This example to illustrate that adequacy and security are interdependent, and that a state which is insecure or/and inadequate leads to unreliability [38].

2.1.4 Analytical and Simulation Methods

Analytical (e.g. probability convolution and state enumeration) or simulation (e.g. non-sequential and sequential Monte Carlo) methods can be used. The probability convolution combines the probability density function of the generation system and the load to evaluate mathematically the reliability of the power system. The state enumeration method enumerates all the possible states of the system and their probability of occurrence, and evaluates the reliability of each state to finally sum them with their respective weights to obtain a single value. The non-sequential Monte Carlo method builds a system state by drawing the status (e.g. available/unavailable) of each system component, then evaluates the reliability, and repeats the process to be able to evaluate the reliability with a certain confidence level. The sequential Monte Carlo method which is performed over a chronological time period builds a chronological system state timeserie by drawing the status (e.g. available/unavailable) duration of each system component, then evaluates the reliability for each state of the considered time period, and repeats the process to be able to evaluate the reliability over the time period with a certain confidence level.

Depending on the HL, and the complexity of the system, certain methods are preferred. On the one hand, analytical methods are fast and exact but are usually limited to small scale systems or HL1 studies. On the other hand, simulation methods are slower, and their accuracy depends on the number of iteration but they are preferred for complex systems and are suitable for HL2 studies.

2.1.5 The chosen approach: sequential Monte Carlo simulations

In our case, we want to assess the generation-transmission (HL2) adequacy of a rather complex power system (220/380 kV Belgian grid) composed of time-dependent features, i.e a high share of renewable energy sources, storage units, and flexibility mechanisms (load shifting). For this reason, we choose the sequential Monte Carlo approach. Indeed, this method allowing chronological behavior, is suitable for large systems, and is compatible with HL2 studies.

2.1.6 Probabilistic adequacy assessment metrics for generation-transmission systems

According to the reference book *Reliability Assessment of Electric Power Systems Using Monte Carlo methods* published by R. Bilinton and W. Li in 1994 [39], different reliability indices are used for each hierarchical level HL1, HL2, and HL3. These indicators are listed below. Two types of HL1 and HL2 indicators are developed in details, the ones relating to the number of hours concerned by loss of load, and the ones relating to the unsupplied demand corresponding to these hours.

1. HL1: Resource/Generation system adequacy

- Loss-Of-Load Expectation LOLE [hours/year][2]: is the most used indicator, and represents the number of hours which experience at least one loss of load.

$$LOLE = 8760 \sum_{i \in S} p_i$$

with p_i the probability of system state i and S the set of all systems states experiencing loss of load.

- Loss-Of-Energy Expectation LOEE [MWh/year]: quantifies the yearly unsupplied energy demand.

$$LOEE = 8760 \sum_{i \in S} C_i p_i$$

with C_i the loss of load [MW] for system state i.

- Other indicators are also referenced for HL1: i) the Loss-Of-Load Frequency LOLF [occurrence/year] which differs from LOLE as it considers the number of times per year the system experiences a loss of load independently from its duration, and ii) the loss-Of-Load Duration LOLD [hours/occurrence] which defines the average duration of a loss of load.

2. HL2: Generation-Transmission/Composite system adequacy

- Probability of Load Curtailment PLC [-]: represents the probability of the system to experience a loss of load.

$$PLC = \sum_{i \in S} p_i$$

- Expected Duration of Load Curtailment EDLC [hours/year] is similar to the LOLE definition in HL1. Of course, in this case, loss of load is not necessarily due to lack of generating capacity, but can also be due to a lack of transmission infrastructure.

$$EDLC = 8760 * PLC$$

- Expected Energy Not Supplied EENS [MWh/year] is similar to the LOEE definition in HL1.

$$EENS = 8760 \sum_{i \in S} C_i p_i$$

[2] It should be noted that in North America, they use the [days/year] system unit for LOLE. Care should be considered when changing from one to the other: a reliability standard of 1 day in 10 years cannot be interpreted as 24 hours in 10 years [40].

- Expected Demand Not Supplied EDNS [MW] represents the expected loss of load during an hour.

$$EDNS = \sum_{i \in S} C_i p_i = \frac{EENS}{8760}$$

- Bulk Power/Energy Curtailment Index BPECI [MWh/MW-year] represents the per-unit equivalent number of hours experiencing loss of load equal to the annual peak load.

$$BPECI = EENS/L$$

  with L the annual system peak load [MW].

- Modified Bulk Power Curtailment MBPCI [MW/MW] represents the equivalent per-unit average power loss during a loss of load of the annual peak demand.

$$MBPCI = \frac{EDNS}{L} = \frac{EENS}{8760 * L}$$

- Other indicators are also referenced for HL2: i) Expected Frequency of Load Curtailment EFLC [occurrence/year], ii) Average Duration of Load Curtailment ADLC [hours/disturbance], iii) Expected Load Curtailments ELC [MW/year] which sums the power of each loss of load independently of the duration of the latter, iv) Bulk Power Interruption Index BPII [MW/MW-year] which represents the equivalent per-unit interruption of the annual peak load, vi) Bulk Power-Supply Average MW Curtailment Index BPACI [MW/disturbance] which represents the average unsupplied power for each loss of load, vii) Severity Index SI [system minutes/year] which represents BPECI indicator in minutes.

3. HL3: Distribution systems
   The different indicators are listed below, but will not be commented in this work.

   - System Average Interruption Frequency Index SAIFI [interruptions/system customer/year], System Average Interruption Duration Index SAIDI [hour/ system customer/year], Customer Average Interruption Frequency Index CAIFI [interruptions/customer affected/year], Customer Average Interruption Duration Index CAIDI [hours/customer interruption], Average Service Availability Index ASAI [-], Average Service Unavailability Index ASUI [-], Energy Not Supplied ENS [kWh/year], Average Energy Not Supplied AENS [kWh/customer/year], Average Customer Curtailment Index ACCI [kWh/customer affected/year].

Firstly, it is interesting to insist on the difference between an hour experiencing loss of load, and an actual loss of load event (LOLEV) which can last less, or more than one hour which means that 2 loss of load events can occur during one hour: LOLEV > LOLE, or one LOLEV can last more than 1 hour: LOLEV < LOLE. Secondly, only HL2 has both absolute and relative indicators, making it possible for systems of different sizes comparison. Thirdly, the BPECI and MBPCI which represent a relative manner to express the EENS could be normalized differently. Variants of these indicators could use L to represent the yearly demand, or the average power demand for example, which could also make sense. Fourthly, some HL1 and H2 indicators are similar, but have different names: LOLE/EDLC, LOEE/EENS. In this work, for HL1 and HL2 studies, the following unique notation will be kept: LOLE and EENS. However, to identify the HL1 or HL2 context, it will always be mentioned if network constraints are considered.

2.2 Methodology for Establishing Reliability Standards in the European context

Due to the liberalization of electricity markets, the integration of intermittent RES, and the flexible usage of electricity grids, there is a strong need to have a clear evaluation of the security of supply for countries in the EU. The the Agency for the Cooperation of Energy Regulators (ACER) is willing to harmonize the LOLE standard for all EU countries. In accordance with Article 23(6) of Regulation (EU) 2019/943 of the European Parliament and of the Council of 5 June 2019 on the internal market for electricity, ACER has defined a methodology to calculate a reliability standard [41]. According to this reference, the LOLE threshold « reflects an economic optimization between the marginal cost of a new capacity resource (CONE[3]) or a renewal/prolongation (CORP[4]) where relevant, and the marginal reduction of energy-not-served cost». The following expression describes this minimization problem:

$$\text{minimize} \overbrace{\sum_{t\in\mathcal{T}} \left(\Delta t \cdot \Gamma_t(Q)\right)}^{\text{energy-not-served cost}} + \overbrace{\sum_{t\in\mathcal{T}} \left(\Delta t \cdot C_t^{op,var}(Q)\right)}^{\text{operation cost}} + \overbrace{C^{inv,fixed}(Q)}^{\text{investment cost}} \tag{2.1}$$

[3]CONE: Cost Of New Entry
[4]CORP: Cost Of Renewal/Prolongation

where t represents a time step, $\mathcal{T}$ the time period set considered, Δt the duration of a time step [hours], Q the installed capacity of resources [MW] in the power system, Γ_t the cost [€/h] due to the energy not served at time step t, $C_t^{op,var}$ the operational costs [€/h] of capacities at time step t, $C_t^{inv,fixed}$ the investment costs [€] of the capacities. The variable of decision in this minimization formulation is Q, the installed capacity. If we derive this expression with respect to Q:

$$\sum_{t\in\mathcal{T}^S} \Delta t \left(\overbrace{\frac{d\Gamma_t(Q)}{dQ}}^{a} + \overbrace{\frac{dC_t^{op,var}(Q)}{dQ}}^{b} \right) + \sum_{t\in\mathcal{T}^{NS}} \Delta t \left(\overbrace{\frac{d\Gamma_t(Q)}{dQ}}^{c} + \overbrace{\frac{dC_t^{op,var}(Q)}{dQ}}^{d} \right)$$
$$+ \underbrace{\frac{dC^{inv,fixed}(Q)}{dQ}}_{e} = 0 \tag{2.2}$$

where $\mathcal{T}^S$ the scarcity time period set consisting in the hours where energy is not served, and $\mathcal{T}^{NS}$ the non-scarcity time period set consisting in the hours where no scarcity is observed. Term a expresses the variation of cost due to energy-not-served when varying the installed capacity Q. If 1 MW of additional capacity is installed, the energy not served will decrease from 1 MWh in scarcity period, and thus the cost will be reduced by VOLL, the value-of-lost-load [€/MWh], so term a is equivalent to $-VOLL$. Term b expresses the variation in operational costs when adding 1 MW of installed capacity during scarcity period, and is equivalent to $CONE^{var}$, the variable cost of new entry [€/MWh]. Term c is zero as energy not-served does not occur in non-scarcity periods. Term d expresses the variation in operational costs when adding 1 MW of installed capacity during non-scarcity period. This term should be zero if the additional capacity is located at the end of the merit of order, and negative if located within the merit of order. This term will be denoted $-z$ for sake of clarity. Term e expresses the variation in investment costs when adding 1 MW of installed capacity, which is equivalent to the $CONE^{fixed}$, the fixed cost of new entry [€/MW]. This leads to the following expression:

$$\overbrace{\sum_{t\in\mathcal{T}^S}}^{f} \Delta t\,(-VOLL + CONE^{var}) \overbrace{-z}^{g} + CONE^{fixed} = 0 \tag{2.3}$$

In this expression, term f is equivalent to the optimal number of loss-of-load LOL^* [hours], set at the loss-of-load expectation threshold. Term g is a complex term $z \in \mathbb{R}^+$ that can as previously said be neglected in some cases. Rearranging expression 2.3, finally gives an expression for $LOLE_{threshold}$ which depends on $CONE^{var}$, $CONE^{fixed}$, and $VOLL$, and in some cases on z:

$$
\begin{aligned}
& LOL^*(-VOLL + CONE^{var}) - z + CONE^{fixed} = 0 \\
\leftrightarrow \quad & LOLE_{threshold} = LOL^* = \frac{CONE^{fixed} - z}{VOLL - CONE^{var}}
\end{aligned} \tag{2.4}
$$

The calculation of VOLL and CONE are described in details in [41]. VOLL is calculated by «evaluating for different inadequacy situations, the maximum electricity price that customers are willing to pay to avoid a supply interruption in situations where capacity resources are insufficient to meet the demand» [41], and is achieved with surveys. The CONEs are calculated for each reference technology with technical specifications. Using this methodology for Belgium's existing grid results in a reliability standard of 3 hours [42]. The following sections (2.2.1 and 2.2.2) summarize the methodology used to calculate these values for Belgium.

2.2.1 Evaluation of the CONE

The variable and fixed CONE are calculated following the methodologies developed by ACER [41] for each reference technology able to enhance resource adequacy. These technologies can include generation capacities, storage facilities, and demand side response. A technology is defined as a reference technology if two criteria are satisfied:

1. the technology is standard: reliable and generic data concerning the costs are available, the construction costs from one project to another are of the same order of magnitude, and the development of the technology is not limited by technical constraints.
2. the technology has a potential for new entry: the technology has been developed, is in process of development, or is planned for development and future developments are allowed.

The fixed CONE for each reference technology is defined as:

$$CONE_{fixed,RT} = \frac{EAC_{RT}}{K_{d,RT}} \tag{2.5}$$

with $K_{d,RT}$ the derating factor, and EAC_{RT} the equivalent annual cost of the reference technology[5].

The derating factor K_d is defined as the ratio between a technology's average contribution during near scarcity hours and its reference power. This factor [%] defines the contribution to security of supply of each technology. Technologies can be divided into 5 categories: i) thermal TSO-connected, ii) weather dependent technologies, iii) energy-limited technologies, iv) DSO-connected technologies, and v) interconnections with external regions. Derating factors are calculated based on input data from a given scenario, and the results of an adequacy assessment (analysis of near-scarcity periods) except for thermal TSO-connected. More information on its calculation can be found in [43].
The variable CONE for each reference technology includes the costs related to the fuel consumption, to the CO_2 emission costs, and other variable OPEX costs such as consumable materials, by-products handling, variable operation and maintenance costs [41].

In Belgium, the Direction Générale (DG) de l'Énergie from the FPS Economy [6] has been designated as the competent authority to evaluate the Cost of New Entry (CONE). Based on the criteria mentioned above, the selected reference technologies are : open cycle gas turbine (OCGT), combine cycle gas turbine (CCGT), gas internal combustion (IC) engines, combined heat and power (CHP) units, photovoltaic (PV), wind onshore, wind offshore, battery storage, demand side response (DSR). Their variable and fixed CONE are summarized in Table 2.1.

[5] The EAC can be calculated with the following equation:

$$EAC_{RT} = \left(\sum_{i=1}^{X} \frac{CC(i)}{(1+WACC)^i} + \sum_{i=X+1}^{X+Y} \frac{AFC(i)}{(1+WACC)^i} \right) \frac{WACC(1+WACC)^{X+Y}}{(1+WACC)^Y - 1} \tag{2.6}$$

with

- X: period of construction [years]
- Y: economical lifetime [years]
- i: each year during the period of construction and the economical lifetime (X+Y)
- CC(i): estimation of investment costs during the construction period X [€/MW/year]
- AFC(i): estimation of fixed annual costs during economical lifetime Y [€/MW/year]
- WACC : estimation of the weighted average cost of capital [-]

[6] The Direction Générale de l'Energie is the energy department of the Federal Public Service in charge of the economy in Belgium. This service is inter alia responsible for the security of supply of the country.

Table 2.1: Data related to the cost of new entry for each reference technology in Belgium: equivalent annual cost EAC, derating factor K_d, fixed CONE $CONE_{fixed,RT}$, and variable CONE $CONE_{var,RT}$ [44].

Reference technology	EAC [€/MW/year]	Kd [-]	$\mathbf{CONE_{fixed,RT}}$ [€/MW/y]	$\mathbf{CONE_{var,RT}}$ [€/MWh]
Open cycle gas turbine (OCGT)	60 700	0.91	67 000	80
Combine cycle gas turbine (CCGT)	88 400	0.92	96 000	49.8
Internal combustion engines (IC engines) - Gas	60 300	0.65	93 000	93.9
CHP	141 400	0.93	152 000	53.1
Photovoltaic (PV)	88 200	0.01	8 823 000	0
Wind onshore	163 300	0.09	1 814 000	0
Wind offshore	360 600	0.13	2 774 000	0
Battery storage	43 300	0.31	140 000	N/A
Demand Side Response (DSR)	20 000	0.66	30 000	736.7

Below, some examples of technologies that cannot be considered as reference technologies in Belgium:

- Nuclear power plants have no potential for new entry because of the Act of January 31, 2003 on the phasing out of nuclear power for industrial electricity generation purposes (amended on 26 April 2024).
- Coal-fired power plants are considered as a non-reasonable option and not to have any potential for new entry because of Belgian and European climate objectives.
- Hydro power and pumped-hydro storage are considered to have no potential for new entry because their potential is very limited in Belgium.
- Waste incineration are not considered as standard. The costs of this technology are high, and the energy production of these plants is a byproduct and their main purpose is waste management.

Finally, a unique reference technology has to be chosen to determine the $LOLE_{threshld}$. The selected technology should be the most economical in terms of fixed costs. For Belgium, after several discussions, DSR is finally chosen with $CONE_{fixed} = 30000$ [€/MW/year] and $CONE_{var} = 736.7$ [€/MWh] [45].

2.2.2 Evaluation of the VOLL

The process of finding a value for the lost-load (VOLL) aims at defining the economic and societal cost due to an electricity outage.

Because the evaluation of the VOLL is imperfect - consumers mis-evaluate their dependency on electricity, this evaluation is dependent on many factors such as the duration of the outage and whether a notification is sent in advance, and several methodologies are proposed by ACER and can lead to different results - the results of the VOLL evaluation must be carefully analyzed with criticism. Countries remain free to fix their own security of supply [46].

The most recent evaluation of the Belgian VOLL was conducted in 2022. The *Direction Generale de l'Energie* and the *Bureau Fédéral du Plan* have launched a public tender to conduct a consumer survey to estimate the VOLL, which was won by SIA Partner. They have calculated the VOLL to be 12 832.48 [€/MWh] [47].

The VOLL represents the economic and societal cost of not having electricity for consumers, both residential and industrial. The amount of 12 832.48 €/MWh can seem very high, and let's see who drives this cost among the participants of the survey.

The survey is addressed to households (B2C), and companies (B2B), and tries to evaluate i) their willingness-to-pay (WTP), which is the maximum amount they are ready to pay to avoid an electricity interruption, ii) their willingness-to-accept (WTA), which is the minimum amount they are ready to accept as compensation to undergo an electricity shortage, iii) their DC (direct cost), which is the overall real cost the B2B consumer will incur due to an electricity shortage.

To do so, 1000 households (B2C), and 200 companies (B2B) have been solicited to answer the survey concerning a potential 1-hour loss load (noticed 24 hours in advance) occurring during a cold winter day at 10:30 for companies, and at 18:00 for households. Combining these WTP/WTA/DC with the actual loss load at that time, a VOLL can be found:

$$VOLL = \frac{\text{cost}}{\text{loss-load}}$$

where the cost [€] can be a weighted sum of the WTP, WTA, and DC, and the loss-load is the electrical quantity [kWh] that it not served to the consumer.

The statistics of the collected and filled survey of B2C and B2B consumers concerning WTP, WTA, and DC are summarized in Table 2.2, and 2.3 respectively.

Table 2.2: Statistics of the WTP and WTA for B2C consumers.

B2C	WTP [€]	WTA [€]
mean	3.32	8.42
std	10.27	18.96
min	0	0
25%	0	0
50%	0	1
75%	3	10
max	100	100

Table 2.3: Statistics of the WTP, WTA, and DC for B2B consumers.

B2B	WTP [€]	WTA [€]	DC [€]
mean	812.75	3661	5290
std	5579.98	30676.61	34328.89
min	0	0	0
25%	1	1	54
50%	10	12	170
75%	70	80	500
max	50000	300000	335000

To calculate a single VOLL value, it has been assumed that i) only WTP was considered, and that ii) the B2C consumers would account for 40% and B2B for 60%. Firstly, thanks to the average loss load and WTP for each consumer type (B2C and B2B), a B2B and B2C VOLL are calculated and are displayed in Table 2.4. Secondly, by considering the respective weights of the B2C and B2B consumers, the single VOLL = 0.4*3506.9 + 0.6*19049.5 = 12.832,5 €

Table 2.4: WTP, Lost Load, and VOLL of different consumers category.

	WTP [€]	Lost Load [kWh]	VOLL [€/MWh]
B2C	3.32	0.95	3506.9
B2B	812.8	42.67	19049.5

It should be noted that it is a difficult task to evaluate WTP, WTA, and DC. Taking the WTP value for the VOLL calculation is pulling the value to lower bounds (WTA, and DC have higher values). It is mainly the B2B consumers that drive the high VOLL value.

2.3 Reliability Standards

2.3.1 Legislation and reliability standards in Belgium

This section has been written taking into account the legislation in application on today's date, 4th July 2024.

Article 7 undecies, §7 [48] of the Law on the organization of the electricity market mentions among other things that:

- The Direction Générale de l'Energie of the FPS Economy, in collaboration with the Bureau fédéral du Plan and the regulator (CREG [7]), is designated as the competent authority to draw up the single estimate of the cost of non-distributed energy (VOLL), as referred to in Article 11 of Regulation (EU) 2019/943, and has to be approved by the King.
- The Direction Générale de l'Energie of the FPS Economy is designated to determine the cost that a new entrant (CONE), referred to in Article 23, paragraph 6, of Regulation (EU) 2019/943 and has to be approved by the King.
- Based on the VOLL and CONE evaluation, the regulator (CREG) proposes a reliability standard based on the method referred to in Article 23(6) of Regulation (EU) no. 2019/943.
- The Direction Générale de l'Energie of the FPS economy and the grid operator (Elia) give their opinion on this proposal.
- The King determines the reliability standard.

Based on this law, the following events have occurred:

- The Direction Générale de l'Energie calculated a VOLL of 12 832.48 €/MWh [47].
- The Direction Générale de l'Energie of the FPS Economy proposed a variable and fixed CONE for each reference technology and recommends to use the variable and fixed CONE associated to the demand side reponse (DSR) technology (736.73 €/MWh, and 30 000 €/MW/year respectively) to calculate the reliability standards [44].
- Based on these estimation, the regulator (CREG) proposes a reliability standard but takes the open cycle gas turbine (OCGT) as reference technology (and not the DSR as recommended by the Direction Générale de l'Energie). This leads to a $LOLE_{threshold}$ [8] = 5.254 [hours/year] = 5 h 15 min per year [49].

[7] The CREG is the Commission for Electricity and Gas Regulation.

[8] $CONE_{var,OCGT}$ = 80 €/MWh and $CONE_{fixed,OCGT}$ = 67 000 €/MW/year

- On the one hand, Elia thinks the reference technology should be DSR, and thus the $\text{LOLE}_{\text{threshold}}$ = 2.48 [hours/year] = 2h29min per year [50]. On the other hand, the Direction Générale de l'Energie states the reliability standard should be set to 3 hours partly because they approve Elia's opinion, but also because they think it is not desirable to relax this reliability standard (previously set to 3 hours) [51].

Finally, the royal decree sets reliability standard to 3 hours [42].

2.3.2 Adequacy Evaluation for Belgian Network

In Belgium, Elia is responsible in making the adequacy studies for the Belgian grid. They use an existing tool named Antares Simualator [52], which is developed and maintained by RTE (French TSO).

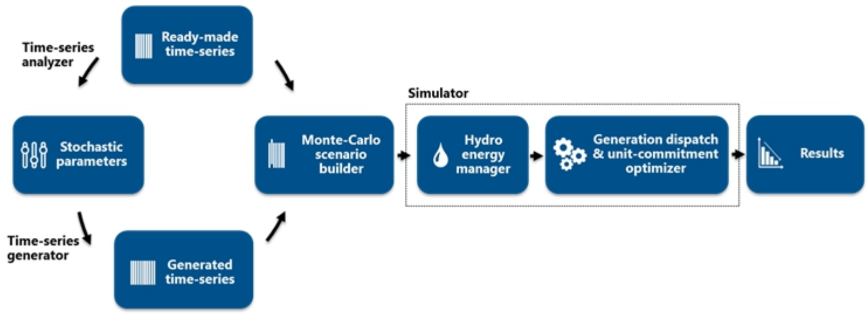

Figure 2.1: Schematic representation of Antares Simulator tool [52] by Antares.

Its functioning is illustrated in Fig. 2.1. From historical time series, synthetic ones can be generated. Firstly, a time-series analyzer extracts the intrinsic characteristics of their stochastic behavior (daily and yearly seasonalities, probability density functions, autocorrelation functions, and spatial correlations). Secondly, from these statistical characteristics, synthetic ones can be generated. Antares considers 5 stochastic inputs under the form of time series: the availability of thermal power plants, load, wind and solar power capacity factors, and hydraulic inflows. Finally, the Monte Carlo scenario builder groups all these generated time series to form a random Monte Carlo year scenario.

Once the Monte Carlo year scenario is built, the simulator is operated. Antares optimizes the unit-commitment economic dispatch formulation with an hourly resolution.

The optimization has a weekly horizon, and is thus performed on each week of the year sequentially. However, hydro reservoirs need to be managed on a longer horizon than a week. For this reason, a coupling between weeks has to be done to model correctly the reservoir's state-of-charge for example. Once this is done, the unit commitment economic dispatch formulation is optimized. This is repeated for each week of the year.

Hourly and yearly operational (unit-commitment and generation level of each unit, flow through each line) and adequacy (loss-of-load duration, energy-not-served) results are the output of the model. This simulator is repeated for each Monte Carlo year scenario which then gives, expected values (average) of our indicators of interest, and permits a probabilistic analysis.

2.3.3 Adequacy Evaluation for European Network

Similar studies are also performed at the European level by ENTSOE. The European Network of Transmission System Operators for Electricity (ENTSO-E) is the association for the cooperation of the European TSOs. It represents 36 countries (40-member TSOs), and together they form the largest interconnected electrical grid in the world. All TSOs member are responsible for ensuring a secure and coordinated operation of the European grid. Its creation in 2009 has the objective to promote a harmonized, efficient, and secured grid management in the context of an integrated European energy market. It delivers pan-European outlooks of the power system in the short, mid, and long term. Based on future scenarios, ENTSO-E performs i) long term studies, named *Ten-Year Network Development Plan* (TYNDP) which define the needs in terms of infrastructure for 2030, 2040, and 2050, ii) midterm studies, named *European Resource Adequacy Assessment* (ERAA) which study the probabilistic adequacy of the European power system for the 10 years ahead, and iii) short-term studies, *Summer and Winter Outlooks*, where they identify critical periods for the security of supply due to extreme weather conditions.

These studies are reviewed by ACER (Agency for the Cooperation of Energy Regulators) and they give their approval or amendment. Concerning the ERAA 2023 study, ACER identified improvements to brought into the 2024 study like *applying a more robust approach to model investment decisions, using flow-based capacity calculation to model cross-border electricity flows to reflect trade opportunities, and fine-tune the modeling of investor's risk aversion via hurdle rates and applying current market* *rules* [53].

CHAPTER 3

Power-to-Hydrogen models in Adequacy Studies

Chapter overview

- Two Power-to-Hydrogen (P2H) models (non-linear and linear) describing the steady-state behavior of a large-scale electrolyzer are developed.
- They are then integrated into a simple adequacy computation tool: an economic dispatch looped into a sequential Monte Carlo process.
- The application is illustrated on a simplified study case representative of the Belgian power system, and both electrolyzer models will be compared.

This chapter is a modified and extended version of the peer-reviewed conference paper:
A. Hernandez, F. Vallée and E. De Jaeger, "Integration of Power-to-Hydrogen Models in Power Systems Adequacy Assessments," 2022 17th International Conference on Probabilistic Methods Applied to Power Systems (PMAPS), Manchester, United Kingdom, 2022, pp. 1-6, doi: 10.1109/PMAPS53380.2022.9810562.

While Chapter 1 underlines the significant role hydrogen might play in the future, and the importance of adequacy studies, a first step is to decide how these power-to-hydrogen, i.e. electrolyzers will be modeled in these studies. In this Chapter, two Power-to-Hydrogen (P2H) models (non-linear and linear) describing the steady-state behavior of large-scale electrolyzer are developed.The first P2H model which describes the relation between the hydrogen production and the electrical power consumption is non-linear. As non-linear models require higher computational time, a second P2H model which is a linear interpolation approximating the response of the non-linear model is elaborated to speed up the calculations. Both models are integrated into an economic dispatch and the effective performance of the linear approximation is assessed through a comparison of the results, and the computational time. Then, several scenarios defined by different annual quantities of hydrogen demand and different hourly profiles combinations will be tested on the Belgian power system. This allows to assess the impact of hydrogen production through electrolyzers on the adequacy of power systems.

> The Chapter is structured according to the following sections: Section 3.1 outlines the generic P2H model and its linearized counterpart is developed in Section 3.2. Section 3.3 details the hydrogen demand profiles that are integrated into the case study. Section 3.4 resumes the sequential Monte Carlo process used to assess the power system adequacy. Section 3.5 describes the case study which is representative of the Belgian power system. Section 3.6 compares both models and analyses the results of the different scenarios. Section 3.7 concludes the study.

3.1 Power-to-Hydrogen Model

The P2H conversion chain is composed of a rectifier, a buck converter and an electrolyzer stack. The rectifier transforms the AC voltage from the grid into a DC voltage, and the buck converter is used to control the voltage given to the electrolyzers terminal to adapt the production of hydrogen. Indeed, electrolyzers need to be fed by a DC-voltage source, and the current flowing through them determines the quantity of hydrogen produced. In this work, the power electronics are considered ideal and have an efficiency of 1, i.e the P2H conversion chain model represents mainly the electrolyzer stack.

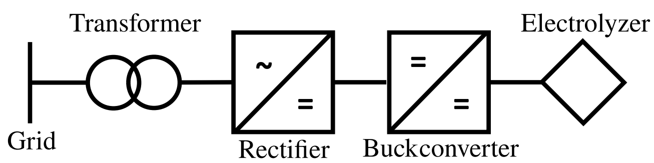

Figure 3.1: Conversion chain of electrolyzer.

3.1.1 Electrolyzer technologies

Electrolyzers use electricity to split the water molecule H_2O into hydrogen and oxygen. For the time being, only Alkaline and Polymer Electrolyte Membrane (PEM) electrolyzers are commercially available. Though the Alkaline technology is the most mature, PEM electrolyzers are the most promising for future applications and still can be improved in terms of current density, dynamics and efficiency unlike the Alkaline technology that has reached its maximum performances [54]. For these reasons, PEM electrolyzers are considered in this study.

3.1.2 Voltage of electrolysis cell

The energy required to initiate the electrolysis, $\Delta H = \Delta G + T\Delta S$ does not have to be entirely supplied by electrical energy. Since entropy ΔS increases in this process of dissociation, part of the energy of reaction can be brought from the environment at a certain temperature T. The amount of energy that has to be brought under the form of electricity is the Gibbs free energy ΔG. The electrical contribution is supplied to the PEM cell under the form of an electrical potential, also called the reversible voltage :

$$V_{rev} = \frac{\Delta G}{zF} \tag{3.1}$$

where $z = 2$ is the number of electrons transferred during the reaction and $F = q_e N_A = 96485.3$ [C] the Faraday's constant.

However, in practice, the electrical potential is higher than the reversible voltage because of thermodynamic irreversibilities. Indeed, when current flows through the cell, losses of different nature appear.

- *Ohmic losses* represent the resistance of the electrodes and cell components to the electron flux and the resistance of the membrane to the ion flux [54].
- *Mass transport losses* represent the limited supply of reactant water to the process and the reduction of catalyst utilisation due to diffusion and bubbles phenomena respectively [54].
- *Activation losses* represent the electrochemical kinetics of the half reactions at the cathode and anode, i.e. the energy required to transfer the electrical charge between chemical species and electrodes [54].

3.1.3 Equivalent electrical circuit (EEC) of large-scale PEM electrolyzer

When dealing with large-scale electrolyzers, some assumptions can be made regarding the losses. In Ayivor's work [55], the following assumptions are made relying on [54]:

- Mass transfer losses are not significant for low and moderate current densities and can be neglected up to 3 A/cm²,
- Activation losses are especially dominant at low current densities,
- Ohmic losses becomes dominant at mid current densities.

The resulting simplified electrical equivalent circuit (EEC) of a large-scale PEM cell in steady-state conditions is illustrated in Fig. 3.2a.

(a) Electrolyzer cell.

(b) Electrolyzer stack.

Figure 3.2: Simplified equivalent electrical circuits

An electrolyzer stack is formed by the connection in series of n electrolysis cells. Thus the EEC of a PEM stack can be modelled by an equivalent reversible voltage $n * V_{rev}$ and a total membrane resistance of $n * R_m$ (see Fig. 3.2b). The mathematical relation between the electrical power injected in the stack and the hydrogen production is developed hereunder.

Stack current

The hydrogen production rate of a cell $m_{H_2,cell}$ is proportional to the current thanks to the derivative with respect to time of the Faraday equation (3.2). Since the cells are in series, the stack production rate m_{H_2} is n times the cell production rate as shown in (3.3) and the current I can thus be expressed in function of the stack production rate.

$$m_{H_2,cell} = \frac{I}{F}\frac{M}{z} \quad \text{[g/s]} \tag{3.2}$$

$$m_{H_2} = n\frac{I}{F}\frac{M}{z} \quad \text{[g/s]} \leftrightarrow I = m_{H_2}\frac{zF}{nM} \quad \text{[A]} \tag{3.3}$$

where M= 2.016 [g/mol] is the molar mass of H_2.

Stack power

The mathematical expression of the stack power depends on the EEC that is used to model the electrolyzer stack. When referring to the equivalent circuit of the electrolyzer stack in Fig. 3.2b, the relation between the stack current and the electrical power can be defined as :

$$\begin{aligned} P_{stack} &= V_{stack} I = (nR_m I + nV_{ocv}) I \\ &= nR_m I^2 + nV_{ocv} I \\ &= R_{m,stack} I^2 + V_{ocv,stack} I \end{aligned} \tag{3.4}$$

with $R_{m,stack}$ referring to the total membrane resistance of the electrolyzer stack, and V_{ocv} the open-circuit voltage of the electrolyzer stack.

Stack power and H_2 production

With (3.3) and (3.4), the relation between the H_2 production and the stack power is derived in (3.5) where the power is expressed in function of the hydrogen production, and vice versa in (3.6).

$$P_{stack} = R_{m,stack} (m_{H_2} \frac{zF}{nM})^2 + V_{ocv,stack} (m_{H_2} \frac{zF}{nM}) \tag{3.5}$$

$$\leftrightarrow m_{H_2} = \frac{1}{2R_{m,stack}} \frac{nM}{zF} \left(- V_{ocv,stack} + \sqrt{V_{ocv,stack}^2 + 4R_{m,stack} P_{stack}} \right) \tag{3.6}$$

3.1.4 Characteristics of the PEM electrolyzer

The characteristics of the PEM electrolyzer used in this study come from Ayivor's work [56] and are referenced in Table 3.1.The relation between electrical power and hydrogen production of the EEC model expressed in (3.5) is represented in Fig. 3.3 (black line). This electrolyzer unit can produce up to 20.65 [kg/h] at its nominal power of 1 MW.

Table 3.1: Characteristics of the PEM electrolyzer stack from [56].

P_{nom}	J_{nom}	$V_{ocv,stack}$	P_{min}	$R_{m,stack}$
1 MW	3 A/cm^2	145 V	0.26 MW	0.015 Ω

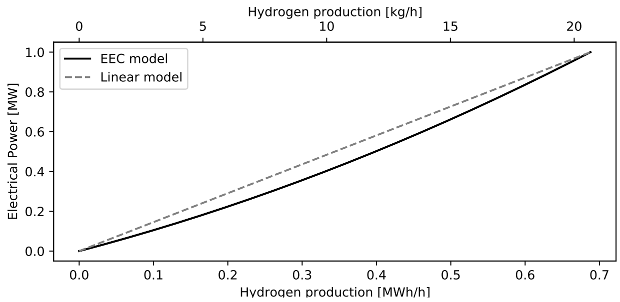

Figure 3.3: Relation between electrical power and hydrogen production of the electrolyzer stack.

The EEC model is quadratic but rather close to linear. It could thus be interesting to establish a linearization of the mathematical relationship and compare both models in the context of adequacy studies.

3.2 Linear Interpolation Model

The mathematical relation of the non-linear EEC model is linearized with the following constraints to guarantee physical consistency:

- No hydrogen is produced when no power is consumed which constrains the linear function to be affine.
- The hydrogen production at the nominal power of 1 MW is maximum and has a value of 20.65 kg/h.

Indeed, we expect the linear model to replicate the exact behavior of the EEC model when not working, or in nominal conditions. This amounts to an interpolation of the quadratic EEC model through the points (0,0) and ($m_{H_2,max}$, P_{nom}). The linearized relation for a large-scale PEM electrolyzer can thus be expressed as:

$$P_{stack} = \frac{P_{nom}}{m_{H_2,max}} \, m_{H_2} \quad [MW] \tag{3.7}$$

Thus, the linear interpolation model of the electrolyzer used in this study is expressed as:

$$P_{stack} = \frac{P_{nom}}{m_{H_2,max}} \, m_{H_2} = \frac{1[MW_{el}]}{20.65[kg_{H_2}/h]} \, m_{H_2} = 48.48[MWh_{el}/ton_{H_2}] \, m_{H_2} \tag{3.8}$$

$$\leftrightarrow m_{H_2} = \frac{m_{H_2,max}}{P_{nom}} P_{stack} = 20.65[kg_{H_2}/MWh_{el}] P_{stack} \tag{3.9}$$

and is represented in Fig. 3.3 (dashed gray line).

One of the many advantages of a linear model, is that electrolyzers can be aggregated together and considered as an equivalent electrolyzer. Indeed, the relation stays linear, unlike with the quadratic EEC model, electrolyzers have to be considered individually and cannot be aggregated together because the relation becomes discrete.

3.3 Hydrogen Demand Profile

In this work, the integration of a hydrogen demand is implemented. In order to distribute an annual hydrogen demand E_{H_2} among the 8760 hours of the year, different hourly profiles will be tested and compared. Firstly the hourly hydrogen demand will be fixed following a day-time, round-the-clock, and wind-correlated profile. Secondly, the annual hydrogen demand will be distributed in an optimal way.

3.3.1 Fixed Profiles

1. Day-time Profile: The annual demand E_{H_2} is divided equally through the days of the year, then an hourly factor distribution f_h (represented by the black line in Fig. 3.4) is applied:

$$E_{H_2,h} = f_h * \frac{E_{H_2}}{365} \quad [MWh] \tag{3.10}$$

2. Round-the-Clock Profile: E_{H_2} is uniformly distributed among the 8760 hours of the year (see gray line in Fig. 3.4):

$$E_{H_2,h} = \frac{1}{24} * \frac{E_{H_2}}{365} \quad [MWh] \tag{3.11}$$

3. Wind-correlated Profile: The hourly distribution is different for each day of the year and is correlated to the hourly offshore wind power load factor lf_h:

$$E_{H_2,h} = \frac{lf_h}{\sum_{h=1}^{8760} lf_h} * E_{H_2} \quad [MWh] \tag{3.12}$$

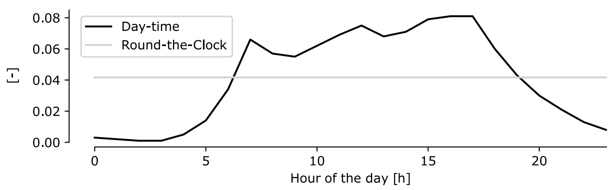

Figure 3.4: Hourly distribution during the day of the day-time profile.

3.3.2 Flexible Profile

The annual hydrogen demand is distributed in an optimal way among the hours of the year. The total hourly production of the 8760 hours of the year will have to equal the annual hydrogen demand.

3.4 Adequacy Tool

An economic dispatch neglecting network constraints is used to assess the adequacy of the power system and this optimization problem is looped into a sequential Monte Carlo (MC) process which samples the outages duration time of the generators. Also, for every new MC year, another wind power profile is generated. The electrical and hydrogen demands are fixed inputs and do not vary from one year to another. This process is depicted in Fig. 3.5.

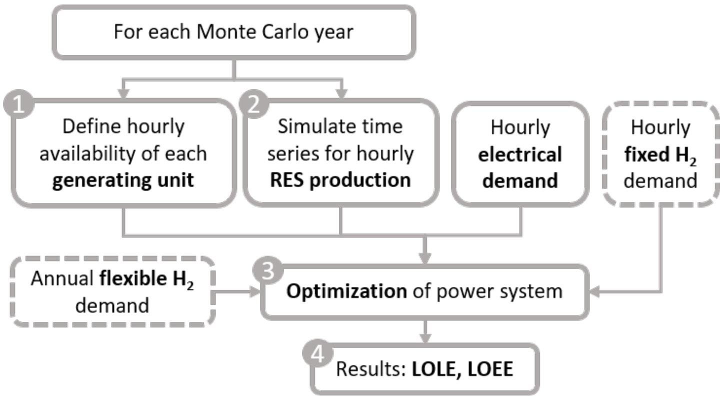

Figure 3.5: Adequacy calculation scheme.

3.4.1 Conventional Generating Units

The availability of the conventional generating units is represented using a two-state model. For each Monte Carlo year, the yearly availability profile of each unit is determined by a random sample draw from the time-to-failure TTF and time-to-repair TTR distributions. TTF and TTR have negative exponential distributions

3.4.2 Wind Power Time series

For each Monte Carlo year, an hourly profile is generated thanks to an auto-regressive and moving average (ARMA) model which is built based on historical data. ARMA models are used to analyze and generate stationary stochastic time series using autoregression and moving average with a polynomial.

3.4.3 Economic Dispatch

The power system optimization consists in a linear optimization representing an economic dispatch problem. It is used to determine the most cost-effective way to operate the system while minimizing load shedding, i.e. dispatch electricity production and storage among the generating and storage units respectively to meet the electricity demand at lower cost and avoid load shedding while considering the operational and technical constraints.

The objective function in (3.13) minimizes the operational costs of generators, and the energy-not-served for both electrical and hydrogen demands, (3.14) represents the electrical balance at each hour, (3.15) and (3.16) limit the power of the conventional units and electrolyzers respectively, (3.17) constrains the energy-not-served for consistency, (3.18)-(3.22) concern the PHS constraints, (3.23) represents the hydrogen balance at each hour, (3.24) defines the flexibility of the hydrogen production, and (3.25) constrains the hydrogen-not-served for consistency.

$$\text{Min} \sum_{t=1}^{8760} \sum_{g=1}^{n_g} c(g) * P(g,t) + voll * Ens(t) + voll_{H_2} * Ens_{H_2}(t) \tag{3.13}$$

subject to :

$$\sum_{g=1}^{n_g} P(g,t) + res(t) + Ens(t) + P_{phs,out}(t) - P_{phs,in}(t)$$
$$= l(t) + C(t) + \left(1 + c_c\right) \sum_{e=1}^{n_e} P_{el}(t) \qquad \forall t \tag{3.14}$$

$$P(g,t) \leq \alpha(g,t) * p_{max}(g) \qquad \forall t, \forall g \tag{3.15}$$

$$P_{el}(e,t) \leq p_{el,max}(e) \qquad \forall t, \forall e \tag{3.16}$$

$$Ens(t) \leq l(t) + (1 + c_c) \sum_{e=1}^{n_e} P_{el}(t) \qquad \forall t \tag{3.17}$$

$$P_{phs,out}(t=1) = 0 \qquad \forall t \tag{3.18}$$

$$Soc_{phs}(t=1) = \eta_{pump} P_{phs,in}(t=1) \qquad \forall t \tag{3.19}$$

$$Soc_{phs}(t) = Soc_{phs}(t-1) + \eta_{pump} P_{phs,in}(t) - \frac{P_{phs,out}(t)}{\eta_{turb}} \quad \forall t > 1 \qquad \forall t \tag{3.20}$$

$$P_{phs,in/out}(t) \leq p_{phs,max} \qquad \forall t \tag{3.21}$$

$$Soc_{phs}(t) \leq soc_{phs,max} \qquad \forall t \tag{3.22}$$

$$\sum_{e=1}^{n_e} q_{el}(P_{el}(e,t)) + Ens_{H_2}(t) = l_{H_2,fixed}(t) + Q_{H_2,flex}(t) \qquad \forall t \tag{3.23}$$

$$\sum_{t=1}^{8760} Q_{H_2,flex}(t) = l_{H_2,flex,year} \qquad \forall t \tag{3.24}$$

$$Ens_{H_2}(t) \leq l_{H_2,fixed}(t) + Q_{H_2,flex}(t) \qquad \forall t \tag{3.25}$$

with $P(g,t)$ the hourly production [MWh/h] of generator g, $Ens(t)$ the hourly energy-not-served [MWh/h], $P_{phs,out}(t)$ and $P_{phs,in}(t)$ the hourly energy [MWh/h] output and input of the pumped hydro storage (PHS), $Soc_{phs}(t)$ the hourly state-of-charge

[MWh] of the PHS, $C(t)$ the hourly curtailed energy [MWh/h], $P_{el}(e,t)$ the hourly consumption [MWh/h] of electrolyzer e, $Q_{H_2,flex}(t)$ the hourly flexible hydrogen production [MWh$_{H_2}$/h], and $Ens_{H_2}(t)$ the hourly hydrogen-not-served [MWh$_{H_2}$/h], being the variables of the formulation and n_g the number of generators, n_e the number of electrolyzers, $c(g)$ the cost [€/MWh] of generator g, $voll$ the value of loss load [€/MWh], $voll_{H_2}$ the value of H_2 loss-load [€/MWh$_{H_2}$], $\alpha(g,t) \in \{0,1\}$ the hourly availability of generator g, $p_{max}(g)$ the maximum capacity [MW] of generator g, $res(t)$ the hourly renewable power [MWh/h], $l(t)$ the hourly load [MWh/h], c_c the hydrogen compression factor, $q_{H_2,fixed}(t)$ the hourly fixed hydrogen production [MWh$_{H_2}$/h], $q_{H_2,flex,year}$ the annual flexible hydrogen demand [MWh$_{H_2}$/year], η_{pump} and η_{turb} the efficiencies of the PHS pump and turbine respectively, and $soc_{phs,max}$ the maximum capacity [MWh] of the PHS, being the parameters of the formulation.

3.4.4 Adequacy metrics

From the economic dispatch, the loss-of-load (LOL) and energy-not-served (ENS) of MC year y can be extracted .

$$LOL_y = \sum_{t=1}^{8760} c_t \tag{3.26}$$

$$ENS_y = \sum_{t=1}^{8760} Ens(t) \tag{3.27}$$

with c_t a boolean variable that equals 1 if load is curtailed at hour h and 0 if not. To compute the adequacy metrics, the process is repeated and LOLE and EENS, which are the average values of LOL, and ENS respectively are calculated.

$$LOLE = \frac{\sum_{y=1}^{n_y} LOL_y}{n_y} \tag{3.28}$$

$$EENS = \frac{\sum_{y=1}^{n_y} ENS_y}{n_y} \tag{3.29}$$

This is done until the convergence criteria is met, i.e. the coefficient of variation (CV) of the expected energy-not-served is below a certain threshold $\epsilon_{threshold}$:

$$CV(EENS) = \frac{\sigma(EENS)}{\mu(EENS)} \leq \epsilon_{threshold} \tag{3.30}$$

3.5 Belgian Power System: Base Case study

The power system studied in this work is representative of the Belgian Power System considered as a 1 node system to which a hydrogen demand is added.

3.5.1 Conventional Generating Units

There are 86 conventional generating units in the system ranging from 5 to 425 MW with a total capacity of 6596.3 MW.

3.5.2 Wind Power Time series

The offshore wind power capacity of Belgium is supposed to be 4.4 GW (forecast value for 2028). The hourly capacity factors for each Monte Carlo year is generated with the following ARMA model and whose order are set with the F-criterion method:

$$\begin{aligned} y_t = {} & 0.236y_{t-1} + 1.482y_{t-2} + 0.167y_{t-3} + 0.563y_{t-4} \\ & + \epsilon_t + 0.71\epsilon_{t-1} - 0.86\epsilon_{t-2} - 0.645\epsilon_{t-3}. \end{aligned} \tag{3.31}$$

The historical data used to build this model are the hourly capacity factors of the aggregated offshore wind power in Belgium [57] during the years 2017-2020, and represented in Fig. 3.6.

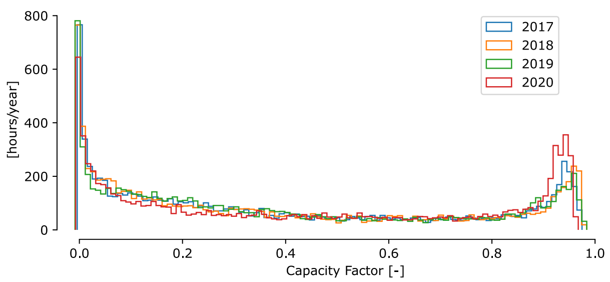

Figure 3.6: Distribution of capacity factors from offshore wind power production in Belgium from 2017 to 2020.

3.5.3 Electrical Load

The hourly mean electrical load of the years 2018-2019 seen by Elia the Belgian Transmission Grid Operator [58] is used as the deterministic load profile.

3.5.4 Annual Hydrogen Demand

According to the European Observatory of Clean Hydrogen [59], Belgium consumed 378.2 kt_{H2} in 2022. This demand is mainly due to refineries (44.5 %), ammonia industry (36 %), other chemicals (11.2 %), and industrial heat (8.2 %). The majority is produced locally with methane (CH_4). In this work, we study the impact of producing a certain share (up to 45 %) of this hydrogen consumption locally with electrolyzers, see Table 3.2.

Table 3.2: Corresponding hydrogen quantity [kt_{H2}/y] for different share of the yearly demand (378.2 kt/year) satisfied locally with electrolyzers.

Share of yearly H_2 consumption [%]	**11.25**	**22.5**	**33.75**	**45**
$[kt_{H_2}/y]$	42.5	85	127.5	170

3.6 Results

Firstly, the EEC model and the linear interpolation model are compared. Secondly, the impact of a local hydrogen demand satisfied with electrolyzers on the Belgian Power System is analyzed.

3.6.1 EEC model vs. Linear Interpolation Model

In this section, we evaluate the linearized electrolyzer model by comparing it to the non-linear EEC model. Both models are integrated into the the economic dispatch one at a time. Depending on the chosen electrolyzer model, our optimization formulation is linear or not. Indeed, $q_{el}(P_{el}(e,t))$ defined in (3.23) can take either form: (3.32) or (3.33).

EEC model :

$$q_{el}(P_{el}(e,t)) = \frac{1}{2R_{m,stack}} \frac{nM}{zF} \left(-V_{ocv,stack} + \sqrt{(V_{ocv,stack})^2 + 4R_{m,stack} P_{el}(e,t)} \right) \quad (3.32)$$

Linear model :

$$q_{el}(P_{el}(e,t)) = \eta_{el} * P_{el}(e,t) \quad (3.33)$$

The linearized electrolyzer model is evaluated in terms of computational time, and accuracy. To do so, we run the economic dispatch on the Belgian case study for a 24-hour period, and with a hydrogen demand of 103.6 [ton_{H_2}] to be satisfied by 432 electrolyzers of 1 MW. This is done 30 times for every hydrogen demand profile (day time, round-the-clock, wind-correlated, and optimized) while considering no outages on the generator units.

Accuracy of linearized model

To evaluate the accuracy of the linearized model, we compare the cost (value of the objective function of economic dispatch), which reflects the operational costs of generators, and the lack of energy through the value-of-loss-load. The cost comparison is illustrated in Fig. 3.7a for each electrolyzer model and hydrogen demand profile combination.

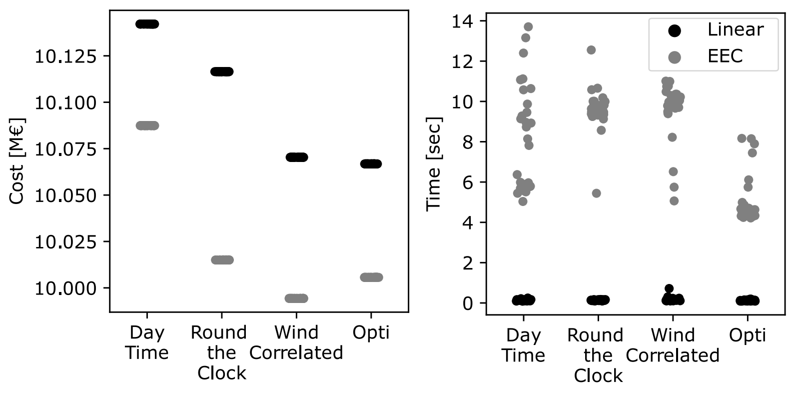

(a) Economic dispatch cost. (b) Economic dispatch computational time.

Figure 3.7: Comparison between EEC and linearized model integrated into an economic dispatch for a 24-hour period.

The errors are summarized in Table 3.3. The hydrogen demand profile influences the error. Indeed, depending the operating load factor of the electrolyzer, the linearized model is closer, or not to the EEC model (see curves in Fig. 3.3). However, the error stays below 1.01 %.

Table 3.3: Accuracy evaluation of the linearized electrolyzer model: comparison of the mean operational cost [M€] value between EEC model (non-linear) and linearized model.

Day Time			Round-the-Clock			Wind-Correlated			Optimized		
Linear model	EEC model	Error [%]	Linear model	EEC model	Error [%]	Linear model	EEC model	Error [%]	Linear model	EEC model	Error [%]
10.142	10.087	0.542	10.116	10.015	1.013	10.070	9.994	0.761	10.067	10.006	0.611

Computational time comparison

The economic dispatch is formulated in the Julia Programming Language. The chosen solvers are Gurobi[1] for the linear formulation and Ipopt for the non-linear formulation, and the run were perfomed on a Intel®Core$^{\mathrm{TM}}$ i7-10610U CPU @ 1.80-2.30 GHz, 4 cores, 8 threads, 32 Go RAM, and SSD 512 Go.

In Fig. 3.7b, for each electrolyzer model and hydrogen demand profile combination, the different computational times are plotted. We can visually assess that the linear formulation is clearly advantageous. The ratio between computational times are reported in Table 3.4. The linearized model can be up to 70 times faster than the EEC model. For longer time period (e.g. 8760 hours for a year), the gain can be huge. Moreover, integrated into a sequential Monte Carlo process, the gain can be ultra competitive.

Table 3.4: Time gain evaluation of the linearized electrolyzer model: comparison of the mean computational time [seconds] value between EEC model (non-linear) and linearized model.

Day Time			Round-the-Clock			Wind-Correlated			Optimized		
Linear model	EEC model	Ratio [-]	Linear model	EEC model	Ratio [-]	Linear model	EEC model	Ratio [-]	Linear model	EEC model	Ratio [-]
0.1357	8.2206	60.6	0.1381	9.5696	69.3	0.1816	9.5808	52.7	0.1252	5.0839	40.6

[1] Acknowledgments for the free academic license

3.6.2 Sensitivity Analysis of the Hourly Distribution of the Hydrogen Demand

The Belgian power system presented in Section 3.5 with different hourly distribution of a hydrogen demand is optimized within an economic dispatch over a whole year and its probabilistic adequacy metrics are obtained with a sequential Monte Carlo process. The LOLE and EENS are represented in Fig. 3.8.

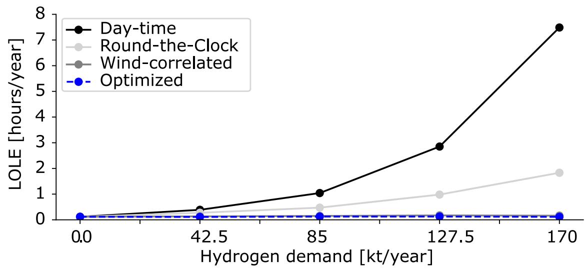

(a) LOLE indicator [hours/y]

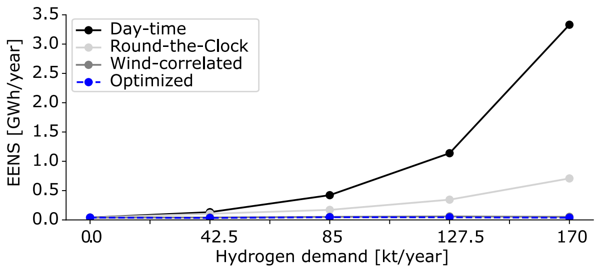

(b) EENS indicator [GWh/y]

Figure 3.8: Adequacy indicators of the different scenarios with progressive hydrogen demand (170 kt/year corresponds to 45% of the annual hydrogen consumption).

All scenarios except the optimized one show an exponential increase of the indicators, but with different exponents. For each replacement share, Table 3.5 gives the increase factor of the LOLE and EENS indicators compared to the situation where no hydrogen demand is added to the system, that is:

$$\text{LOLE Increase factor} = \frac{LOLE_{sh}}{LOLE_{noH_2}} \tag{3.34}$$

$$\text{EENS Increase factor} = \frac{EENS_{sh}}{EENS_{noH_2}} \tag{3.35}$$

where $LOLE_{sh}$ is the LOLE of the scenario with a specific local H_2 consumption share sh and $LOLE_{noH_2}$ the LOLE of the Belgian Power System without any hydrogen produced with electrolyzers.

Table 3.5: The increase factor of the LOLE and EENS indicators of scenarios with different local hydrogen demands.

	Local H_2 annual demand [kt/year]	**42.5**	**85**	**127.5**	**170**
	Share of yearly H_2 consumption [%]	11.25	22.5	33.75	45
LOLE	Day-time	3.3	8.83	24.17	63.46
	Round-the-Clock	2.32	4.01	8.32	15.52
	Wind-correlated	1.13	1.28	1.4	1.4
	Optimized	1	1	1	1
EENS	Day-time	3.35	10.7	28.86	84.45
	Round-the-Clock	2.67	4.34	8.75	17.95
	Wind-correlated	1.05	1.32	1.41	1.41
	Optimized	1	1	1	1

A first observation is that when the annual hydrogen demand is optimized throughout the year (flexible H_2 demand), no impact is observed on the adequacy until 170 [$kton_{H_2}$/year] of local hydrogen demand while for the other scenarios (fixed H_2 demand), the impact is more or less significant depending on the scenario.

Already at 42.5 [$kton_{H_2}$/year] of local hydrogen demand, the hourly distribution of hydrogen throughout the year has an impact on the adequacy indicators. Indeed, the LOLE and EENS of the day-time scenario increase by a factor 3.3 and 3.35 respectively while the LOLE and EENS of the round-the-clock scenario increase by a factor 2.3 and 2.7 respectively. This difference gets more significant as the local hydrogen demand share increases. The wind-correlated scenario has a very low impact on the adequacy indicators and is very close to the optimized scenario. It can be deduced that both scenarios produce hydrogen at similar moments, i.e. when wind power is important.

At 85 [$kton_{H_2}$/year] of local hydrogen demand, the LOLE of the day-time scenario is impacted 7 times more than the wind-correlated scenario, and the round-the-clock scenario, 3 times more than the wind-correlated scenario. At 170 [$kton_{H_2}$/year] of local hydrogen demand, the LOLE of the day-time and round-the-clock scenarios are respectively 45 and 11 times more impacted than the wind-correlated scenario.

The results show clearly that the hourly profile of the hydrogen demand has a significant impact on the adequacy of power systems and that optimising the hydrogen demand, or correlating it to wind power is relevant.

3.7 Conclusion

This study presents the impact that a local hydrogen demand can have on power systems adequacy assessments. To do so, a Power-to-Hydrogen (P2H) model is integrated into an economic dispatch looped into a sequential Monte Carlo process. In this work, two models i.e a non-linear equivalent electrical circuit and its linear interpolation counterpart have been tested and compared.
As a first result, it has been observed that the linear interpolation approximation does not impact the accuracy of the economic dispatch results (less than 1.01% error for the operational cost) and that it can reduce drastically the computational time. Reducing computational time is very useful, especially when the economic dispatch is then integrated within the Monte Carlo process. Then, the probabilistic adequacy tool is applied to the Belgian power system over a yearly time period and different hydrogen demands and hourly profiles are analyzed. In this study, the linearized electrolyzer model is considered. A second important result is that the hourly profile of local H_2 demand has a significant impact on the adequacy indicators. Firstly, when optimizing the local H_2 demand, no impact is observed on the adequacy. Secondly, the LOLE of the power system with day-time and round-the-clock hourly H_2 local demand distributions are much more impacted than with an hourly H_2 distribution profile correlated with the offshore wind power production. This clearly shows the relevance to optimize the local H_2 demand profile or correlate it to wind power to reduce the hydrogen demand impact on power systems adequacy.

CHAPTER **4**

Adequacy Assessment Tool with the integration of the hydrogen energy vector

Chapter overview

- Core description of the probabilistic adequacy tool integrating hydrogen and based on sequential Monte Carlo simulations.
- Development of a crucial block of this tool, i.e. the multi-period DC OPF.
- Validation of the DC OPF on PGLib benchmark.

This chapter is based on a peer-reviewed conference paper and on a non-peer-reviewed submitted article:

A. Hernandez, F. Vallée and E. De Jaeger, "Integration of Hydrogen in Sequential Monte Carlo Power Systems Adequacy Assessment," 2023 IEEE Belgrade PowerTech, Belgrade, Serbia, 2023, pp. 1-6, doi: 10.1109/PowerTech55446.2023.10202671.

Hernandez, Aurélia and De Jaeger, Emmanuel and Vallée, François, Linking Hydrogen to Power Systems in Adequacy Computations. Available at SSRN: http://dx.doi.org/10.2139/ssrn.4898181.

After an introduction to the general theory of reliability an risk assessments in Chapter 2, we have chosen to work with sequential Monte Carlo simulations. Although this method can be computationally intensive as it requires a large number of simulations for accurate results, it can handle complex systems with many components. In Chapter 3, to illustrate the impact of integrating power-to-hydrogen models into an adequacy assessment, a first basic adequacy tool was developed: a sequential Monte Carlo simulation tool to generate yearly states of the system, combined with an economic dispatch neglecting network constraints to analyze the states of the system.

In this Chapter, we present the core of the final and advanced probabilistic adequacy tool integrating hydrogen that has been developed. This tool is also based on sequential Monte Carlo simulations to generate yearly states of the system, but here it is combined with an economic dispatch that takes into account network constraints, i.e. a DC optimal power flow problem to analyze the states of the system over the studied period. Firstly, we outline each block of the adequacy tool, and then, the main block, i.e the multi-period DC OPF formulation integrating hydrogen is detailed, and the mathematical equations are formulated and explained. Finally, this main block is tested on various test systems from the PGLib benchmark.

> The Chapter is structured according to the following sections: Section 4.1 introduces the different blocks of the probabilistic adequacy tool integrating hydrogen. Section 4.2 thoroughly develops the multi-period DC OPF, and Section 4.3 tests the formulation on a benchmark for verification purposes.

4.1 The probabilistic adequacy tool with hydrogen integration

To assess the adequacy of a coupled hydrogen-electricity system in a probabilistic framework:

- a sequential sampling is undertaken to account for uncertain hourly time series, including potential unit outages and the variability of offshore wind power throughout the year. These sequential samplings allow for the characterization of each year's uniqueness considering both contingencies and climatic conditions.
- a hydrogen-integrated multi-period DC optimal power flow is developed to optimize the system operation, determining the optimal generation schedule fo each unit to meet the electrical and hydrogen demand while being constrained by technical limits, e.g maximum power capacity of technologies. This optimiza-

tion permits to identify energy shortfalls at specific hours and thus define the adequacy indicators (loss-of-load, energy-not-served).

- a Monte Carlo loop is developed to repeat the two aforementioned steps. This iterative process allows testing a large range of possible years, and ensure a robust evaluation of those adequacy indicators (loss-of-load-expectation, and expected-energy-not-served).

The methodology is schematized in Fig. 4.1, and each block of the scheme is detailed in the following subsections.

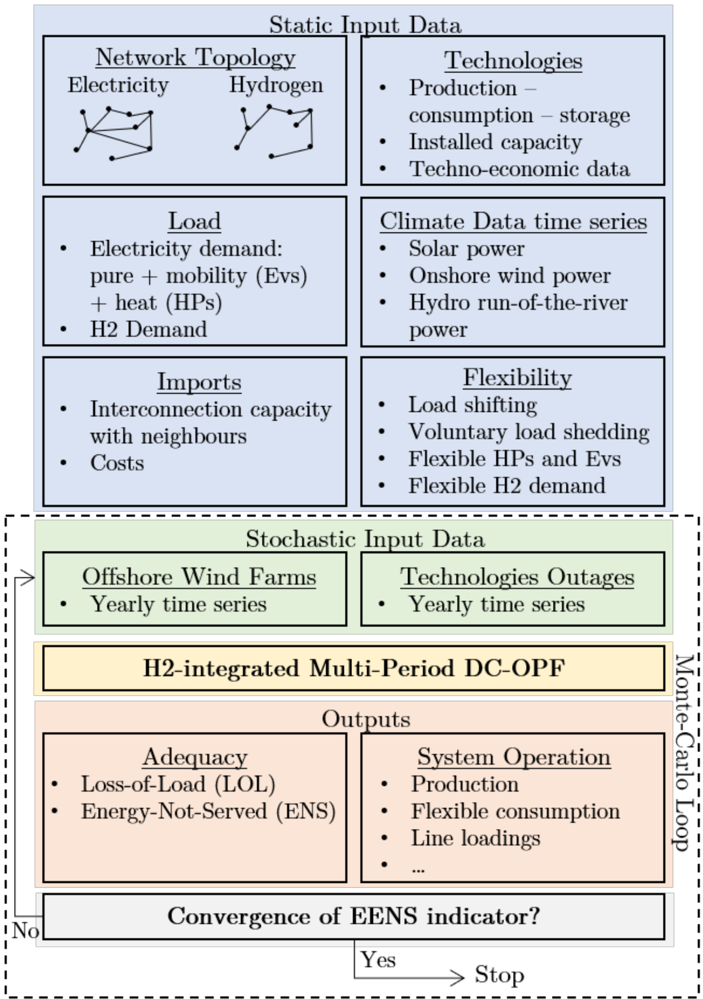

Figure 4.1: Schematic of the developped adequacy tool.

4.1.1 Static Input Data

The probabilistic hydrogen-integrated adequacy framework requires some fixed parameters, that do not vary from one simulation to another. They consist in: electrical and hydrogen network topology, techno-economic data of the different production/consumption/storage technologies, of the electrical and hydrogen interconnections with foreign countries, and of the different flexibilities (flexible loads, voluntary shedding, and smart heat-pumps and electric vehicles). Moreover, electrical and hydrogen demands, hourly capacity factors [1] of the distributed renewable energy sources (PV, onshore wind power, hydro run-of-river power) throughout the year are set as constant time series although they have a stochastic behavior in reality.

4.1.2 Stochastic Input Data

Offshore Wind Farms Production

A set of 100 annual time series has been generated for each wind farm. For each Monte-Carlo year, a yearly time series is randomly selected from the existing set.

Technologies Unplanned Outages

The availability of the different technologies is represented using a two-state model. The first state being available for operation, and the second one, in outage and unavailable for operation. The time after which an outage occurs is defined as the time-to-failure (TTF) [hours], and the time it takes to repair, the time-to-repair (TTR) [hours]. Based on historical data, the behavior of these random variables (TTF,TTR) has been observed, and it appears that their probability density function follows a negative exponential distribution:

$$f(x;\kappa) = \begin{cases} \kappa e^{-\kappa x} & \text{if } x \geq 0, \\ 0 & \text{if } x < 0. \end{cases}$$

where $\kappa > 0$ is the rate parameter, and represents in our case the failure λ or the repair μ rate. One property of the random variables following this negative exponential distribution $X \sim \text{Exp}(\kappa)$ is that its expected value $\mathbb{E}(X) = 1/\kappa$. For $TTF \sim \text{Exp}(\lambda)$, the expected value $\mathbb{E}(TTF) =$ MTTF (mean-time-to-failure) and is equal to $1/\lambda$. Similarly, $TTR \sim \text{Exp}(\mu)$, the expected value $\mathbb{E}(TTR) =$ MTTR (mean-time-to-repair) and is equal to $1/\mu$. In the literature, the failure/repair rate λ/μ, and/or the mean-time-to-failure/repair MTTF/MTTR of technologies are given and allow thus to construct their probability density function and draw different TTF/TTR values following a distribution that is representative of their behavior based on historical data[2] . The construction of the yearly availability profile (vector of 8760 elements taking a value $\in \{0, 1\}$) of

[1] In this work, the hourly capacity factor is defined as the hourly average power generated by a unit divided by its peak or installed capacity.

[2] A distinction is made between mean-time-to-failure MTTF and mean-time-between-failures MTBF: MTTF is a metric for outages requiring replacements, whereas MTBF is used for outages that are repairable. In our case, the outages can be of both nature, and we will keep the MTTF notation.

each unit is determined by juxtaposing the status of samples drawn from the TTF and TTR distributions respectively, as depicted in Fig. 4.2. The status is set available (1) for the TTF durations, and in outage (0) for the TTR durations. TTF and TTR samples are drawn until their sum ≥ 8760.

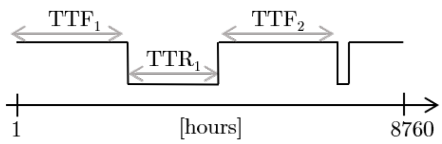

Figure 4.2: Construction of the availability profile of a unit.

The inverse transform sampling method allows to draw samples from any non-uniform probability density functions if the cumulative distribution function is known. This method is developed hereunder and is applied to samples of negative exponential probability density functions:

If $f(t)$ represents the failure/repair density function,

1. Calculate $F(t) = \int_{-\infty}^{t} f(t')dt'$ representing the cumulative function of $f(t)$, i.e. $F(t) = P[t_{failure} \leq t]$:

$$F(t) = \int_0^t \kappa e^{-\kappa t'} dt' = [-e^{-\kappa t'}]_0^t = 1 - e^{-\kappa t}$$

2. Calculate the inverse function $F^{-1}(u)$.

$$F^{-1}(u) = -\frac{1}{\kappa} \ln(1-u)$$

3. Draw a sample u from a uniform distribution, and $F^{-1}(u)$ will give you a sample from $f(t)$.

$$\begin{aligned} TTF_{sample} &= - \overbrace{\frac{1}{\lambda}}^{MTTF} * \ln(1-u) \quad [hours] \\ TTR_{sample} &= - \underbrace{\frac{1}{\mu}}_{MTTR} * \ln(1-u) \quad [hours] \end{aligned}$$

Technologies can also undergo planned outages. For generators, they occur mainly during the summer and autumn season but are still present during the autumn/winter season. To consider them, Elia makes the hypothesis that i) if the maintenance dates are known and available on the transparency platforms in advance, they are explicitly taken into account, and ii) if not known, a maintenance rate is used, and there scheduling is generated before the simulation. In this case, no planned outages occur during winter and autumn [60].

In this work, planned outages are neglected. It is assumed, that because they are planned, they will never occur during periods where energy-not-served is close to happen, and thus does not have an impact on the results obtained in terms of adequacy.

4.1.3 H2-integrated Multi-Period DC-OPF

The model used is a hydrogen-integrated multi-period DC optimal power flow. It has an hourly resolution and is specifically tailored for horizons of a year. The formulation is a linear optimization problem and is detailed in Section 4.2.

4.1.4 Outputs

After each Monte Carlo year, the outputs consist in all the variables of the model (see nomenclature in Section 4.2). Although, all the variables are not saved for each year, because of space and time constraints, the user is free to change and save precise data for every year. However, the main outputs are the yearly adequacy indicators: loss-of-load (LOL), and energy-not-served (ENS):

$$ENS_y = \sum_{t=1}^{8760} Ens(t) \tag{4.1}$$

$$LOL_y = \sum_{t=1}^{8760} [Ens(t) > 0] \tag{4.2}$$

where $Ens(t)$ is a variable (output result) from the H2-integarted MP-DC-OPF, and represents the hourly energy-not-served [MWh].

From these outputs, we can calculate the expected-ENS (EENS), and the LOL-expectation (LOLE) which are typical adequacy indicators for transmission systems:

$$EENS_y = \overline{ENS_y} = \frac{\sum_{\psi=1}^{y} ENS}{y} \tag{4.3}$$

$$LOLE_y = \overline{LOL_y} = \frac{\sum_{\psi=1}^{y} LOL}{y} \tag{4.4}$$

where $y = 1$ is the first Monte Carlo year, $y = 2$ the second, etc.

4.1.5 Convergence of EENS indicator

The Monte Carlo loop stops whenever the expected-energy-not-served (EENS) has converged. The convergence of this indicator is defined as the rolling median of the β' indicator with a window of 30 samples: $\tilde{\beta'}_{y,30}$

$$\tilde{\beta'}_{y,30} = \text{median of } [\beta'_{y-29}, \beta'_{y-28}, ..., \beta'_{y}] \tag{4.5}$$

$$\text{with } \beta'_y = \frac{\mid \beta_y - \beta_{y-1} \mid}{\beta_{y-1}} \tag{4.6}$$

$$\text{and } \beta_y = \frac{\sigma(EENS)_y}{\mu(EENS)_y} = \frac{\sigma([EENS_1, EENS_2, ..., EENS_y])}{\mu([EENS_1, EENS_2, ..., EENS_y])} \tag{4.7}$$

The simulation process stops at year y when the convergence indicator $\tilde{\beta'}_{y,30} < 0.001$. More details on the choice of this convergence indicator can be found in Appendix A.

4.2 The Multi-Period DC Optimal Power Flow (MP-DC-OPF) Formulation

A multi-period DC optimal power flow is an optimization problem which consists in minimizing a certain quantity – usely the cost which depends on the decision variables of the problem – under several constraints – which translate different realities and bound the solution. In this formulation, Variables are denoted with an upper case letter as first letter, and parameters with a lower case letter.

4.2.1 Objective function

The costs related to the operation of conventional generating units [3] P_{gen}, the electrical and hydrogen imports P_{imp},$Q_{H_2,imp}$, the electrical and hydrogen energy-not-served

[3]In this manuscript, conventional generating units refer to thermal power plants.

Ens,Ens_{H_2}, the shifted energy demand S_{rem} and the voluntary load shedding E_{v-shed} are minimized and detailed in (4.8).

$$\begin{aligned}
&\text{Min} \sum_{t=1}^{8760} \left(\sum_{g=1}^{n_g} c_{gen}(g) * P_{gen}(g,t) + \sum_{i=1}^{n_i} c_{imp}(i) * P_{imp}(i,t) + \sum_{j=1}^{n_j} c_{H_2} * Q_{H_2,imp}(j,t) \right) \\
&+ \sum_{t=1}^{8760} \sum_{n=1}^{n_n} \Bigg(voll * Ens(n,t) + voll_{H_2} * Ens_{H_2}(n,t) + c_{shift} * S_{rem}(n,t) \\
&+ c_{v-shed} * E_{v-shed}(n,t) \Bigg)
\end{aligned} \tag{4.8}$$

4.2.2 Constraints

Electrical balance

At each hour t of the year and at each node n of the system, electrical energy has to comply with the conservation of energy. This constraint is detailed in (4.9). The power produced - by the conventional generators P_{gen}, the offshore wind farms res, the electrical imports P_{imp}, and the hydrogen-to-power (H2P) units P_{H2P} - has to satisfy the demand - i.e. the fixed residual electrical load l_{resi}, the consumption of electrolyzers and their compression needs $(1 + \eta_c) * P_{el}$ - with the support of flexiblity - such as storage faclities (i.e. pumped hydro storage $P_{phs,in/out}$, batteries $P_{batt,in/out}$) , voluntary load shedding E_{v-shed}, load shifting S_{rem}/S_{add}, a flexible heat demand $P_{flex,heat}$, and a flexible mobility charging demand $P_{flex,mob}$. If imbalance occurs, production is curtailed C (excess) or energy is not served Ens (lack).

$$\begin{aligned}
&\sum_{g\in G_n} P_{gen}(g,t) + \sum_{r\in R_n} res(r,t) + \sum_{i\in I_n} P_{imp}(i,t) + \sum_{h\in H_n} P_{H2P}(h,t) \\
&+ \sum_{p\in P_n} \Big(P_{phs,out}(p,t) - P_{phs,in}(p,t) \Big) + \sum_{b\in B_n} \Big(P_{batt,out}(b,t) - P_{batt,in}(b,t) \Big) \\
&+ \sum_{l\in L_{to,n}} F(l,t) - \sum_{l\in L_{from,n}} F(l,t) + Ens(n,t) - C(n,t) = l_{resi}(n,t) \\
&+ P_{flex,heat}(n,t) + P_{flex,mob}(n,t) + (1+\eta_c) * \sum_{e\in E_n} P_{el}(e,t) \\
&+ S_{add}(n,t) - S_{rem}(n,t) - E_{v-shed}(n,t) \qquad \forall n, \forall t
\end{aligned} \tag{4.9}$$

The fixed residual load l_{resi} consists of the traditional electrical demand [4] l , and the non-flexible (fixed) heat $l_{hp,fixed}$ and mobility $l_{ev,fixed}$ demands, to which the distributed production - distributed renewable production from photovoltaics $lf_{pv} * p_{pv,max}$, onshore wind turbines $lf_{onsh} * p_{onsh,max}$, hydro run-of-river $lf_{hydro} * p_{hydro,max}$, and distributed conventional units $lf_{dist-gen} * p_{dist-gen,max}$ (e.g. small CHPs) - is substracted. It represents the load seen at the interface between the 220/380 kV transmission grid and the lower voltage levels i.e. subtransmission and distribution grids, and is detailed in (4.10).

$$\begin{aligned} l_{resi}(n,t) &= d_l(n) * l(t) + d_{ev}(n) * l_{ev,fixed}(t) + d_{hp}(n) * l_{heat,fixed}(t) \\ &- d_{dist-gen}(n) * lf_{dist-gen}(t) * p_{dist-gen,max} \\ &- d_{pv}(n) * lf_{pv}(t) * p_{pv,max} - d_{onsh}(n) * lf_{onsh}(t) * p_{onsh,max} \\ &- d_{hydro}(n) * lf_{hydro}(t) * p_{hydro,max} \qquad \forall n, \forall t \end{aligned} \tag{4.10}$$

Conventional Generators

Production of conventional generators [5] P_{conv} is limited by their minimum/maximum power capacity $p_{conv,min/max}$, and by their availability $\alpha_{gen} \in \{0,1\}$ at each time step t in (4.11). The unavailbailities represent unplanned forced outages.

$$\alpha_{gen}(g,t) * p_{gen,min}(g) \leq P_{gen}(g,t) \leq \alpha_{gen}(g,t) * p_{gen,max}(g) \qquad \forall g, \forall t \tag{4.11}$$

Electrical Imports

The interconnections i with neighboring regions permit the import of electricity P_{imp}. These imports are of course limited by the capacity of each interconnection $p_{imp,max}$, and the availability of the latter α_{imp} in (4.12). The availability parameter defines if the interconnection line is available and if the neighboring region has the possibility to transmit power. The total imports are also limited in power by a certain threshold $p_{imp,max,tot}$ in (4.13) to keep a stable domestic network. Finally in (4.14), the yearly imports of each interconnection is limited by a certain value $e_{imp,max,yearly}$.

[4] In this manuscript, the traditional electrical demand is referred to lighting, electronics, industrial appliances, etc., which were traditionally electrified, and excluding any usage for heating or transportation.

[5] In this manuscript, conventional generators refers to the units producing electrical energy from coal, oil, or natural gas.

$$P_{imp}(i,t) \leq \alpha_{imp}(i,t) * p_{imp,max}(i) \qquad \forall i, \forall t \tag{4.12}$$

$$\sum_{i=1}^{n_i} P_{imp}(i,t) \leq p_{imp,max,tot} \qquad \forall t \tag{4.13}$$

$$\sum_{t=1}^{n_t} P_{imp}(i,t) \leq e_{imp,max,year}(i) \qquad \forall i \tag{4.14}$$

Power Load Flow

Electricity flows through electrical lines from generating units to consuming units. These flows are limited by the maximum capacity of the lines f_{max} in (4.15).

$$-f_{max}(l) \leq F(l,t) \leq f_{max}(l) \qquad \forall l, \forall t \tag{4.15}$$

Furthermore, these flows are constrained by the physics of the load flow. In this model, the approximation of a DC load flow is considered [6] , i.e. the power flowing through a line F is directly linked to the susceptance of the line b_{pu}, and to the phase angle θ difference between the two nodes bounding the line, as shown in (4.16). Additionally, the hourly availability of the lines α_l are considered to constraint the flow to zero if an outage occurs on that line.

$$F(l,t) = \alpha_l(l,t) * s_{base} * b_{pu}(l) * \big(\Theta(n_{from}(l),t\big) - \Theta\big(n_{to}(l),t)\big) \qquad \forall l, \forall t \tag{4.16}$$

Also, the phase angle difference between two adjacent nodes bounding a line is also limited by $\Delta\Theta_{max}$ in (4.17).

$$-\Delta\Theta_{max} \leq \Theta\big(n_{from}(l),t\big) - \Theta\big(n_{to}(l),t\big) \leq \Delta\Theta_{max} \qquad \forall l, forallt \tag{4.17}$$

Finally, because only the relative phase angle values matter, and not their absolute values, a phase angle node n_{ref} is set as the reference node, and its value to zero in (4.18).

$$\Theta(n_{ref},t) = 0 \qquad \forall t \tag{4.18}$$

[6]The DC-OPF is a linearization of the AC-OPF formulation. This simplification requires the following assumptions [61]: i) the reactance of the line (X) is much greater than its resistance (R), $X >> R$, ii) the voltage magnitude at each bus is considered to be 1.0 per unit, iii) the phase angle difference between two adjacent buses is small. These hypothesis imply that lines are lossless (R=0), and that reactive power is negligible. These assumptions apply for high voltage transmission systems. Moreover, the DC approximation is a game changer in terms of computational time for large systems while maintaining a relatively low error.

Curtailment

The curtailment C, i.e. the excess production of electricity is bounded at each hour t, and each node n by the local production (centralized/distributed conventional/renewable generation). This equation is detailed in (4.19) and makes sure that an excess of power is curtailed at the location of excess and not elsewhere. This constraint avoids inconsistencies such as curtailed power at a node with no local production and fed from a neighbouring node with excess power production.

$$\begin{aligned} C(n,t) \leq \sum_{r \in R_n} res(r,t) + \sum_{g \in G_n} P_{gen}(g,t) + d_{dist-gen}(n) * lf_{dist-gen}(t) * p_{dist-gen,max} \\ + d_{pv}(n) * lf_{pv}(t) * p_{pv,max} + d_{onsh}(n) * lf_{onsh}(t) * p_{onsh,max} \\ + d_{hydro}(n) * lf_{hydro}(t) * p_{hydro,max} \qquad \forall n, \forall t \qquad (4.19) \end{aligned}$$

Energy-Not-Served

The energy-not-served Ens, i.e. the energy lacking to serve the load is bounded at each hour t and each node n by the local consumption (pure electrical load, flexible and fixed loads from electric vehicles and heat-pumps) in (4.20).

$$\begin{aligned} Ens(n,t) \leq d_l(n) * l(t) + d_{ev}(n) * l_{ev,fixed}(t) + d_{hp}(n) * l_{heat,fixed}(t) \\ + P_{flex,heat}(n,t) + P_{flex,mob}(n,t) \qquad \forall n, \forall t \qquad (4.20) \end{aligned}$$

Electrolyzers

Hydrogen can be produced using electrolyzers with a certain efficiency η_{el}. The installed capacity of electrolyzers $p_{el,max}$ is fixed, and thus limits the electrical power consumption of the latter in (4.21).

$$P_{el}(e,t) \leq \alpha_{el}(e,t) * p_{el,max}(e) \qquad \forall e, \forall t \qquad (4.21)$$

Hydrogen-to-Power units

These units convert hydrogen into electrical power with a certain efficiency η_{H2P}. The installed capacity of hydrogen-to-power units $p_{H2P,max}$ is fixed, and thus limits the electrical power production of the latter in (4.22).

$$P_{H2P}(h,t) \leq \alpha_{H2P}(h,t) * p_{H2P,max}(h) \qquad \forall h, \forall t \qquad (4.22)$$

Load Shifting

A certain energy quantity can be shifted during the day. This implies that a certain quantity S_{rem} can be supplied at another time during the day by S_{add} (see (4.23)). Of course, the daily amount of shifted energy is limited at each node by a percentage d_s of the maximum daily shiftable energy $e_{shift,max,daily}$ allowed in the system in (4.24). Also the shifted quantity (removed) is limited at each node and each time step by a percentage d_s of the maximum shiftable power $p_{rem,max}$ in (4.25).

$$\sum_{t=24(d-1)+1}^{24d} S_{rem}(n,t) = \sum_{t=24(d-1)+1}^{24d} S_{add}(n,t) \qquad \forall n, \forall d \qquad (4.23)$$

$$\sum_{t=24(d-1)+1}^{24d} S_{rem}(n,t) \leq d_s(n) * e_{shift,max,day} \qquad \forall n, \forall d \qquad (4.24)$$

$$S_{rem}(n,t) \leq d_s(n) * p_{rem,max} \qquad \forall n, \forall t \qquad (4.25)$$

Voluntary load shedding

A certain quantity of the electrical demand can also be shed voluntarily E_{v-shed} thanks to contracts defined in advance. Same here, in (4.26) this daily flexibility is limited at each node by the maximum daily shedable energy $e_{v-shed,max,day}$. Further more, this voluntary shedding is limited in power by the maximum shedable power $p_{v-shed,max}$ at each node, and each time step in (4.27).

$$\sum_{t=24(d-1)+1}^{24d} E_{v-shed}(n,t) \leq d_{sh}(n) * e_{v-shed,max,day} \qquad \forall n, \forall d \qquad (4.26)$$

$$E_{v-shed}(n,t) \leq d_{sh}(n) * p_{v-shed,max} \qquad \forall n, \forall t \qquad (4.27)$$

Flexible demands: mobility, heat, and hydrogen

Part of the hydrogen, heat and mobility demands are set flexible within a day. The daily quantities to be satisfied are $l_{H_2,flex,daily}$, $l_{heat,flex,daily}$, and $l_{mob,flex,daily}$ for hydrogen, heat, and mobility demands respectively. Firstly, the hourly and nodal consumptions $Q_{H_2,flex}$, $P_{heat,flex}$, and $P_{mob,flex}$ are constrained by the daily demands in (4.28-4.30). The daily flexibility constrains a daily production but allows a flexibility within the hours of the day. Secondly, the consumption of heat-pumps for flexible heat demand is constrained by the power of installed heat pumps that operate in a flexible way in (4.31), , where n_{hp} represents the total number of individual heat-pumps, w_{hp1m} the share of heat-pumps operating in a flexible way, and $p_{hp,individual}$ the capacity of an individual heat-pump. Thirdly, the hourly consumption of electric vehicles is constrained by the number of electric vehicles that are connected to flexible charging stations in (4.32) where n_{ev} represents the total number of electric vehicles, w_{v1m} the share of electric vehicles connected to a flexible charging station, and $p_{charger}$ the power of the charging station.

$$\sum_{t=24(d-1)+1}^{24d} Q_{H_2,flex}(n,t) = d_{H_2}(n) * \frac{l_{H_2,flex,year}}{365} \qquad \forall n, \forall d \tag{4.28}$$

$$\sum_{t=24(d-1)+1}^{24d} P_{heat,flex}(n,t) = d_{hp}(n) * l_{heat,flex,day} \qquad \forall n, \forall d \tag{4.29}$$

$$\sum_{t=24(d-1)+1}^{24d} P_{mob,flex}(n,t) = d_{ev}(n) * l_{mob,flex,day} \qquad \forall n, \forall d \tag{4.30}$$

$$P_{heat,flex}(n,t) \leq d_{hp}(n) * n_{hp} * w_{hp1m} * p_{hp,individual} \qquad \forall n, \forall t \tag{4.31}$$

$$P_{mob,flex}(n,t) \leq d_{ev}(n) * n_{ev} * w_{v1m} * \alpha_{v1m}(t) * p_{charger} \qquad \forall n, \forall t \tag{4.32}$$

Storage management: PHS and batteries

Electricity can be stored thanks to storage systems with a certain round trip efficiency $\eta_{in} * \eta_{out}$. The following equations are detailed for the pumped-hydro storage units, but apply similarly for batteries. To do so, the *phs* subscript shall be replaced by *batt*, and the indices *p* by *b*. It is assumed that the storage units are empty at the beginning of the year in (4.33)-(4.34). The state-of-charge of the storage system Soc_{phs} is updated at each time step *t* in (4.36). The storage capacity Soc_{phs} is limited in (4.37) by the size of the installation $soc_{phs,max}$. The input/output power flows of these facilities are also limited in (4.39)-(4.38) by the maximum power of the pump $p_{phs,in,max}$ and the maximum power of the turbine $p_{phs,out,max}$.

$$Soc_{phs}(p, t = 1) = \eta_{phs,in}(p) * P_{phs,in}(p, t = 1) \qquad \forall p \qquad (4.33)$$

$$P_{phs,out}(p, t = 1) = 0 \qquad \forall p \qquad (4.34)$$

$$Soc_{phs}(p, t) = Soc_{phs}(p, t - 1) + \eta_{phs,in}(p) * P_{phs,in}(p, t) \qquad (4.35)$$

$$- P_{phs,out}(p, t)/\eta_{phs,out}(p) \qquad \forall p, \forall t > 1 \qquad (4.36)$$

$$Soc_{phs}(p, t) \leq soc_{phs,max}(p) \qquad \forall p, \forall t \qquad (4.37)$$

$$P_{phs,in}(p, t) \leq p_{phs,in,max}(p) \qquad \forall p, \forall t \qquad (4.38)$$

$$P_{phs,out}(p, t) \leq p_{phs,out,max}(p) \qquad \forall p, \forall t \qquad (4.39)$$

Hydrogen balance constraint

Hydrogen also has to comply with the conservation of energy at each hour t of the year and at each node n of the system. Hydrogen produced by electrolyzers $P_{el} * \eta_{el}$, and imported from outside the system $Q_{H_2,imp}$ has to feed the hydrogen demand (flexible $Q_{H_2,flex}$ and fixed $l_{H_2,fixed}$), and the H2P units P_{H2P}/η_{H2P} with the support of hydrogen storage $Q_{H_2,sto,in}//Q_{H_2,sto,out}/$. Hydrogen can also be transported through pipelines F_{H_2} . Unserved hydrogen demand Ens_{H_2} can occur. This constraint is detailed in (4.40).

$$\sum_{e \in E_n} P_{el}(e, t) * \eta_{el} + \sum_{j \in J_n} Q_{H_2,imp}(j, t) + \sum_{q \in Q_n} \Big(Q_{H_2,sto,out}(q, t) - Q_{H_2,sto,in}(q, t) \Big)$$

$$+ \sum_{j \in K_{to,n}} F_{H_2}(j, t) - \sum_{j \in K_{from,n}} F_{H_2}(j, t) = d_{H_2}(n) * l_{H_2,fixed}(t) + Q_{H_2,flex}(n, t)$$

$$+ \frac{P_{H2P}(n, t)}{\eta_{H2P}} - Ens_{H_2}(n, t) \qquad \forall n, \forall t \qquad (4.40)$$

Hydrogen Pipelines

Hydrogen can be transported through pipelines. Hydrogen flows F_{H_2} are limited by the maximum transfer capacity of the pipelines $f_{H_2,max}$ in (4.41).

$$-f_{H_2,max}(k) \leq F_{H_2}(k, t) \leq f_{H_2,max}(k) \qquad \forall k, \forall t \qquad (4.41)$$

Hydrogen Imports

Hourly hydrogen imports $Q_{H_2,imp}$ are limited by a maximum value $q_{H_2,imp,max}$ at each interconnection j in (4.42).

$$Q_{H_2,imp}(j,t) \leq q_{H_2,imp,max}(j) \qquad \forall j, \forall t \tag{4.42}$$

Hydrogen storage management

Hydrogen can be stored under the form of compressed gas. It is assumed that the hydrogen storage is empty at the beginning of the year in (4.43)-(4.44). The state-of-charge of the hydrogen storage units Soc_{H_2} is updated at each time step t in (4.45). The storage capacity is limited in (4.46) by the installed capacity $soc_{H_2,sto,max}$.

$$Soc_{H_2,sto}(q,t=1) = Q_{H_2,sto,in}(q,t=1) \qquad \forall q \tag{4.43}$$

$$Q_{H_2,sto,out}(q,t=1) = 0 \qquad \forall q \tag{4.44}$$

$$\begin{aligned} Soc_{H_2,sto}(q,t) = {} & Soc_{H_2,sto}(q,t-1) + Q_{H_2,sto,in}(q,t) \\ & - Q_{H_2,sto,out}(q,t) \qquad \forall q, \forall t > 1 \end{aligned} \tag{4.45}$$

$$Soc_{H_2,sto}(q,t) \leq soc_{H_2,sto,max}(q) \qquad \forall q, \forall t \tag{4.46}$$

4.2.3 Summary

Figure 4.3 gives a visual support for the two main constraints of this model: the electrical and hydrogen balance and highlights the links between electricity and hydrogen energy vectors.

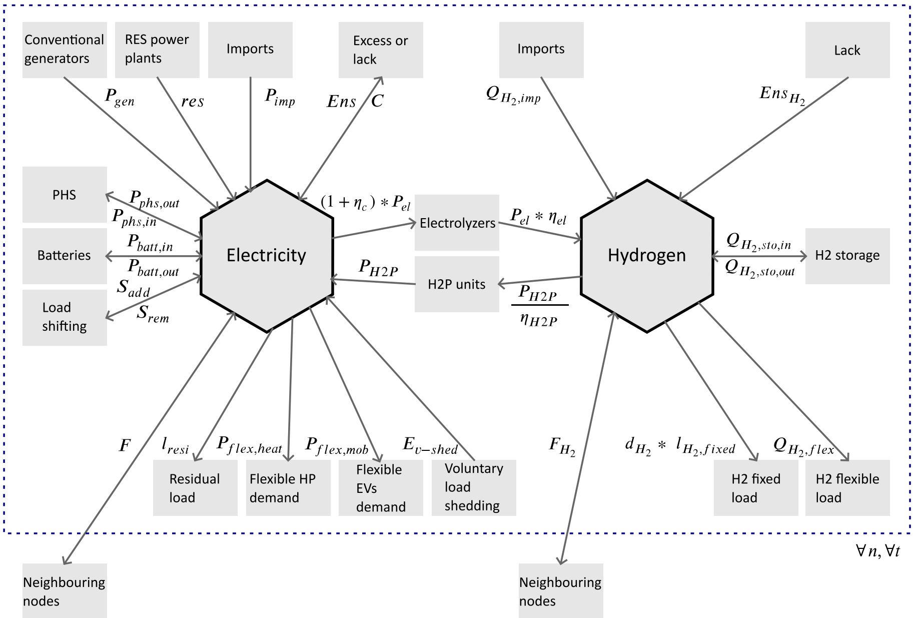

Figure 4.3: Summary of the electricity-hydrogen link in the adequacy tool for a particular node n, and time step t.

4.3 Verification of the model with a benchmark

A benchmark library called "Power Grid Lib - Optimal Power Flow" [7] is available online to verify developed models solving the AC optimal power flow problem. Although this library's first objective is the AC-OPF verification, it also permits to compare results for variants of the OPF formulation, such as the DC-OPF. The developed DC-OPF of our adequacy tool is compared to all test cases of the library and the results are listed in Table 4.1 and 4.2. Out of 66 test cases: 40 are verified (error < 0.3%) - 2 cases with an error between 1-2 % - 11 cases with different results - 13 cases that did not converge with our DC-OPF.

[7] managed and maintained by the IEEE PES Task Force on Benchmarks for Validation of Emerging Power System Algorithms, available on github: : `https://github.com/power-grid-lib/pglib-opf`

Table 4.1: Comparison between developed DC-OPF and the benchmark "Power Grid Lib - Optimal Power Flow" [1/2] `https://github.com/power-grid-lib/pglib-opf`

Test cases	# Buses	# Edges	My DC-OPF [$/h]	Benchmark DC-OPF [$/h]	Diff rel [%]	Validation
case10000_goc	10000	13193	2.34E+06	1.35E+06	7.38E+01	✗
case10192_epigrids	10192	17043	1.69E+06	1.67E+06	1.50E+00	~
case10480_goc	10480	18559	2.22E+06	2.22E+06	1.16E-03	✓
case118_ieee	118	186	9.31E+04	9.31E+04	2.90E-04	✓
case1354_pegase	1354	1991	1.22E+06	1.22E+06	1.47E-03	✓
case13659_pegase	13659	20467	8.76E+06	8.77E+06	7.75E-02	✓
case14_ieee	14	20	2.05E+03	2.05E+03	1.28E-03	✓
case162_ieee_dtc	162	284	1.01E+05	1.01E+05	2.22E-03	✓
case179_goc	179	263	7.52E+05	7.52E+05	1.35E-04	✓
case1803_snem	1803	2795	8.77E+04	8.77E+04	1.20E-02	✓
case1888_rte	1888	2531	1.33E+06	1.35E+06	1.33E+00	~
case19402_goc	19402	34704	1.90E+06	1.90E+06	3.25E-04	✓
case1951_rte	1951	2596	2.03E+06	2.03E+06	2.84E-01	✓
case197_snem	197	286	1.47E+00	1.47E+00	2.37E-04	✓
case200_activ	200	245	-	2.75E+04	-	-
case2000_goc	2000	3639	3.66E+04	9.43E+05	9.61E+01	✗
case20758_epigrids	20758	33368	2.58E+06	2.57E+06	1.29E-01	✓
case2312_goc	2312	3013	-	4.40E+05	-	-
case2383wp_k	2383	2896	1.80E+06	1.80E+06	5.33E-04	✓
case24_ieee_rts	24	38	6.10E+04	6.10E+04	3.94E-04	✓
case240_pserc	240	448	3.27E+06	3.27E+06	1.14E-03	✓
case24464_goc	24464	37816	2.51E+06	2.51E+06	4.36E-04	✓
case2736sp_k	2736	3504	-	1.28E+06	-	-
case2737sop_k	2737	3506	-	7.64E+05	-	-
case2742_goc	2742	4673	2.60E+05	2.60E+05	1.37E-03	✓
case2746wop_k	2746	3514	-	1.18E+06	-	-
case2746wp_k	2746	3514	1.55E+06	1.58E+06	2.12E+00	✗
case2848_rte	2848	3776	1.23E+06	1.27E+06	2.99E+00	✗
case2853_sdet	2853	3921	2.15E+06	2.04E+06	5.72E+00	✗
case2868_rte	2868	3808	1.97E+06	1.97E+06	2.15E-02	✓
case2869_pegase	2869	4582	2.39E+06	2.39E+06	1.20E-02	✓
case3_lmbd	3	3	5.70E+03	5.70E+03	7.20E-05	✓
case30_as	30	41	7.68E+02	7.68E+02	2.74E-04	✓
case30_ieee	30	41	7.47E+03	7.47E+03	1.96E-04	✓
case300_ieee	300	411	5.18E+05	5.18E+05	9.27E-03	✓
case30000_goc	30000	35393	1.09E+06	1.09E+06	1.07E-03	✓
case3012wp_k	3012	3572	2.32E+06	2.51E+06	7.54E+00	✗
case3022_goc	3022	4135	-	5.99E+05	-	-
case3120sp_k	3120	3693	1.66E+06	2.09E+06	2.05E+01	✗
case3375wp_k	3374	4161	7.13E+06	7.32E+06	2.62E+00	✗
case39_epri	39	46	1.37E+05	1.37E+05	2.25E-04	✓
case3970_goc	3970	6641	9.34E+05	9.34E+05	7.29E-05	✓
case4020_goc	4020	6988	7.95E+05	7.95E+05	2.00E-04	✓
case4601_goc	4601	7199	7.94E+05	7.94E+05	4.77E-04	✓
case4619_goc	4619	8150	4.57E+05	4.57E+05	8.02E-04	✓
case4661_sdet	4661	5997	3.46E+06	2.22E+06	5.60E+01	✗
case4837_goc	4837	7765	8.50E+05	8.50E+05	3.81E-04	✓
case4917_goc	4917	6726	-	1.38E+06	-	-
case5_pjm	5	6	1.75E+04	1.75E+04	5.90E-04	✓
case500_goc	500	733	-	4.41E+05	-	-
case5658_epigrids	5658	9078	1.20E+06	1.20E+06	2.83E-03	✓
case57_ieee	57	80	3.48E+04	3.48E+04	1.50E-04	✓

Table 4.2: Comparison between developed DC-OPF and the benchmark "Power Grid Lib - Optimal Power Flow" [2/2] `https://github.com/power-grid-lib/pglib-opf`

Test cases	# Buses	# Edges	My DC-OPF [$/h]	Benchmark DC-OPF [$/h]	Diff rel [%]	Validation
case588_sdet	588	686	-	3.10E+05	-	-
case60_c	60	88	9.07E+04	9.07E+04	1.12E-13	✓
case6468_rte	6468	9000	-	1.98E+06	-	-
case6470_rte	6470	9005	-	2.14E+06	-	-
case6495_rte	6495	9019	-	2.56E+06	-	-
case6515_rte	6515	9037	-	2.56E+06	-	-
case73_ieee_rts	73	120	1.83E+05	1.83E+05	2.03E-03	✓
case7336_epigrids	7336	11521	1.85E+06	1.86E+06	4.17E-01	✓
case78484_epigrids	78484	126146	6.10E+07	1.51E+07	3.05E+02	✗
case793_goc	793	913	7.54E+05	2.58E+05	1.92E+02	✗
case8387_pegase	8387	14561	2.50E+06	2.50E+06	6.81E-02	✓
case89_pegase	89	210	1.05E+05	1.05E+05	1.15E-01	✓
case9241_pegase	9241	16049	6.03E+06	6.03E+06	2.54E-02	✓
case9591_goc	9591	15915	1.03E+06	1.03E+06	3.79E-03	✓

CHAPTER 5

Analysis on test systems

Chapter overview

- Description of the modified Roy Bilinton Test System (RBTS).
- Application of the probabilistic adequacy tool integrating hydrogen on the RBTS study case.
- Study of the impact of hydrogen on adequacy and system operation.

This chapter is based on a peer-reviewed conference paper:

A. Hernandez, F. Vallée and E. De Jaeger, "Integration of Hydrogen in Sequential Monte Carlo Power Systems Adequacy Assessment," 2023 IEEE Belgrade PowerTech, Belgrade, Serbia, 2023, pp. 1-6, doi: 10.1109/PowerTech55446.2023.10202671.

In this Chapter, we apply the probabilistic adequacy tool (previously presented in Chapter 4) to a modified Roy Bilinton Test System (RBTS). While this application uses an earlier version of the tool, the results and conclusion remain robust and unaffected. This exercise serves to illustrate the tool's functionality and to validate its core principles before moving on to a more intricate study case, i.e the Belgian power system in 2030. Through this simpler study case, we demonstrate the impact that hydrogen can have in terms of demand, storage, production, and imports.

> The work presented in this Chapter is structured according to the following sections: Section 5.1 describes the case study. Section 5.2 presents and analyses results for different scenarios, and Section 5.3 concludes the work of this Chapter.

5.1 Description of the test case

The methodology was first tested on a simple case, i.e. the Roy Billinton Test System (RBTS) [62] which is modified to represent future transmission power systems, i.e. high offshore wind penetration level located at the outskirts of the system, with one remote hydrogen system located near the renewable energy source, and another centered near the consumers. The system originally consists in 6 buses, 9 lines, a 185 MW peak load, and 11 generators (thermal and hydro) located at Bus 1 and 2 respectively with a total capacity of 240 MW. This test system is modified (see Fig. 5.1) by removing a 40 MW thermal unit at Bus 1, adding a wind farm (WF) at Bus 1, a hydrogen system - consisting of an electrolyzer, a hydrogen storage (H_2 Sto.) unit, and a hydrogen-to-power (H2P) unit - at Buses 1 and 5, and a hydrogen pipeline linking both hydrogen assets.

The offshore wind power time series are generated as follows: thanks to historical data of the offshore power capacity (production normalized by the installed capacity), an ARMA model was built to generate the capacity factors. A set of 100 time series has been build, and they are multiplied by the considered wind farm power capacity of the considered scenario. The outages are intrinsically taken into account as historical data concerns power production, and not wind speeds.
Different sizes of hydrogen systems will be tested, but it will always follow the following configuration:

$$
\begin{aligned}
p_{H2P,max}(e) &= p_{el,max}(e) && \forall e \\
soc_{H_2,sto,max}(e) &= R \cdot p_{el,max}(e) && \forall e
\end{aligned}
$$

with R refering to the hydrogen storage ratio [1] . The efficiency of the electrolyzers and H2P units are set to $\eta_{el} = 0.7$ and $\eta_{H2P} = 0.43$ respectively. These values are taken

[1] In this study, the storage ratio is defined as the value linking the power of the electrolyzer, and the energy that can be stored in the storage unit. This value expresses the size of the hydrogen storage unit relative to the power of the electrolyzers.

arbitrarily from ranges proposed by [63]. The hydrogen pipelines are assumed to have a 100 MW maximum capacity.

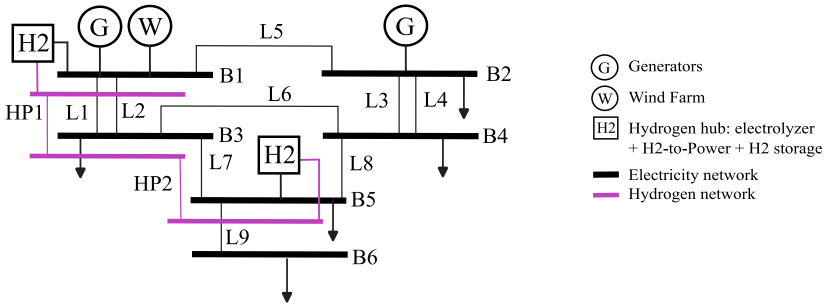

Figure 5.1: Line-diagram of the modified Roy Bilinton Test System (RBTS)

5.2 Results

5.2.1 Impact of H_2 storage units

Scenario 1: 100 MW wind farm, 10/20/30 MW electrolyzers, H_2 storage ratio $R = 3$, no H_2 demand, no H_2 imports.

The empirical probability distribution function of the Loss-of-Load is plotted in Fig. 5.2. There is a clear correlation between the hydrogen system size and the LOLE (see vertical line projected on x-axis). When installing 10 MW (2x5 MW: 5 MW at Bus 1 and 5 MW at Bus 5) of electrolyzers, the LOLE decreases by 41%, and when reaching 20 (2x10 MW) and 30 MW (2x15 MW), it decreases by 48% and 63% respectively. For the sake of clarity, the x-axis of Fig. 5.2 has been cut and the figure does not show extreme cases that can reach high values of LOL and LOE. The same analysis can be made for the LOEE in Fig. 5.2. It decreases by 29.5, 32.5 and 46% when installing 10, 20 and 30 MW of electrolyzers respectively.

Stating that the adequacy enhances when the electrolyzers' installed capacity increases could be misleading. In this case, increasing the installed capacity of the hydrogen system (electrolyzer, storage, and hydrogen-to-power units) improves the adequacy of the system. Indeed, this allows a higher power and energy flexibility to the system.

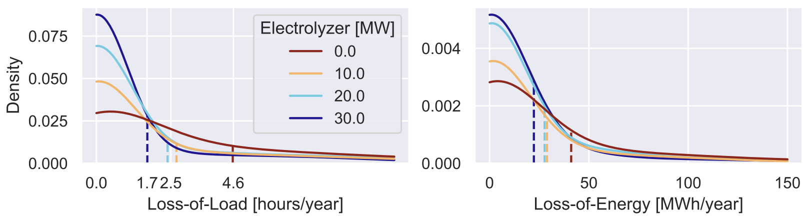

Figure 5.2: Kernel Distribution Estimate (KDE) [a] of the LOL and LOE for every electrolyzer capacity - Scenario 1 : modified RBTS with 200 MW conventional generators, 100 MW Wind Farm, $R = 3$, No H_2 Demand, No H_2 Imports.

[a] Kernel Distrbution Estimation is a non-parametric method to estimate the probability density function of a random variable which allows smoothing a histogram.

These results can be put into perspective by observing outputs other than the adequacy indicators. The yearly curtailment (see Fig. 5.3) decreases when the hydrogen system capacity increases. Initially around 5 GWh/year, it decreases by 46, 70, and 82% when installing 10, 20, and 30 MW of electrolyzers respectively.

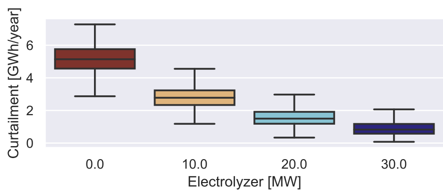

Figure 5.3: Distribution of the yearly curtailment for every electrolyzer capacity - Scenario 1: modified RBTS with 200 MW conventional generators, 100 MW Wind Farm, $R = 3$, No H_2 Demand, No H_2 Imports.

The yearly production of generators increases slightly when adding hydrogen storage systems. Indeed, it increases by 1% when adding 30 MW of electrolyzers. This is due to the system trying to reduce its cost by increasing and storing cheap hydro power in order to use it instead of expensive thermal power plants when hydro plants are already at their maximum production. However, going through the hydrogen storage system leads to additional losses (round-trip efficiency of 30%), so this strategy increases the overall production of conventional generators.

The yearly resume of the operation of hydrogen assets, i.e. the energy consumed and produced by electrolyzers and H2P plants, as well as the number of equivalent cycles in the hydrogen storage facility q defined as:

$$\text{Eq. Nb. Cycles } (q) = \frac{\sum_{t=1}^{8760} Q_{H_2,sto,in}(q,t)}{soc_{H_2,sto,max}(q)} \tag{5.1}$$

are illustrated in Fig. 5.4. Firstly, electrolyzers and H2P consume/produce more when the installed capacity of electrolyzers and H2P increases (Fig. 5.4: top-mid row). However it should be put into perspective with the evolution of their respective utilization factor. Indeed, the load and capacity factor of the latter can be found in Table 5.1. They decrease when the installed capacity increases. Secondly, the equivalent number of cycles of the hydrogen storage (Fig. 5.4: bottom row) gives an insight on the utilization of the hydrogen storage. In this scenario, the mean value lies between 412 and 428 equivalent cycles. When increasing the electrolyzer capacity, the values decrease a bit due to the fact that the load factor of electrolyzers decreases as well. These rates could seem quite high for hydrogen storage units. Indeed, they are usually used as seasonal storage. However, in this study a simplified system is analyzed, and hydrogen storage is the only storage mean. Thus, for this reason, the system has no other shifting strategy, and hydrogen storage is the only flexibility.

Table 5.1: Evolution of the capacity and load factors [%] of the hydrogen assets when increasing the electrolyzers installed - Scenario 1: modified RBTS with 200 MW conventional generators, 100 MW Wind Farm, $R = 3$, No H_2 Demand, No H_2 Imports.

H2 Technology	2x5 MW	2x10 MW	2x15 MW
Electrolyzer Node 1	7.5	6.5	5.8
Electrolyzer Node 5	7.17	5.89	5.06
H2P Node 1	2.52	2.24	2.04
H2P Node 5	1.89	1.5	1.59

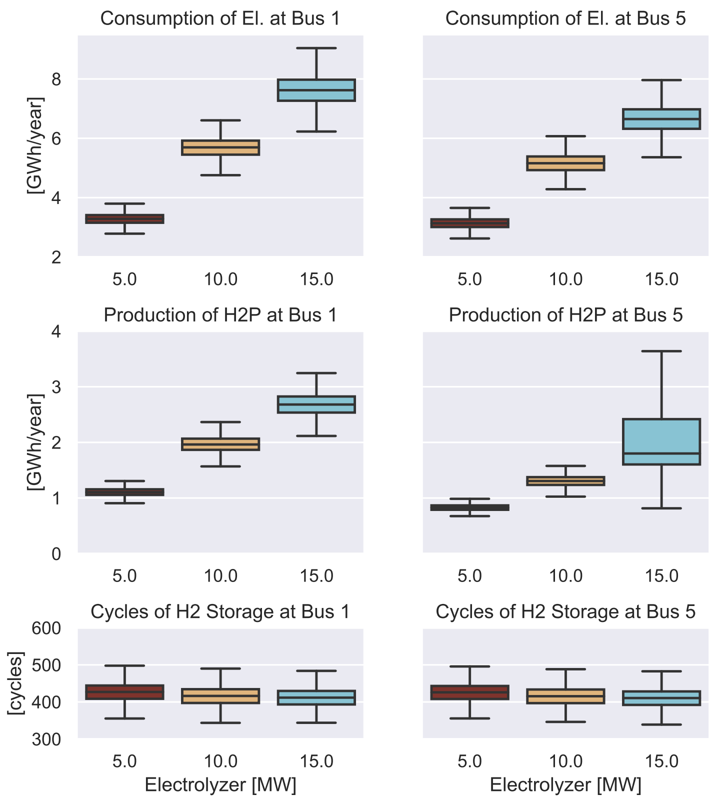

Figure 5.4: Distribution of energy consumption/production of the hydrogen assets for every electrolyzer capacity. Top row: Electrolyzers at Node 1 and 5. Mid row: H2P at Node 1 and 5. Bottom row: Equivalent number of cycles of the H2 storage - Scenario 1: modified RBTS with 200 MW conventional generators, 100 MW Wind Farm, $R = 3$, No H_2 Demand, No H_2 Imports.

5.2.2 Impact of wind farm capacity and H_2 storage units size

Sensitivity analysis of Scenario 1: 100/200 MW wind farm, 10/20/30 MW electrolyzers, H_2 storage ratio $R = 2/3/6$, no H_2 demand, no H_2 imports.

Two scenarios (WF = 100 and 200 MW) with their variants (H_2 storage ratio R = 2,3,6) are compared and studied in this section. Their adequacy results (LOLE and LOEE) are plotted and compared in Fig. 5.5. Firstly, the hydrogen system size, the hydrogen storage ratio, and the wind penetration level are favourable to the adequacy of the system. Secondly, these positive effects overlap at some point. Indeed, when 10 MW of electrolyzers are installed, having a 100 MW or a 200 MW wind farm can be equivalent in terms of adequacy if the hydrogen storage is increased by a factor 3, i.e. from 20 MWh ($R = 2$), to 60 MWh ($R = 6$). The same analysis is made when 20 MW of electrolyzers are installed, having a 100 MW or a 200 MW wind farm can be equivalent in terms of adequacy if the hydrogen storage is increased by a factor 2, i.e. from 60 MWh ($R = 3$), to 120 MWh ($R = 6$). Moreover, above 20 MW of electrolyzers installation, the test system with a 100 MW wind farm can be more reliable than with a 200 MW wind farm for a certain hydrogen storage capacity.

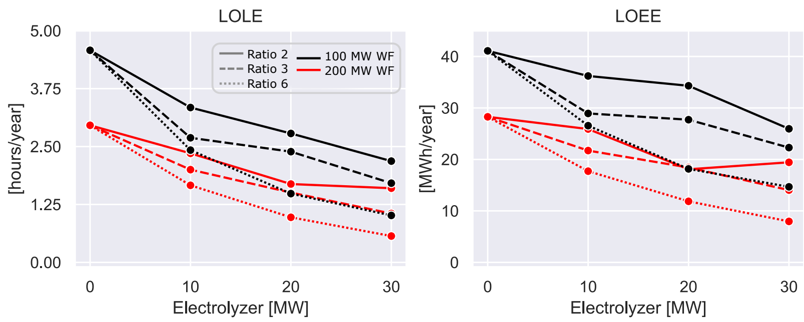

Figure 5.5: LOLE and LOEE evolution when increasing the electrolyzer capacity size for different scenarios - Scenario 1: modified RBTS with 200 MW conventional generators, 100 MW Wind Farm, $R = 3$, No H_2 Demand, No H_2 Imports.

5.2.3 Impact of H_2 demand

Scenario 2: 300 MW wind farm, 30/60/90/120 MW electrolyzers, H_2 storage ratio $R = 3$, with H_2 Demand, no H_2 Imports.

The integration of a hydrogen demand is studied in this section. Two cases are compared: a yearly flexible vs. a non-flexible hydrogen demand and the adequacy results are plotted in Fig. 5.6. For each hydrogen demand (0.75-1.5-2.25-3 kt/year), a different electrolyzer capacity (30-60-90-120 MW) is installed to satisfy this demand. The flexible case is almost not impacted by the integration of a hydrogen demand, while the non-flexible case increases its LOLE and LOEE by a factor 6 and 6.7 respetively when integrating a yearly demand of 3 ktons of hydrogen.

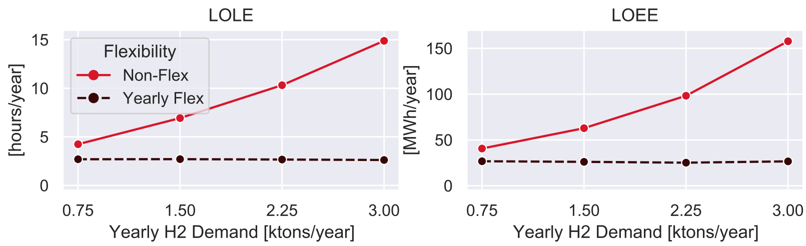

Figure 5.6: LOLE and LOEE evolution when increasing the yearly hydrogen demand - Scenario 2: modified RBTS with 200 MW of conventional generators, 300 MW Wind Farm, Varying Hydrogen System, With Hydrogen Demand, No H_2 Storage, No H_2 Imports.

5.2.4 Impact of H_2 storage with H_2 imports

Scenario 3: removal of 40 conventional generators, 100 MW wind farm, 10 MW electrolyzers, H_2 storage ratio $R = 3$, no H_2 demand, with H_2 imports.

In this section, hydrogen imports are permitted and integrated into the test system. Two cases are compared: the modified RBTS with 200 MW vs. 160 MW (removal of an extra 40 MW thermal unit) of conventional power units. Firstly, it can be observed in Fig. 5.7 that for both cases, allowing hydrogen imports enhances adequacy. The LOLE and LOEE can be reduced up to 46 and 55% for RBTS 160 and RBTS 200 MW respectively when allowing 15 MWh/h of hydrogen imports. Secondly, the distribution of the yearly hydrogen imports for the different cases is depicted in Fig. 5.8. Their is an order of magnitude between both cases. Indeed, RBTS 200 MW is already highly reliable (LOLE $\sim$ 2.5 hours) and thus only imports when lacking energy which is rare while the case RBTS 160 MW is not reliable (LOLE $\sim$ 65 hours) and thus imports much more hydrogen to produce electricity with the H2P units.

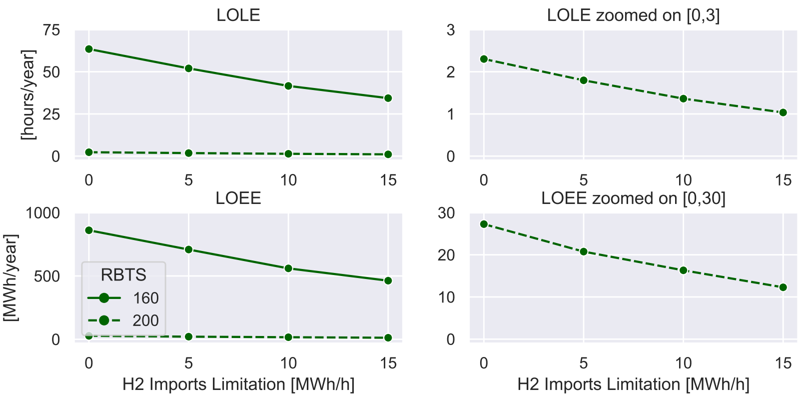

Figure 5.7: LOLE and LOEE evolution when increasing the hydrogen importation limit - Scenario 3.

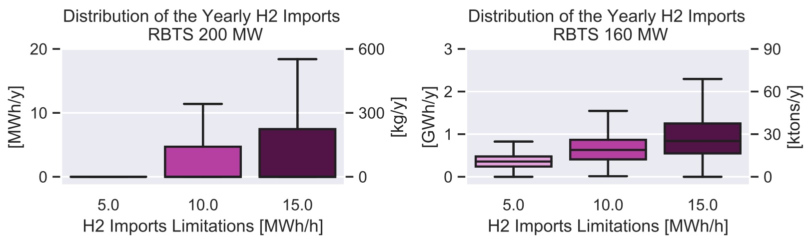

Figure 5.8: Distribution of the yearly H2 imports - Scenario 3.

5.3 Conclusion

This study presents the impact that hydrogen can have on power system adequacy assessments. To do so, a novel sequential Monte Carlo adequacy tool based on a multi-period DC optimal power flow model is developed. In this model, the hydrogen energy carrier is integrated, as well as the assets that link hydrogen to the power system, i.e. electrolyzers, and hydrogen-to-power units, and hydrogen storage units. The methodology is applied to a modified Roy Billinton Test System and different scenarios are analysed.

The first scenario highlighted the positive effect of different hydrogen system assets on the systems adequacy and operation: hydrogen systems with a power capacity of 10-20-30 MW and a hydrogen storage of 30-60-90 MWh could reduce the LOLE by 41-48-

63 % and the LOEE by 29.5-32.5-46 % respectively, and reduce the curtailment by 46-70-82 %. The results also showed that though consumption/production of electricity from electrolyzers, and H2P units increase with the capacity installed, their respective load/capacity factor decreases. Moreover, the effect of wind farm capacity, hydrogen storage ratio, and hydrogen system size was also analysed. This sensitivity analysis underlines the importance of a compromise between different installed capacity of the assets and highlights the relevance of optimising these capacities in further studies.
The second scenario analysed the effect of introducing a certain hydrogen demand, and showed that allowing some flexibility can help the system cope with this additional indirect electrical demand.
The third scenario integrated hydrogen imports. It is clearly beneficial for the power system and especially if the system does not have sufficient conventional generators, and relies on hydrogen-to-power units and hydrogen imports.

CHAPTER 6

Analysis of the Belgium 2030 case

Chapter overview

- Description of the Belgium 2030 study case with its variants.
- Application of the probabilistic adequacy tool integrating hydrogen on the Belgium 2030 study case.
- Insights on performances and challenges of the future power system.

This chapter is based on a non-peer-reviewed submitted article:

Hernandez, Aurélia and De Jaeger, Emmanuel and Vallée, François, Linking Hydrogen to Power Systems in Adequacy Computations. Available at SSRN: http://dx.doi.org/10.2139/ssrn.4898181.

In this Chapter, we apply the probabilistic adequacy tool (previously presented in Chapter 4) to the Belgium 2030 study case, exploring a range of future conditions. We analyze scenarios with and without grid extensions, as well as those featuring full versus reduced offshore wind farm developments. Additionally, we evaluate the impact of incorporating flexibility and the implications of setting a minimum local hydrogen production. Each scenario is assessed and compared to one another in terms of adequacy indicators and system operation, including production (from conventional units, offshore wind farms, and imports), production curtailment, hydrogen production (from local electrolyzers and imports), and line loadings to identify potential congestion points. By applying the tool to this future scenario, we gain detailed insights into the performances and challenges of the Belgian power system.

> The Chapter is structured according to the following sections: Section 6.1 describes the study case of Belgium in 2030 and its variants that are analyzed. Section 6.2 gives some pre-results, obtained from input data directly, without using the tool and enables to gain some insights on the results. Section 6.3 presents extensive results both from an adequacy and system operation perspective. Finally, the main conclusions are exposed in Section 6.4.

6.1 Input Data and scenarios

The probabilistic adequacy framework is applied to a realistic and complex study case, i.e. the Belgian hydrogen-electricity system in 2030. The construction of this study case is both comprehensive and intricate. To ensure clarity and avoid disrupting the flow of the main text, the complete description, including all hypotheses and detailed steps, is provided in Appendix B. This appendix serves as an essential resource, offering in-depth understanding of the methodology used to develop the final Belgian study case. Additionally, all related data can be accessed through the following GitHub repository: `aurelhern/Data4Belgium2030`. The main aspects of the study case are summarized in the following subsections.

6.1.1 Topology

Electricity and hydrogen networks are represented in Fig. 6.1, as well as the potential extension [1] of the transmission grid: Boucle du Hainaut and Ventilus (BHV) projects. This system consists in 47 nodes, 93 electrical branches, and 6 hydrogen branches (pipelines). The 380 and 220 kV level of the transmission grid is considered when analyzing Belgium. The lower voltage level 150 KV (and even lower levels down to 30 kV) are neglected. Indeed, taking into account the 150 kV level could explode the computational time as it represents a very wide system. Moreover, the 150 kV level lines have limited lengths and transmission capacity which highlights their regional and local purposes of electricity transport. The system is also connected to neighboring countries with HVDC, and HVAC transmission lines.

[1] This supposes the reinforcement of the Belgian high-voltage grid at two locations: 1) between Avelgem and Courcelles: Boucle du Hainaut project, and 2) between Slijkens and Izegem: Ventilus project. Both reinforcement, consist in 6 GW connection at 380 kV.

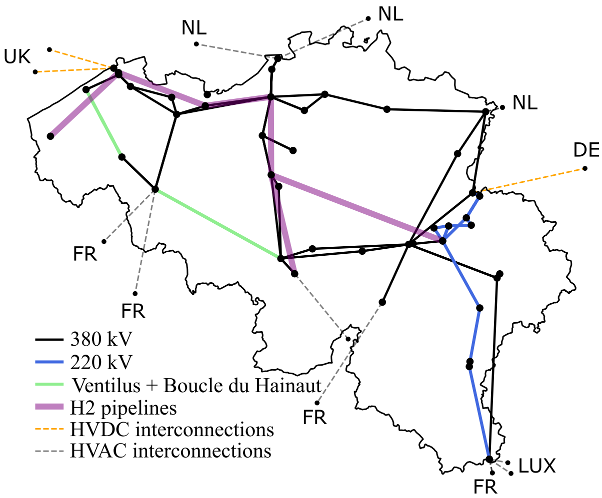

Figure 6.1: Topology of the hydrogen-electricity system in 2030.

6.1.2 Large conventional production units

The system consists in 76 large-scale conventional units. Two nuclear power units (Doel 4: 1038 MW, Tihange 3: 1038 MW) are supposed to remain in operation, and two new CCGTs (non-existing today, Seraing: 885 MW and Flémalle: 890 MW) appear in the region of Liège. Their nodal distribution is illustrated in Fig. 6.2, and their sizes depicted in Fig. 6.3. All together, they have a power capacity of 9665.1 MW. Nuclear units, as well as biomass and waste units are constrained to work at 100% of their maximum capacity, and CHPs at minimum 60% of their maximum capacity at all hours of the year, except when undergoing an outage.

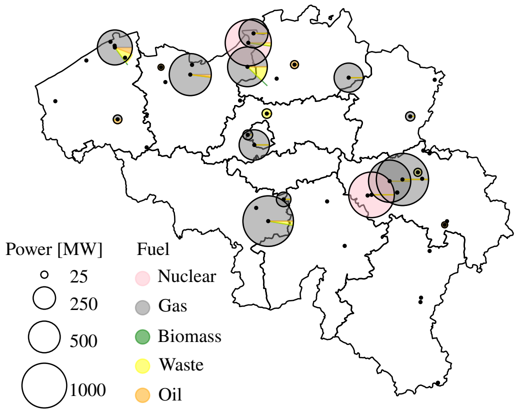

Figure 6.2: Spatial distribution of large-scale conventional generating units.

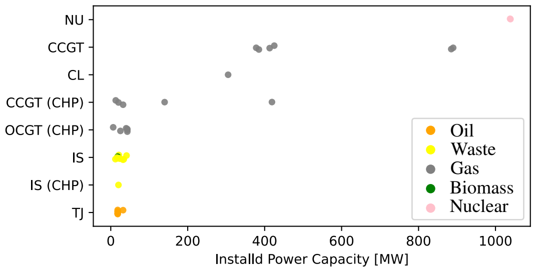

Figure 6.3: Large-scale conventional generating units sorted by types and size. Legend: CCGT (Combined Cycle Gas Turbine) - CL (Classical) - GT (Gas-Turbine) - IS (Incinerator) - NU (Nuclear) - OCGT (Open Cycle Gas Turbine) - ST (Steam Turbine) - TJ (Turbojet).

6.1.3 Offshore wind farms

In the Belgian waters, 9 wind farms next to one another (see Fig. 6.4b) are present today, with a total amount of 2262 MW of installed capacity [64].

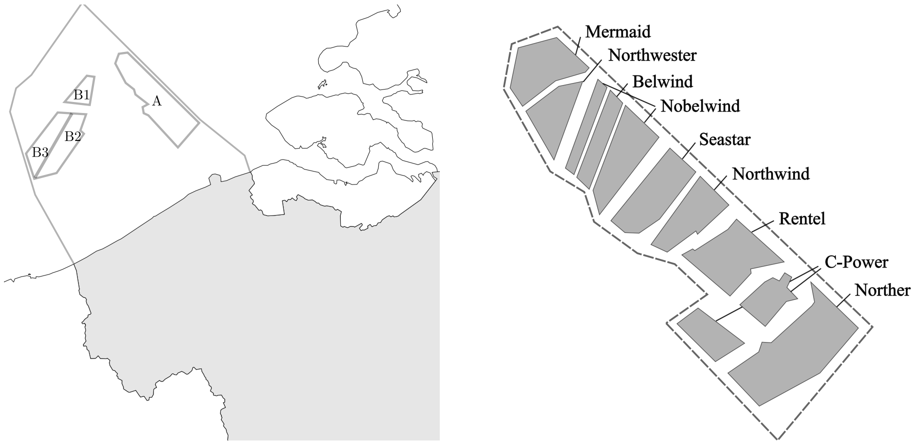

(a) Zone A: existing - Zone B: Princess Elisabeth Zone (PEZ), to be constructed.

(b) Zoom on existing wind farms (Zone A)

Figure 6.4: The planned belgian offshore wind farms for 2030.

New wind farms are planned for installation in a new area called Princess Elisabeth Zone (PEZ), as shown in Fig. 6.4a [65]. It is assumed that this new zone will consist of 15 MW wind turbines, totaling 3500 MW: a first zone with 728 MW (49 turbines), and a second and third zone with a combined total of 2782 MW (185 turbines). This will increase the existing offshore wind power capacity to 5710 MW.

Time series of offshore wind farms production are generated thanks to a machine learning-based model that accounts for aerodynamic effects (turbulence and wake effects) developed by Nguyen et al. [66]. Time series are generated for each wind farm with this methodology.

6.1.4 Imports

Belgium is studied as an isolated system and neighboring countries are not considered. It has been stated that for this study case, Belgium could import from all interconnections, at any hour during the year, except when the latter were undergoing an unplanned outage. However, annual imports [TWh], the hourly aggregated imports entering the Belgian grid [GW], and hourly imports at each interconnection [GW] are limited in energy and power respectively as detailed in the description of the equations of the adequacy tool in Section 4.2.

6.1.5 Distributed renewable energy sources

The forecast installed capacities for 2030 are 14.1 GW for photovoltaic, 5.3 GW for onshore wind turbines, and 0.151 GW for run-of-the-river hydro units according to Elia [67]. The capacity factors time series are plotted in Fig. 6.5. The annual capacity factors considered are 11.8% for photovoltaic, 24.3 % for onshore wind turbines, and 48.4 % for run-of-the-river hydroelectricity units.

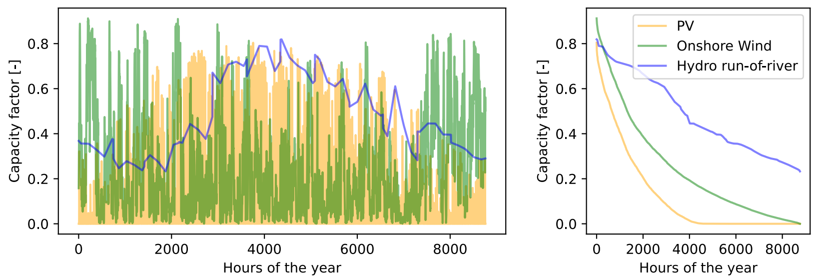

(a) Time distribution: hourly profile.

(b) Monotonic curve.

Figure 6.5: Capacity factors representations for distributed renewable energy sources.

Also the spatial distribution is considered similar as today, and is illustrated in Fig. 6.6.

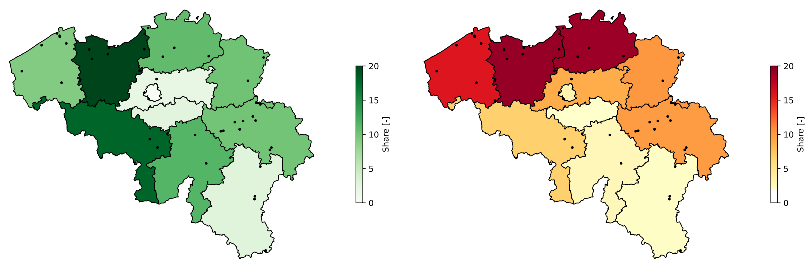

(a) Onshore wind turbines.

(b) Photovoltaic.

Figure 6.6: Spatial distribution of distributed renewable energy sources per province in Belgium in 2024.

6.1.6 Distributed small-scale conventional units

These are considered in an aggregated manner, and not individually. Small gas CHPs represent 1379 MW, small biomass units 503 MW, and small waste units 46 MW. Their production is not optimized in the model and is fixed to 60% of their installed capacity for each hour of the year.

Also, their spatial distribution is considered identical as the traditional electrical load.

6.1.7 Storage units

Two pumped-hydro storage units. Coo with a power of 1161 MW, and storage capacity of 5600 MWh. Plate-Taille, a smaller one, with a power of 144 MW, and a storage capacity of 700 MWh. The round-trip efficiency of both units is supposed to be 75%.

6.1.8 Electrolyzers

Their installed capacity is supposed 447 MW , distributed equally among the shore (Zeebrugge) , and the industrial hub: Ghent, Antwerpen, Brussels, Liège, and Hainaut (74.5 MW at each hub). They have an efficiency of 70%, and are equipped with a hydrogen storage system capable of storing 10 hours of full-load production.

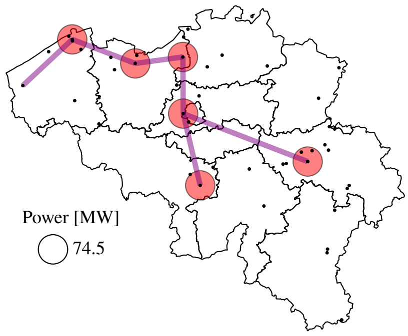

Figure 6.7: Spatial distribution of electrolyzers per node.

6.1.9 Electrical demand

The future load will consist in the traditional load (104.2 TWh/year), electric vehicles (5.1 TWh/year), and heat-pumps (2.9 TWh/year).

Traditional Load

The spatial and time distribution of the load is depicted in Fig. 6.8.

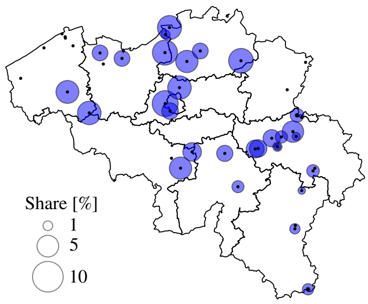

(a) Spatial distribution.

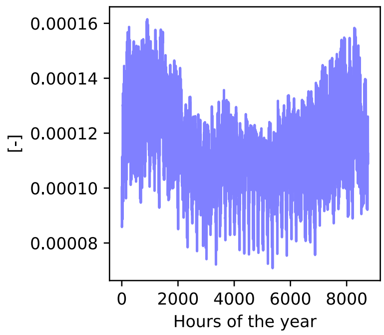

(b) Time distribution: hourly profile normalized by the annual demand.

Figure 6.8: Electrical Load excluding heat-pumps and electric vehicles.

Electric vehicles

This annual demand is distributed equally among the days of the year (~14 GWh/day). However the distribution among the hours of the day is not uniform, and depends on the EV type.

Four types of electric vehicles can co-exist depending on their charging behavior :

1. V0: natural charging profile (pre-defined time series) with a peak in the evening (plain line in Fig. 6.9)
2. V1H: delayed charging profile (pre-defined time series) with a peak in the middle of the night (dashed line in Fig. 6.9)
3. V2H: bi-directional charging profile (pre-defined time series) where the EV has a battery behavior, charging during the night and restituting during the evening (dashdotted line in Fig. 6.9)
4. V1M: smart charging profile (result of the optimisation) concerning EVs that are flexible and produce optimally during the day. The share of the smart EV fleet connected to a flexible charger during the day is not constant and represented in Fig. 6.10.

Their nodal distribution is considered to be similar to the photovoltaic distribution. Also, flexible chargers are supposed to have a power of 7 kW.

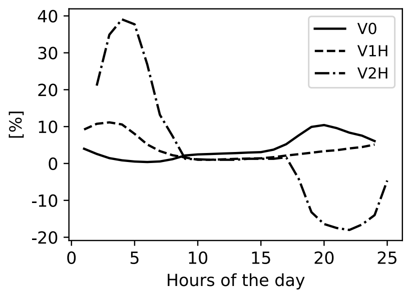

Figure 6.9: V0 (classical) and V1H (smart) charging profiles [67].

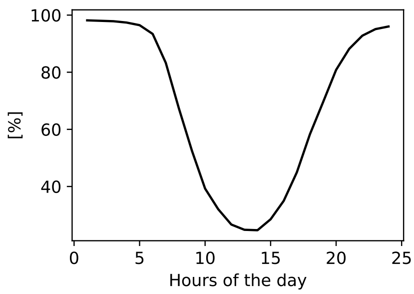

Figure 6.10: Share of the flexible EV fleet connected to a flexible charger during the day [67].

Heat-pumps

This annual demand is distributed among the different months as shown in Fig. 6.11 and the distribution among the hours of the day depends on the HP type.

They are splitted into 3 categories depending on their behaviors:

1. HP0: natural profile (pre-defined time series) with a peak in the morning, and in the evening (plain line in Fig. 6.12)
2. HP1H: pre-heated profile (pre-defined time series) with an additional peak (compared to HP0) during the day, which reduces the evening peak (dashed line in Fig. 6.12)
3. HP1M: smart profile (result of optimisation) concerning HPs that are flexible and produce optimally during the day.

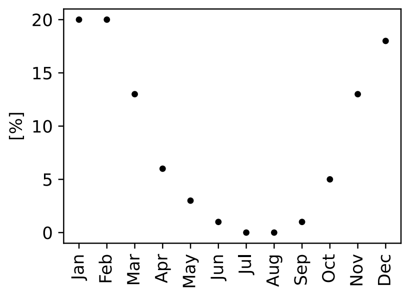

Figure 6.11: Monthly distribution of annual heat-pump demand inspired by [67] (simplification applied)

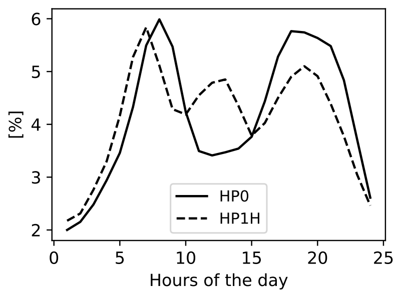

Figure 6.12: HP0 (classical) and HP1H (smart) charging profiles [67].

Their nodal distribution is considered to be similar to the photovoltaic distribution.

6.1.10 Hydrogen demand

The yearly demand is set to 800 [kt/year] = 26.6 [TWh_{H2}/year]. Its spatial distribution is illustrated in Fig. 6.13.

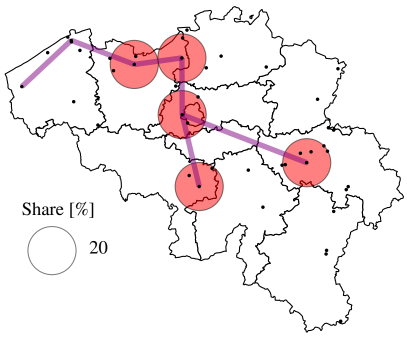

Figure 6.13: Spatial distribution of hydrogen load per node.

6.1.11 Hydrogen imports

Hydrogen imports are unlimited and the different interconnections are shown in Fig. 6.14.

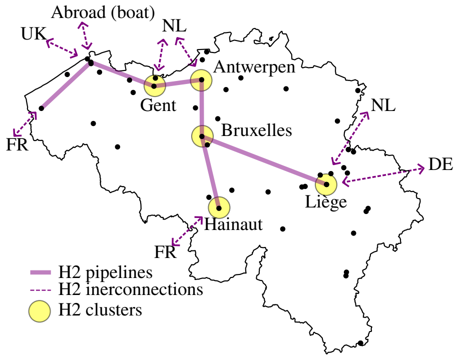

Figure 6.14: H_2 pipeline network with its corresponding clusters.

6.1.12 Additional flexibility

Three different types of flexibility means will be tested in this study case: batteries, load shifting, and flexible heat-pumps and electric-vehicles.

- **Batteries:** A total installed power capacity of 2982 MW, being able to charge 3.5 hours at full-load (10 464 MWh) and distributed among the six industrial hubs.
- **Load shifting:** A daily quantity of 18 630 MWh can be shifted daily with a power of 1000 MW maximum.
- **Flexible EVs:** A share of 30 % has a fixed natural charging profile (V0: peak in the evening), 45 % has a fixed delayed charging profile (V1H: peak in the middle of the night), 20% has a charging profile optimized by the model (V1M: constraint on daily demand), and 5% has a fixed bi-directional charging profile (V2H: battery behavior, charging during the night and restituting during the evening).
- **Flexible HPs:** A share of 59 % has a fixed natural charging profile (HP0: peak in the morning and in the evening), 31 % has a fixed delayed charging profile (HP1H: peak in the morning, middle of the day, and in the evening), and 10% has a charging profile optimized by the model (HP1M: constraint on daily demand).

6.1.13 Scenarios

Two main uncertainties are present in this study case: the transmission grid and offshore wind farm potential extensions. For this reason, we choose to analyze the three following scenarios:

1. **no BHV - w2800:** Reduced offshore wind farm extension of 2800 MW, and no grid extension.
2. **no BHV - w3500:** Full offshore wind farm extension of 3500 MW, and no grid extension.
3. **BHV - w3500:** Full offshore wind farm extension of 3500 MW, with the grid extension.

Moreover, for each scenario a variant is studied with/without additional flexibility (described in Section 6.1.12).

6.2 Pre-results

Analyzing pre-results is a good way to generate insights on the results that are obtained after simulating a scenario. These pre-results are an estimation of the maximum yearly available production and a comparison with the yearly demand. In Fig. 6.15 the available yearly production is shown next to the yearly demand. Although, in both cases, the production is a little greater than the demand, it can be observed in Fig. 6.16 that imbalance appears which will imply the intervention of flexibility and imports to match the hourly demand. Moreover, it is to be noted that network constraints are not considered and might cause difficulties.

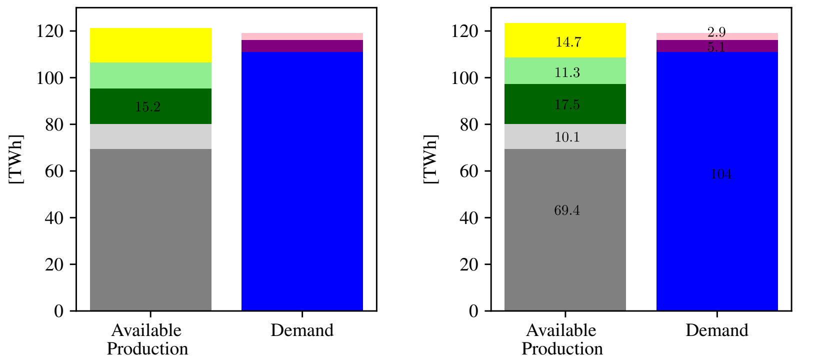

(a) Offshore wind power extension = 2800 MW

(b) Offshore wind power extension = 3500 MW

Figure 6.15: Yearly potential production vs. yearly demand. Legend: Large conventional units - Distributed small conventional units - Offshore wind power - Onshore wind power - PV - Traditional load - EVs - HPs . Note: the offshore production is the only difference between both scenarios in this figure. Hypothesis: yearly equivalent availability of large conventional units = 82 %, of offshore wind farms = 77.6 % - yearly capacity factor of offshore wind farms = 44 %, of onshore wind farms = 23.3 %, of photovoltaic panels = 11.8 %, of distributed small conventional units = 60 %.

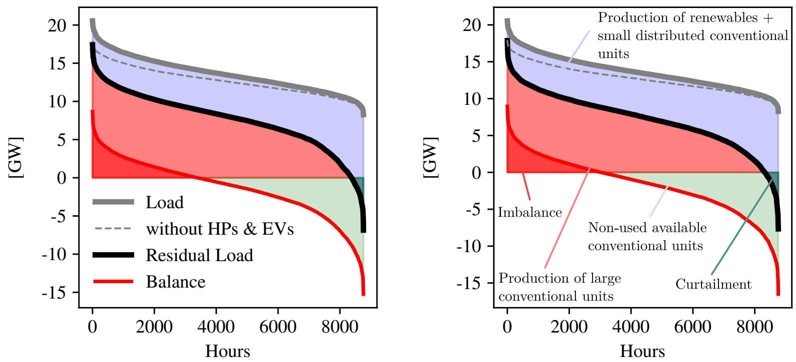

(a) Offshore wind power extension = 2800 MW

(b) Offshore wind power extension = 3500 MW

Figure 6.16: Monotonic curve of the electrical balance. Notes: Residual Load = Load - PV - Onshore/Offshore Wind Power - Hydro Power - Distributed Generation from small conventional units, Balance = Residual Load - Production from large conventional units available. Imbalance will have to be fulfilled thanks to imports and flexibility.

6.3 Results

6.3.1 Adequacy indicators

In Fig.6.17, it is clear that allowing for flexibility into the system for each scenario enhances its adequacy. The mean values, i.e. EENS, and LOLE are summarized in Table 6.1. When adding flexibility, the EENS drops in all scenarios, reaching values between 0.002 and 0.03 [GWh]. When observing the LOLE, and having in mind the adequacy threshold for Belgium of 3 hours, we can conclude that adding flexibilities, can for all three scenarios, make the system adequate (LOLE $<$ 3 hours), droping from 4.71-4.98 [hours] to 0.05-0.09 [hours].

Although flexibility enhances the adequacy indicators (the smaller the better), the size of the offshore wind farm extension in the range of 2800-3500 (+700) MW does not affect the adequacy indicator. The reason is that hours with unserved demand (ENS) are usually characterized by a very low renewable production (offshore wind and irradiation being very low), and a high load. During these hours, no matter the size of the offshore wind farm, the production is often close to zero.

It could have been a possibility that the grid and wind expansion had an impact on the adequacy indicators. When observing the scenarios that consider additional flexibilities, $EENS_{BHV-w3500} < EENS_{noBHV-w3500} < EENS_{noBHV-w2800}$ which might lead us to believe that grid and wind expansion have very little impact. However, when observing the scenarios that do not consider additional flexibilities, the indicators do not follow the expected order in terms of value. This leads us to refute the hypothesis that grid and wind expansions have (very little) impact. It can be concluded that the differences in EENS between scenarios are due to the randomness of outages that occurred more or less frequently, or were more or less severe, even though the convergence threshold was reached.

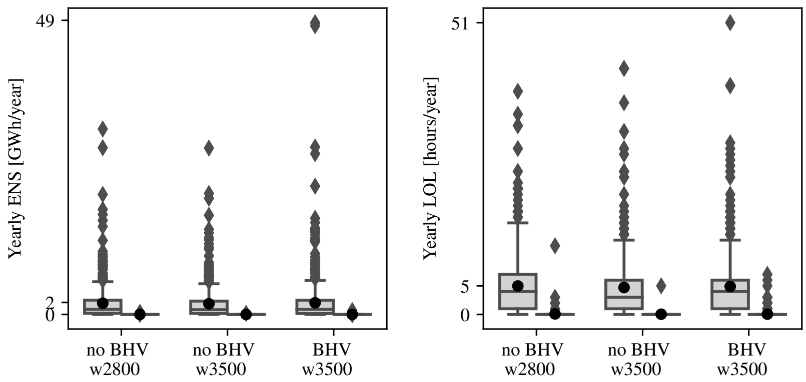

(a) (b)

Figure 6.17: Distribution of the energy-not-served (a) and loss-of-load (b) for each scenario comparing cases without flexibility [ ], and with flexibility [ ].

Table 6.1: Adequacy indicators fo each scenario.

Scenario	Flexibility	LOLE [hours/year]	EENS [GWh/year]
no BHV - w2800	No	4.98	1.864
	Yes	0.08	0.021
no BHV - w3500	No	4.71	1.781
	Yes	0.07	0.003
BHV - w3500	No	4.88	1.941
	Yes	0.05	0.002

The correlation between the LOL, and ENS is plotted in Fig. 6.18. A Pearson correlation coefficient of 0.859 is observed. In this figure, it is clear that, for the same ENS, different LOL can be obtained. Moreover, the objective function of the MP-DC-OPF minimizes the ENS. For this reason, the Monte Carlo loop is based on the convergence of the average of the ENS indicator.

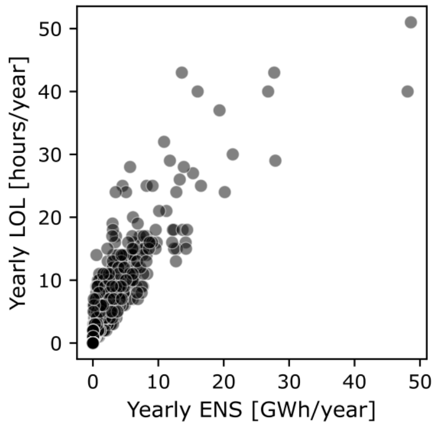

Figure 6.18: Correlation between the loss-of-load and loss-of-energy for every Monte Carlo year of every scenario. The Pearson correlation coefficient is 0.859.

6.3.2 Electrical Production

Figure 6.19 plots the distribution of the annual production of the conventional generators, and the corresponding capacity factors. With flexibility, the total production of generators reduces by 1.3-1.4 TWh in average (-2.3-2.5%). Indeed, flexibility permits to maximize the use of renewable production by shifting the production/demand to more convenient hours, and thus reduce a little the production of conventional units. This leads to a general decrease of the overall capacity factor of the generators of 1-2 %. Moreover, allowing a full extension of the offshore wind farms, reduces again the production of generators by 1.1-1.2 TWh, and if allowing the grid extension, an additional 0.3-0.4 TWh can be saved.

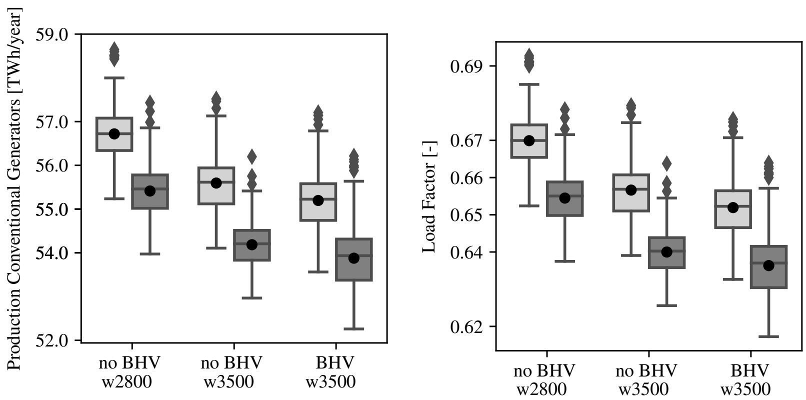

Figure 6.19: Distribution of the total production of conventional generators (a), and the corresponding equivalent capacity factor (b) for each scenario comparing cases without flexibility [ ], and with flexibility [ ].

Table 6.2: Average production of large conventional units for each scenario

Scenario	Flexibility	Production [TWh/year]
no BHV - w2800	No	56.7
	Yes	55.4
no BHV - w3500	No	55.6
	Yes	54.2
BHV - w3500	No	55.2
	Yes	53.9

The operation of individual generators can also be analyzed. For the sake of clarity, and because all scenarios are quite similar in terms of individual behavior, only the scenario with grid extension (BHV), a wind farm extension of 3500 MW (w3500), and with the integration of flexibilities is illustrated.

The distribution of their yearly capacity factor is represented in Fig 6.20. Some units work very close to 100% on average, such as the nuclear units (13: Doel, 65: Tihange), the incinerators (5,6,8-10,29,39-42,56,32), and one classical biomass CHP unit (60). Nuclear units and units fueled by waste and biomass are constrained in the model to operate at their maximum power ($P_{min} = P_{max}$) except when an outage occurs. Also the operation of CCGTs (that are not CHPs) varies from one unit to another and reaches between 31.5% and 79% on average. The higher capacity factors (2: Amercoeur, 27: New Seraing, 30: New Flémalle, 66: T-Power) have higher efficiencies (58-61%). The classical unit which burns blast furnace gas, and converter gas operates at a low rate of 4% because its efficiency is lower (42%). Also, CHPs are constrained in the model to operate at minimum 60% of their max power ($P_{min} = 0.6P_{max}$). For this reason, they tend to have an average capacity factor around 60 % and no more except for four of them: either because they are CCGTs with great efficiencies (36,70), or because they are units fueled with biomass or waste (32,60) constrained by the model to operate at their maximum value. Finally, turbojets do not operate during the year in this scenario, and OCGTs operate during a negligeable amount of hours (<17 hours for 17: Angleur, and <288 hours for 21: Ham), except for Seraing which operates at 22% as it has a good efficiency (52 %).

The yearly energy production can also be observed in Fig. 6.21, and is complementary to the Fig. 6.20 because it outlines the importance of a unit and illustrates well which units are the big producers. The nuclear power plants (13: Doel, 65: Tihange), and the two new CCGTs in Liège (27: New Seraing, 30: New Flémalle) produce on average 29 TWh of electricity. The other CCGTs produce individually on average between 1 and 3 TWh. Although CHPs are numerous and operate over 60 % on average, due to their limited size, they produce a limited amount of electricity. On average, they individually produce less than 1 TWh except for Zandvliet (70) which produces on average almost 4 TWh because it is a big unit with a high capacity factor. All together, CHPs produce 9 TWh. Although incinerators run at 100%, they produce only a small part of the electricity: 2.4 TWh (non-chps) and 0.2 (CHPs). Finally, turbojets do not produce and OCGTs produce 0.6 TWh. The aggregated production by type of units is represented in Fig. 6.22. The figure illustrates also the scenario with a reduced offshore wind farm extension of 2800 MW. In both cases, the majority of the production is assured by CCGTs, and nuclear power. And contrary to what one might think (due to the large number of relatively small units), IS and CHPs represent as well a non-negligible production. The major difference between scenarios is that with a reduced wind farm extension of 2800 MW, the CCGTs compensate for that energy production.

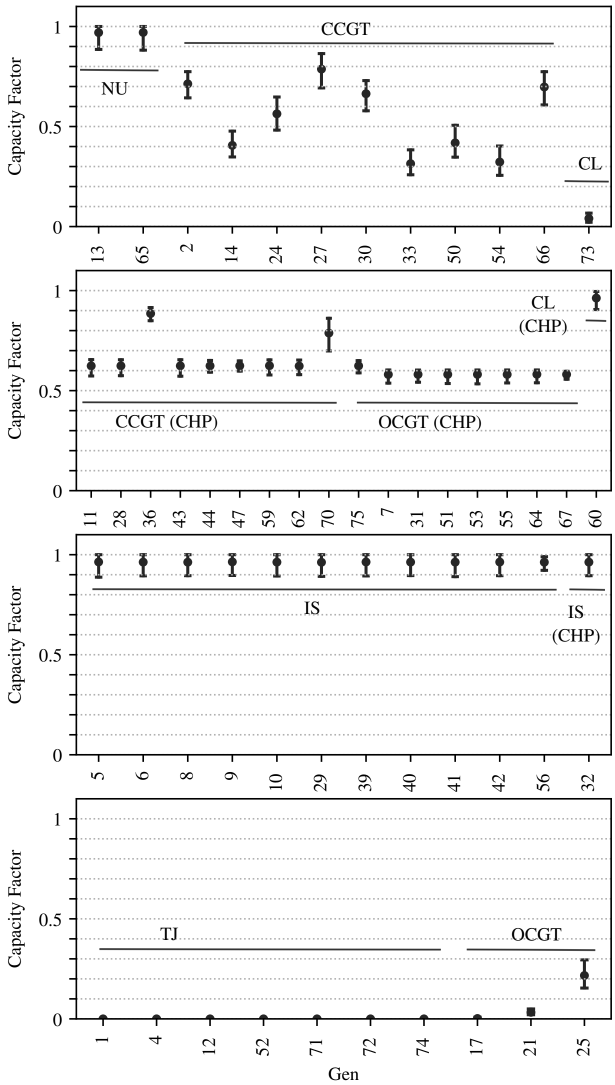

Figure 6.20: Capacity Factors of the generator in the future Belgium 2030 system resulting from the optimization. They are sorted by type: CCGT (Combined Cycle Gas Turbine) - CL (Classical) - GT (Gas-Turbine) - IS (Incinerator) - NU (Nuclear) - OCGT (Open Cycle Gas Turbine) - ST (Steam Turbine) - TJ (Turbojet).

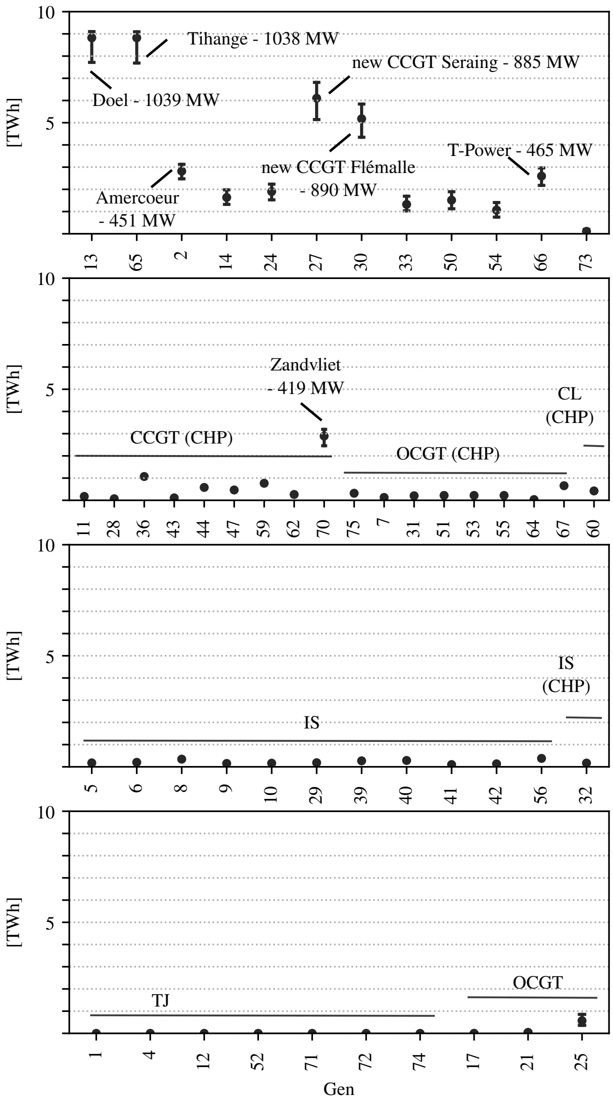

Figure 6.21: Production of conventional generators in the future Belgium 2030 system resulting from the optimization.

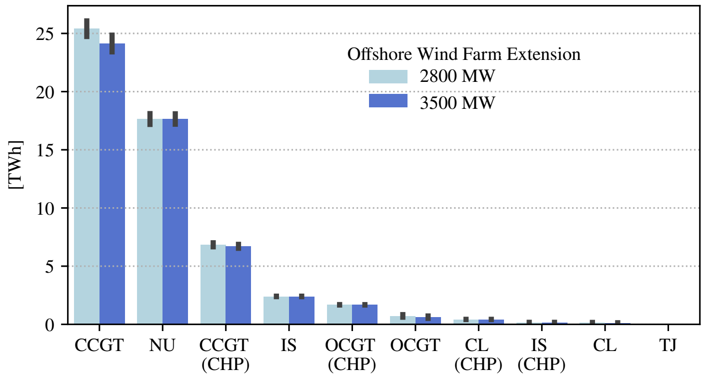

Figure 6.22: Production of conventional generators by type of units. Comparison of two scenarios: no grid extension (no BHV) - with flexibilities (all flex) - offshore wind farm extension of 2800 MW (w2800) vs. grid extension (BHV) - with flexibilities (all flex) - offshore wind farm extension of 3500 MW (w3500) .

6.3.3 Imports

In all scenarios, imports are solicited to their maximum value, i.e 12.36 TWh/year (see Fig. 6.23). The cost of imports are interesting for the system. However, it still has to decide when to import, as the annual and hourly quantities are limited. The system mainly imports when irradiation is low, storages are empty, and load is high.

6.3.4 Offshore wind farms

The production of offshore wind farms is 15.8 TWh and 17.5 TWh with the 2800 and 3500 MW extension respectively and represented in Fig. 6.24. Knowing that the total offshore wind farm is 5010 MW (2800 MW extension), or 5710 MW (3500 MW extension), the overall power factor, taking into account turbine outages, and the variability of wind speed, is of 35-36%. And knowing that the power factor of the offshore wind farms without outages, is 44.5 %, considering turbines outages, can decrease the estimated production by 22.4 %.

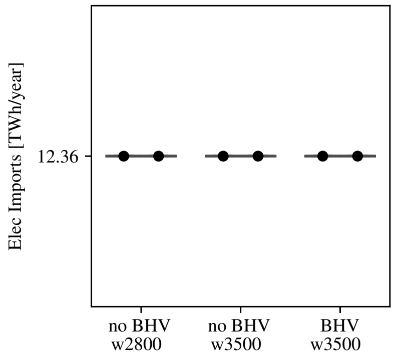

Figure 6.23: Distribution of the total imports for each scenario comparing cases without flexibility [ ], and with flexibility [ ].

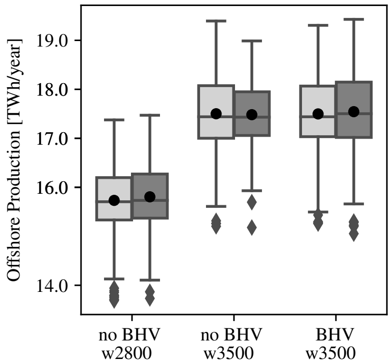

Figure 6.24: Distribution of the total production of offshore wind farms for each scenario comparing cases without flexibility [ ], and with flexibility [ ].

6.3.5 Curtailment

Curtailment usually occurs when the renewable production is high (especially PVs), and demand is low. When integrating flexibility, renewable-based production curtailment is decreased (see Fig. 6.25) for all scenarios. The peak curtailment (see Fig. 6.26) also decreases when introducing flexibility. While grid extension has an impact on the yearly curtailment, it does not seem to have an impact on the peak curtailment.

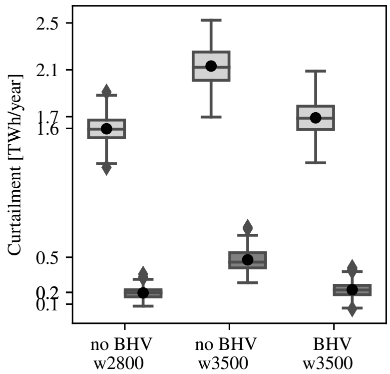

Figure 6.25: Distribution of the total production curtailment for each scenario comparing cases without flexibility [], and with flexibility [].

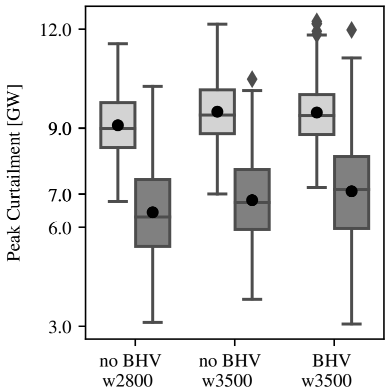

Figure 6.26: Distribution of the peak production curtailment for each scenario comparing cases without flexibility [], and with flexibility [].

6.3.6 Hydrogen

The system has a hydrogen demand of 800 kt/year (26.7 TWh_{H_2}). The majority is imported. Imports are represented in Fig. 6.27, and slightly lower when flexibility is introduced, and the extension of the grid is established. In all scenarios, the imported share represents between 96.4 and 97.1 %.

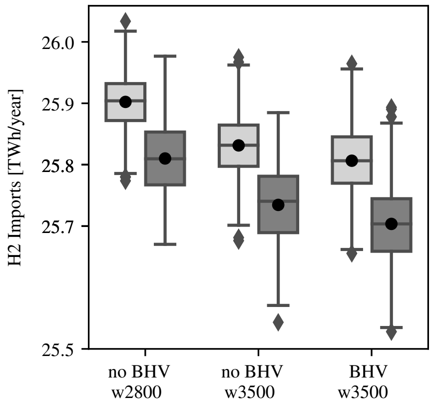

Figure 6.27: Distribution of the hydrogen imports for each scenario comparing cases without flexibility [ ], and with flexibility [ ].

The rest of the hydrogen demand (2.9-3.6 % depending on the scenario), is produced by electrolyzers. They tend to produce a higher share when allowing flexibility in the system and when integrating the grid extension. Their utilization factor is between 28 and 35 %.

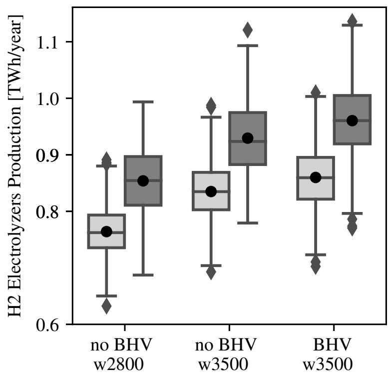

Figure 6.28: Distribution of the hydrogen production from electrolyzers for each scenario comparing cases without flexibility [ ], and with flexibility [ ].

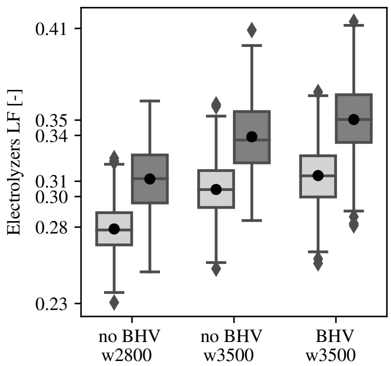

Figure 6.29: Distribution of the electrolyzers load factor for each scenario comparing cases without flexibility [ ], and with flexibility [ ].

The behavior of electrolyzers can be observed in detail for a random Monte Carlo year in Fig. 6.30. It can be observed that hydrogen production mainly happens when renewable energy sources is high, i.e. during mid-day, and during the warmer seasons, or when a lower load is observed, i.e. at night with wind power production. The mid-day, and seasonal pattern is due to solar production, and is clearly observable in Fig. 6.30.

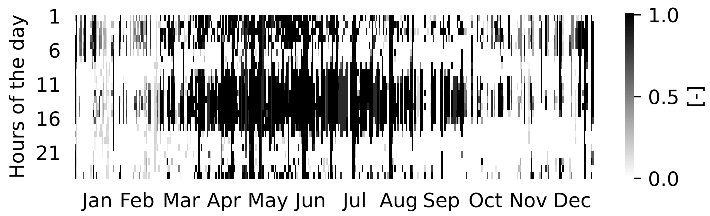

(a) Operation of electrolyzers

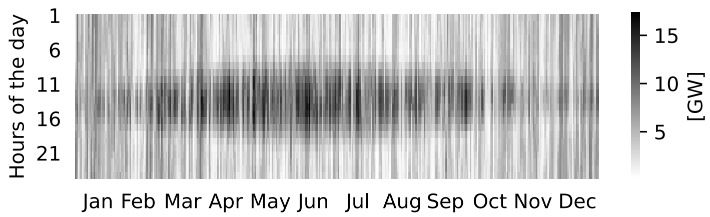

(b) Production of renwable energy sources

Figure 6.30: Hourly results of a random Monte Carlo year. Scenario: Grid extension (BHV) - with flexibilities - offshore wind farm extension (w3500).

In a more distant future like 2050, a deeper integration of RES is foreseen to be installed in order to support a carbon-neutral system. Table 6.3 summarizes the projected and optimal deployments for the Belgian system in 2050, based on three studies, and their respective scenarios. Although all scenarios indicate an increase in capacity, the expansion of photovoltaic is expected to be particularly significantly exceeding that of both onshore and offshore wind. This is primarily due to Belgium's geographic limitations, which restrict the installation of wind turbines.

As a result, the share of PV production in the aggregated renewable energy sources profile is likely to be dominant, way-more than it is for the 2030 scenario. Very high midday power peaks are expected, and the system will try to maximize the operation of electrolyzers during these high-irradiation periods. It is important to note that although for the 2030 scenarios, electrolyzers operation seem to align both with solar (midday) and wind (night) generation, it is very likely that in 2050, due to the overwhelming integration of PV, electrolyzers operation align solely with PV production.

Table 6.3: Deployments of renewable energy sources for 2050 - installed capacity [GW]

Study	Scenario	Wind offshore	Wind onshore	PV
Elia - Roadmap to Net-zero 2050 [3]	BAU x 1.5	5	6	30
	BAU x 3	6	8	40
	BAU x 4	8	9	50
Elia - Belgian electricity system blueprint for 2035-2050 [68]	low	5.8	7.6	29.5
	central	8	9.6	41.5
	high	-	13.6	65.5
	very high	-	-	97.5
X. Rixhon [6]	REF	6	10	59.2
	SMR[a]	6	10	59.2
	Minimum 2050	5	6	29.5
	Maximum 2050	8	13.6	97.5
	2024	2.3 [67]	3.5 [67]	10.4 [69]

6.3.7 Line loadings

Depending on the scenario, the line loadings can vary quite a lot. The average annual loading differs mainly due to the extension of the grid and not due to the wind farms extension. Thus, for the sake of clarity, only the scenarios with an offshore wind farm extension of 3500 MW are illustrated in Fig. 6.31.
Moreover, from Fig. 6.31, it can be observed that in both scenarios, the lines in the eastern part of the country (Liège area) are highly used. The other parts of the grid do not seem to be as congested but the indicator used is an average line loading and does not show if a line is highly loaded during contingencies, or during a certain period of the year. Indeed, those event are hidden behind the average, and a further look on a particular year could give more insights on how lines are used from an hour resolution. The main differences in the average annual loadings between both scenarios is depicted in Fig. 6.32. A blue line means that the average annual line loading decreases when extending the grid and if red, it increases. The lines in dots are the extension of the grid. It is clear that the existing lines at the shore are relieved when extending the grid. The extension of the grid will bring a new path for wind power transport from the shore.

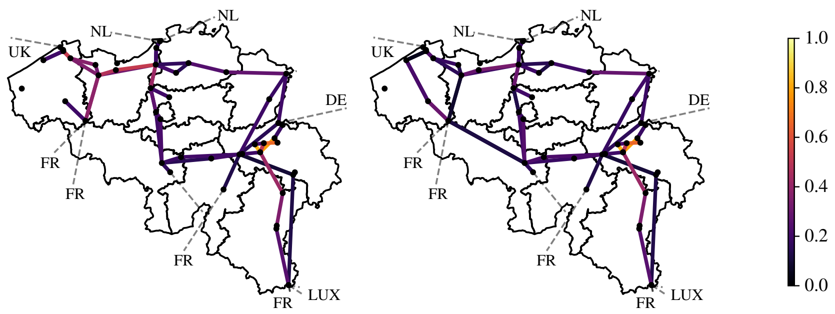

(a) Scenario: No grid extension (no BHV) - with flexibilities - offshore wind farm extension of 3500 MW.

(b) Scenario: Grid extension (BHV) - with flexibilities - offshore wind farm extension of 3500 MW.

Figure 6.31: Average annual line loading.

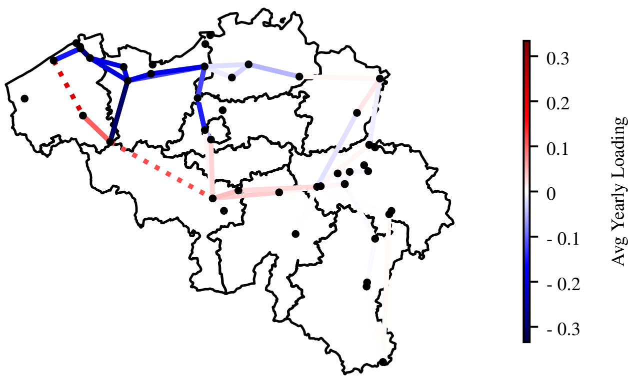

Figure 6.32: Difference in annual line loading when extending the grid (with flexibilities and offshore wind farm extension of 3500 MW.)

To grasp some insights on what is behind an annual line loading factor, let's take a closer look at the results of a random Monte Carlo year. In Fig. 6.33, the congestions are illustrated. In this analysis, a congestion is considered to be a loading > 90%, and on this figure, the lines who have more than 50 hours of congestion are plotted for sake of clarity. The names of the concerned branches are referenced in Table 6.4. In Fig. 6.34 are highlighted for each scenario, the lines where congestions appear during the year. In the scenario without the extension, we observe congestions on the lines close to the shore. This line is a set of 4 lines 4x1076MW=4304 MW and knowing that the offshore wind farm has a installed power of 5710 MW, and that this line is the only path to the internal grid, it seems logical to see overloadings appear. Congestions re-appear a bit further near Gent. Looking at the scenario with the grid extension, all these overloadings near the shore disappear. The remaining overloadings are similar in both scenarios. Liège area is highly overloaded. And some lines which connect our country to our neighbors are highly used as well: the one to the Netherlands (via Van Eyck), to France (via Achene), and to Luxemburg (via Aubange).

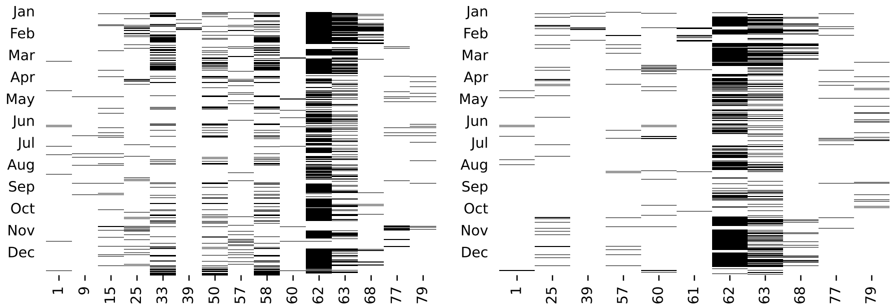

(a) Scenario: No grid extension (no BHV) - with flexibilities - offshore wind farm extension of 3500 MW.

(b) Scenario: Grid extension (BHV) - with flexibilities - offshore wind farm extension of 3500 MW.

Figure 6.33: Hourly line loading of a random Monte Carlo year. Legend: black → > 90%, and white → < 90%.

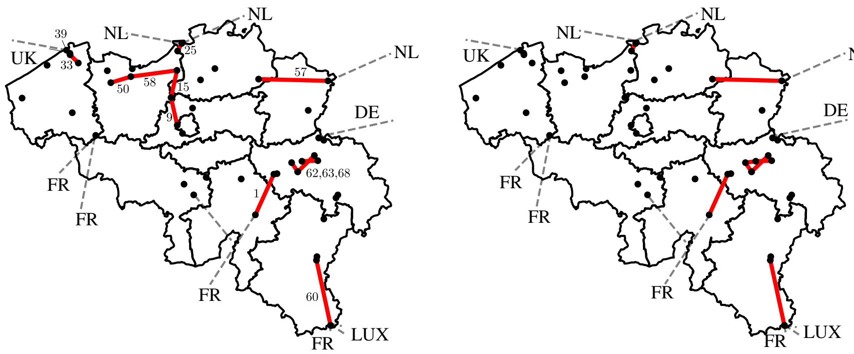

(a) Scenario: No grid extension (no BHV) - with flexibilities - offshore wind farm extension of 3500 MW.

(b) Scenario: Grid extension (BHV) - with flexibilities - offshore wind farm extension of 3500 MW.

Figure 6.34: Highlight of lines that experiment congestions (defined in this analysis as an hourly loading > 90%) during a random Monte Carlo year.

Table 6.4: References of the branches experiencing high line loadings.

Branch	Branch Name
1	ACHENE-GRAMME
9	BRUEGEL-BUGGENHOUT
15	BUGGENHOUT-MERCATOR
25	DOEL-ZANDVLIET
33	GEZELLE-MAERLANT
39	GEZELLE-NEMO
50	HORTA-RODENHUIZE
57	MEERHOUT-VAN EYCK
58	MERCATOR-RODENHUIZE
60	AUBANGE 220-VILLEROUX
62	AWIRS-RIMIRE 220
63	JUPILLE-RIMIERE 220
68	ROMSEE-SERAING
77	LIXHE 380-LIXHE 220
79	RIMIERE 380-RIMIERE 220

6.3.8 Impact of hydrogen on the system

In the previous studies, there were no constraints on the operation of electrolyzers, and hydrogen imports were unlimited. The system thus had the choice between importing or locally producing hydrogen to satisfy the annual demand at the lowest cost. Depending on the scenario, the system was producing a small part of the annual demand locally (2.9-3.6 %), operating the 447 MW electrolyzers at an annual load factor of 28-35 %. Analyzing the previous results, one might ask, is this decision made to avoid energy-not-served and maintain reliability, or because importing is cheaper than producing locally during the rest of the time? In this section, we study inter alia the impact of setting a minimum annual load factor for the electrolyzers.

This study is performed on the scenario with grid and offshore extension, considering all flexibilities (BHV - w3500 - all flex). Four variants of this original scenario will be studied: one where hydrogen demand is removed, and three others where electrolyzers have a minimum annual load factor set to: 70, 80, and 90 %. The three last variants result in imposing an additional electrical demand of 2.74, 3.13, 3.52 [TWh/year] respectively corresponding to the following hydrogen production: 1.92, 2.19, 2.47 [TWh_{H_2}/year]. For the scenarios that have a minimum annual load factor set to the electrolyzers, the following constraint has to be added to the optimization problem:

$$\frac{\sum_{t=1}^{8760}\sum_{e=1}^{n_e} P_{el}(e,t)}{8760 * \sum_{e=1}^{n_e} p_{el,max}(e)} \geq lf_{el,min,year} * \alpha_{el,tot,year} \tag{6.1}$$

with

$$\alpha_{el,tot,year} = \overline{\alpha_{el}(e,t)} = \frac{\sum_{t=1}^{8760}\sum_{e=1}^{n_e} \alpha_{el}(e,t)}{8760 * n_{el}} \tag{6.2}$$

being the average availability over the year of electrolyzers. The inequality in (6.1) constrains the electrolyzers to operate at a minimum annual load factor of $lf_{el,min,year}$ considering that electrolyzers can undergo outages.

The impact of adding hydrogen on the power system is examined in terms of adequacy assessment and system operation. The results show that in terms of adequacy, removing the hydrogen demand or constraining the electrolyzers to operate at a rate between 70 and 90 % does not impact the LOLE, or the EENS compared to the original scenario. This is illustrated in Fig. 6.35a and 6.35b. Two conclusions can be drawn. Firstly, because the original system was only producing hydrogen locally when convenient, and would never put itself in difficulties, removing the hydrogen demand does not enhance the adequacy. Secondly, the original scenario was quite reliable, as when imposing a certain local production, the system is not affected in terms of adequacy. It can be thus stated that the low rate operation of electrolyzers in the original scenario is a choice to lower the costs rather than due to insufficient resources.

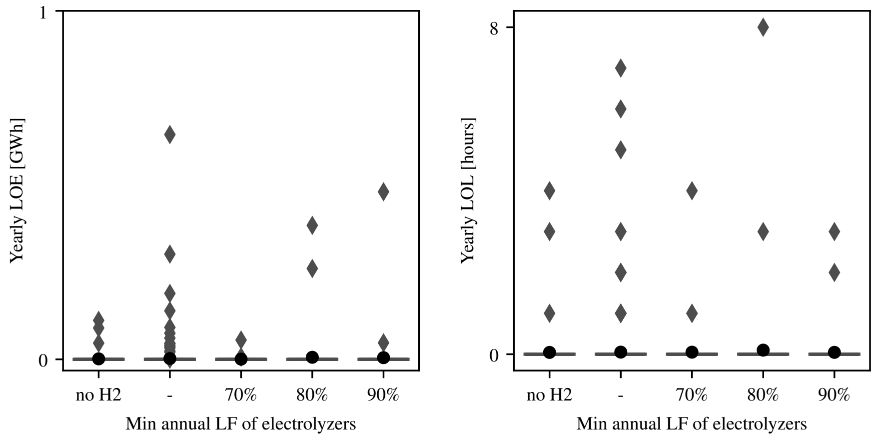

(a)

(b)

Figure 6.35: Distribution of (a) the energy-not-served and (b) the loss-of-load for variants of the scenario with grid and offshore wind farm extensions, and considering flexibility. The variants: (i) no H2: no hydrogen demand, (ii-iv) minimum annual load factor of electrolyzers set to 70, 80, and 90 %.

In terms of operation of the system, the main changes are observable in the production of conventional units. This is illustrated in Fig. 6.36. When removing the hydrogen demand, their production decreases by $\sim$ 1 TWh. Indeed, in the original scenario integrating a hydrogen demand, local production was occurring when: there was excess of must-run production, or when it was more economical to increase a slightly the conventional production, rather than pay the import price of hydrogen. Thus, when removing the hydrogen demand, this additional production disappears and the yearly production decreases. In the three other variants where a local production is imposed, conventional production increases by $\sim$ 1-2 TWh.

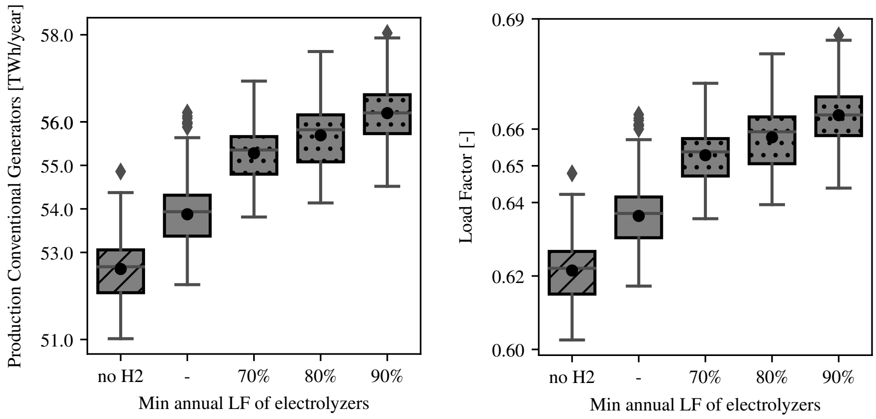

(a) (b)

Figure 6.36: Distribution of (a) the total production of conventional generators and (b) the corresponding equivalent capacity factor for variants of the scenario with grid and offshore wind farm extensions, and considering flexibility. The variants: (i) no H2: no hydrogen demand, (ii-iv) minimum annual load factor of electrolyzers set to 70, 80, and 90 %.

Apart from that, imports are kept at their maximum for all variants and the original scenario itself. Small changes appear in the curtailment, when removing the hydrogen demand. This is illustrated in Fig. 6.37. Indeed, when removing the hydrogen demand, excess production is no longer absorbed by the electrolyzers. The curtailment is not impacted by the fact that electrolyzers have a minimum annual load factor. Indeed, this characteristic does not affect the flexibility that electrolyzers can bring to the system.

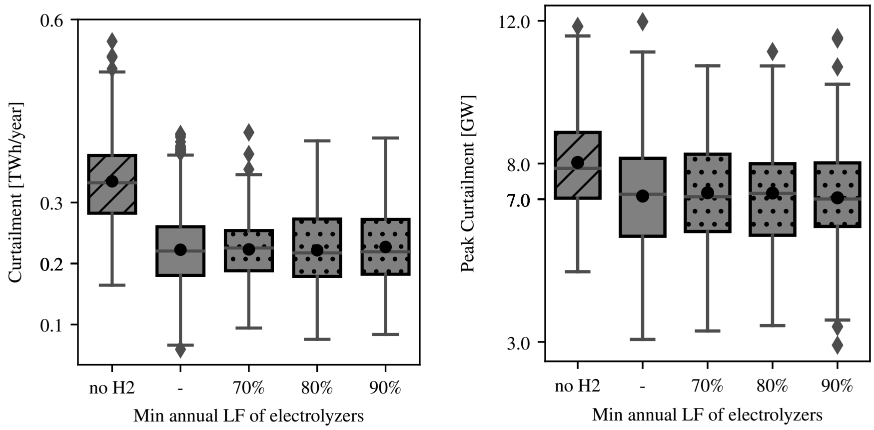

(a) (b)

Figure 6.37: Distribution of (a) the yearly production curtailment and (b) the peak production curtailment for variants of the scenario with grid and offshore wind farm extensions, and considering flexibility. The variants: (i) no H2: no hydrogen demand, (ii-iv) minimum annual load factor of electrolyzers set to 70, 80, and 90 %.

The operation of electrolyzers can be observed in detail for a random Monte Carlo year in Fig. 6.38. A seasonal pattern appears clearly: electrolyzers operate at high rate between March and September, without a clear daily trend, and a constant hourly operation. However, during colder months of October to February, with usually higher electrical demand, a daily trend appears: electrolyzers operate during the night, and at mid-day. The system prefers producing during summer days as irradiation lasts longer, and the load is generally lower, which makes the residual load way lower at those periods, and ideal to produce hydrogen. During colder seasons, the system will operate electrolyzers mainly when the residual load low, i.e. when irradiation occurs, and at night when wind produces and the load is lower.

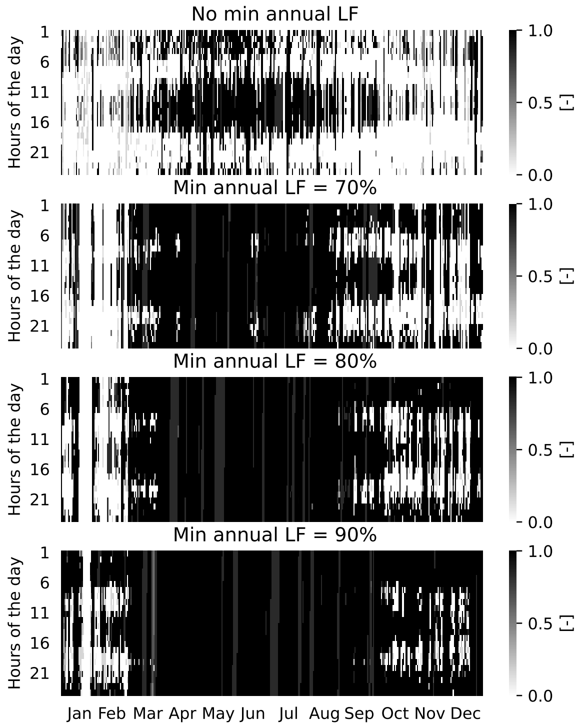

Figure 6.38: Hourly operation of electrolyzers during a random Monte Carlo year for variants of the scenario with grid and offshore wind farm extensions, and considering flexibility. The variants: minimum annual load factor of electrolyzers set to 70, 80, and 90 %.

6.3.9 Computational Time

The tool was run on a machine dating from 2015 with the following characteristics: CPU: Intel E5-2637 (3.5GHz) - RAM: 128GB DDR4 @ 2133MHz - OS: Ubuntu 20.04. The system operation optimization of each Monte Carlo year have been recorded and are plotted in Fig. 6.39. The values vary within a scenario, and from a scenario to the other. For each scenario, three Monte Caro years were run in parallel, but the optimization was not parallelized itself. It should be noted that these run times represent the optimization of each Monte Carlo year which is the most time consuming

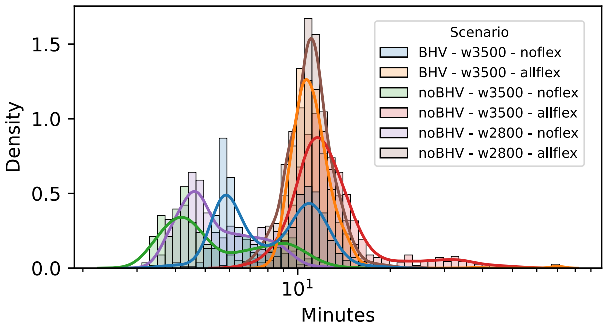

Figure 6.39: Histogram and KDE plot of the run time [minutes] for system operation optimization of a Monte Carlo year.

task, and do not consider the time required to read the input data and build the model at the beginning of each simulation, update parameters and constraint between each MC years, and save data in `.txt` files for each Monte Carlo year, as well as the global results at the end of the simulation.

6.4 Conclusion

The objective of this Chapter was to apply the previously detailed novel probabilistic adequacy tool including hydrogen to a realistic and complex study case, i.e. Belgium for the 2030 horizon. Different scenarios, illustrating current uncertainties, such as the grid extension, or the offshore wind farm extension were analyzed in this study. The integration of additional flexibility was also studied.
The study provided insights into the Belgian system for 2030. Flexibility (load shifting and batteries) plays a crucial role and significantly reduces the adequacy indicators in each scenario. The full offshore wind farm extension and flexibility integration have the same impact in terms of reducing electrical production of conventional units, mainly the CCGTs. The installed capacity of electrolyzer might seem oversized at first, observing that their annual load factor is 28-35% depending on the scenario and that the system prefers to import. However, when imposing a minimum annual load factor of 70, 80, and 90 % to the scenario with grid and offshore extension and integrating flexiblities, the system is not impacted in terms of adequacy. This means that operating electrolyzers at a low rate is a strategy to lower the costs rather than to avoid energy-not-served. However, it is important to bear in mind that this low rate strategy is highly dependent on the import cost of hydrogen. Although

integrating flexibility and 447 MW of electrolyzers reduces the energy curtailed and the curtailment peaks, the latter still reach high values, such as 6-7 GW. These are thus not sufficient to absorb very high renewable energy peaks.

Finally, it is important to state that this study considered Belgium as an isolated system, and that neighboring countries were always capable to export to Belgium which is a very optimistic and unrealistic hypothesis. This choice of imports modeling is clearly favorable for the system and results are surely impacted by this decision. Indeed, the power import limit at each hour is a very impacting parameter on the adequacy results, especially for a study case that has a a limited amount of reliable and controllable generating units.

Conclusions and perspectives

Chapter overview

- Conclusion
- Limitations
- Perspectives

Conclusion

Numerous studies indicate that hydrogen will play a significant role in our future energy system, with a substantial portion of this hydrogen expected to be produced using electrolyzers. This technology transforms water into hydrogen and oxygen using electrical energy, thereby linking the electrical power system with the hydrogen system. However, the additional load from electrolyzers on the electrical grid is not well-understood. The goal is to produce green hydrogen, which means electrolyzer consumption must align with renewable energy production. Consequently, electrolyzers may exhibit variable behavior in response to fluctuations in renewable energy production. This work aimed to quantify the impact of hydrogen production through electrolyzer consumption on the power system, specifically focusing on adequacy studies. To accurately model the future behavior of electrolyzers, we coupled the whole hydrogen energy system with the power system, encompassing electrolyzers, hydrogen storage units, hydrogen pipelines, and hydrogen-to-power units. This approach enabled a comprehensive understanding of electrolyzers' behavior within the broader system.

The objective was to develop a novel probabilistic adequacy tool incorporating hydrogen, tailored for realistic and complex cases such as Belgium. The tool can analyze various time periods, but was specifically designed for a yearly horizon. It evaluates the power system using an economic dispatch approach that optimizes operational costs, and heavily penalizes energy-not-served to minimize load shedding. This formulation considers network constraints through a multi-period DC optimal power flow model, allowing for the extraction of adequacy indicators on a yearly basis. The probabilistic nature is achieved by repeating the process numerous times through Monte Carlo simulations, with indicators being averaged across these simulations. Inputs are varied each year, including the availability timeseries of different technologies (e.g., conventional generators, transmission lines, transformers, imports, electrolyzers, offshore wind turbines) and offshore wind farm production.

After testing the tool on smaller systems, it was applied to a coupled electricity-hydrogen system representative of Belgium in 2030. Various scenarios reflecting current uncertainties, such as grid and offshore wind farm extensions, were analyzed. The economic dispatch formulation included flexibility modeling, testing scenarios with and without various flexibility measures, such as daily load shifting, short-term battery storage, and different consumption strategies for electric vehicles (EV) and heat pumps (HP). For the latter, rather than assuming fixed operating profiles, we explored a range of behaviors: some EVs and HPs maintained their natural charging patterns, others adopted smart charging to shift daily peaks, and some employed fully optimized charging strategies.

The study yielded several key insights for the Belgian system in 2030. Flexibility plays a crucial role, significantly reducing adequacy indicators across all scenarios. Full offshore wind farm extension and flexibility integration similarly reduce the need for conventional electrical production, particularly from Combined Cycle Gas Turbines (CCGTs). The installed capacity of electrolyzers (447 MW) may initially appear oversized, with an annual load factor ranging from 28-35% depending on the scenario. The system tends to prefer imports. However, imposing a minimum annual load factor of 70%, 80%, and 90% in the scenario with grid and offshore extensions, and integrating flexibility, does not impact adequacy. This suggests that operating electrolyzers at a low rate is a cost-saving strategy rather than a necessity for avoiding energy-not-served. It is important to note that this strategy is highly dependent on hydrogen import costs. Despite integrating flexibility and 447 MW of electrolyzers, curtailment peaks remain high, reaching values of 6-7 GW. This indicates that the system is not fully capable of absorbing very high renewable energy peaks.

The results suggest that flexibility must be considered in adequacy studies, especially when intermittent energy sources constitute a significant portion of production as it can enhance adequacy. Given the model's ability to import unlimited quantities of hydrogen to meet the demand, the system will never incur energy-not-served due to a hydrogen demand integration. As long as large-scale imports are permitted, even if both systems are linked, hydrogen will not impact negatively the adequacy of the power system. At best, it improves it with large-scale hydrogen storage but this has challenges. First, the round-trip efficiency of hydrogen storage is low, meaning that a substantial amount of energy is lost during storage and retrieval, and thus to compensate for these losses, a large amount of renewable energy is required which can be not achievable in a country with high-density population, and a limited surface. Secondly, large-scale hydrogen storage requires a suitable environment and cannot be installed everywhere. To assess the impact of a constraining hydrogen demand, constraints on local production and electrolyzer share must be set. In our scenario, a local hydrogen production, if managed flexibly, does not negatively impact system adequacy, though the nature of electricity will need careful consideration to ensure green hydrogen certification.

While the tool effectively accomplishes its intended purpose, there is potential for further enhancement to tackle existing limitations.

Limitations and perspectives

- **Soft-Link with an investment planning model considering multiple energy careers** Evaluating the adequacy of power systems for future horizons is challenging due to uncertainties about future installed capacities. Typically, investment planning models are used to design power systems, including infrastructure topology, and conversion technologies (generating units, storage units, and consumption units). As electrification grows, technologies from other sectors—such as heating, industry, and mobility—are increasingly integrated into power systems. These investment planning models are crucial for envisioning the future composition of power systems, including the technologies and network structures involved. To assess the adequacy of future power systems, it is essential to incorporate the outputs from these investment models as inputs. Therefore, coupling our model with these investment planning models could be valuable for evaluating different far-future power system designs in a quasi-automated manner.

- **Integration of V2G in the model** To study and evaluate future scenarios beyond 2030, such as 2040 or 2050, integrating vehicle-to-grid (V2G) optimization into the model is crucial. By then, the number of EVs could be significantly higher, and it is important to assess the flexibility they can provide, as they essentially function as moving batteries. Although the current model includes a basic form of V2G (Vehicle-to-Home V2H: a fixed time series with nighttime energy retrieval), an optimized version would be more desirable. This cannot be achieved by considering them as classical storage units. Indeed, each cannot be considered individually due to the large number of vehicles which is infeasible due to the excessive time and computational resources required; they are not always connected to the grid; and they move. All these characteristics are significant challenges for V2G integration into power system studies.

- **Modeling of Imports from Neighboring Countries** A code is always a work in progress and can be continuously improved. Certainly, the imports formulation presented in this work could be further refined. Two approaches have been proposed for modeling electrical imports. The first approach uses a single price with limited import windows, allowing imports only at predefined times and capping the import to 25 % of the time. This method is conservative and rigid. The second approach, employed in the Belgium 2030 study, allows for continuous imports (except during interconnection outages) with prices varying throughout the year. While this model provides more flexibility, it may be somewhat optimistic. During scarcity periods, imports are critical, so improving the accuracy of import modeling could enhance the reliability of the analysis. A precise method could involve considering neighboring countries as a complex power system, but may be computationally complicated. Instead, simplifying these neighboring countries to a single node with aggregated technologies and demands for both electricity and hydrogen could ensure they are able to export energy when required. Regarding hydrogen imports, which are currently modeled as unlimited, introducing constraints would be more realistic. Differentiating between hydrogen imports from neighboring countries via pipelines and those transported from farther locations by boat would allow for more accurate modeling, as different constraints may apply based on the source and transportation method.

- **Reduction of the optimization period for system operation** The proposed tool is specifically designed for annual studies (8760 hours), with an optimization period of 8760 hours. However, this decision is questionable. Time computation is a critical and very constraining factor in adequacy studies for large systems. This often leads to the need for simplifications, such as using the DC power flow approximation, and neglecting the unit commitment formulation in this work. While studying a system over a yearly horizon is logical in adequacy studies, considering the entire year as the optimization period might not be necessary. Time steps are inter-linked because of storage units, and flexibility. However, flexibility is usually daily flexibility, and storage units are not seasonal storage units. A more efficient approach could involve breaking the problem into smaller periods, such as weekly optimizations, and linking the final state of one week to the initial conditions of the next one to assure continuity. Computational time could be drastically reduced, as long as the optimization problem scales more than linearly with the cardinality of its input space, which clearly appears to be the case in practice.
  Though this approach would yield a suboptimal solution, it is justifiable for several reasons. First, weekly forecasts for renewable energy production are realistic, whereas forecasting hourly data for an entire year is impractical. Secondly, optimizing over shorter periods, such as a week, better aligns with operational realities. This makes the weekly optimization strategy more relevant and manageable, both in terms of forecast accuracy and operational planning.

- **Application to future hydrogen exporter countries and perform reliability-based location optimization of electrolyzers** It would be interesting to test this adequacy tool on a country that forecasts to be a hydrogen exporter, and to do some reliability-based optimization on the location of electrolyzers. Indeed, Belgium has too few electrolyzers installed to really have interest in the location optimization. Countries like Chile, and Australia for example could be great candidates. However, these countries are also quite big, and it should be assessed if simulating the whole high voltage grid is possible, or parts of it. Indeed, the number of nodes in the grid highly impacts the computational time of the simulation.

- **Model Computational Time** While, it was a concern to have a model that is rather fast, the code has not been optimized for computational efficiency. This presents an opportunity for further improvement. As a first step, conducting a detailed analysis of the model's time-consuming components—such as the number of lines, generators, and flexibility—could provide valuable insights for reducing computation time. Additionally, exploring advanced sampling techniques to address the computational demands of Monte Carlo simulations could be beneficial. Indeed, reducing the number of simulated Monte Carlo years may also be an option to decrease computational time.

List of Figures

List of Tables

List of publications

A. Hernandez, F. Vallée and E. D. Jaeger, "Integration of Power-to-Hydrogen Models in Power Systems Adequacy Assessments," 2022 17th International Conference on Probabilistic Methods Applied to Power Systems (PMAPS), Manchester, United Kingdom, 2022, pp. 1-6, doi: 10.1109/PMAPS53380.2022.9810562.

A. Hernandez, F. Vallée and E. De Jaeger, "Integration of Hydrogen in Sequential Monte Carlo Power Systems Adequacy Assessment," 2023 IEEE Belgrade PowerTech, Belgrade, Serbia, 2023, pp. 1-6, doi: 10.1109/PowerTech55446.2023.10202671.

A. Hernandez, F. Vallée and E. De Jaeger, "Linking Hydrogen to Power Systems in Adequacy Computations," 2024 submitted and under review in Applied Energy Journal.

Other contributions out of the scope of this thesis.

P. Thiran, A. Hernandez, G. Limpens, M. G. Prina, H. Jeanmart, & F. Contino, "Flexibility options in a multi-regional whole-energy system: the role of energy carriers in the Italian energy transition." In proceedings of ECOS 2021 conference.

M. U. Tareen, S. Meyer, P. Thiran, A. Hernandez, S. Quoilin, "Modeling the impact of energy sufficiency measures on European integrated energy systems". In proceedings of ECOS 2024 conference.

Bibliography

[1] EU Comission. Énergie et pacte vert pour l'europe. https://ec.europa.eu/info/strategy/priorities-2019-2024/european-green-deal/energy-and-green-deal_fr, (accessed December 5, 2022).

[2] Federal Planning Bureau. Fuel for the future - More molecules or deep electrification of Belgium's energy system by 2050. https://www.plan.be/publications/publication-2056-en-fuel_for_the_future_more_molecules_deep_electrification_of_belgium_s_energy_system_by_2050, October 2020 (accessed December 5, 2022).

[3] Elia. Roadmap to net zero: Elia group's vision on building a climate-neutral european energy system by 2050. https://www.elia.be/en/news/press-releases/2021/11/20211119_elia-group-publishes-roadmap-to-net-zero, Novemeber 2021 (accessed December 5, 2022).

[4] SPF Economy. Stratégie fédérale belge pour l'hydrogène. https://economie.fgov.be/fr/themes/energie/transition-energetique/strategie-federale-belge-pour, October 2022 (accessed December 5, 2022).

[5] EnergyVille. Perspective and paths for 2050. https://perspective2050.energyville.be/, November 2022 (accessed December 5, 2022).

[6] Xavier Rixhon. *Exploration of uncertainty-aware energy transition pathways : reinforcement learning and principal component analysis-based methods*. PhD

thesis, UCLouvain, 2024. URL `https://dial.uclouvain.be/pr/boreal/fr/object/boreal%3A292281`.

[7] Paolo Thiran. *Exploring options for a fossil-free European energy system : The role of renewable fuels*. PhD thesis, UCLouvain, 2024.

[8] International Energy Agency. Global hydrogen demand by sector in the net zero scenario, 2020-2030, 2023. IEA, Paris, Licence: CC BY 4.0.

[9] Global Hydrogen Review 2023 – Analysis, September 2023. URL `https://www.iea.org/reports/global-hydrogen-review-2023`.

[10] U.S. Environmental Protection Agency. Oxygen Supply Chain- Full Profile. 2022.

[11] Prakash Rao and Michael Muller. Industrial Oxygen: Its Generation and Use. 2007.

[12] Abbas Rabiee, Andrew Keane, and Alireza Soroudi. Green hydrogen: A new flexibility source for security constrained scheduling of power systems with renewable energies. *International Journal of Hydrogen Energy*, 46(37):19270–19284, May 2021. ISSN 0360-3199.

[13] Mingfei Ban, Jilai YU, M. Shahidehpour, and Yiyun YAO. Integration of power-to-hydrogen in day-ahead security-constrained unit commitment with high wind penetration. *Journal of Modern Power Systems and Clean Energy*, 5, April 2017. doi: 10.1007/s40565-017-0277-0.

[14] Mohammad Amin Mirzaei, Ahmad Sadeghi Yazdankhah, and Behnam Mohammadi-Ivatloo. Stochastic security-constrained operation of wind and hydrogen energy storage systems integrated with price-based demand response. *International Journal of Hydrogen Energy*, 44(27):14217–14227, May 2019. ISSN 0360-3199.

[15] Pudong Ge, Qinran Hu, Qiuwei Wu, Xiaobo Dou, Zaijun Wu, and Yiyuan Ding. Increasing operational flexibility of integrated energy systems by introducing power to hydrogen. *IET Renewable Power Generation*, 14(3):372–380, 2020. ISSN 1752-1424. doi: 10.1049/iet-rpg.2019.0663. _eprint: https://onlinelibrary.wiley.com/doi/pdf/10.1049/iet-rpg.2019.0663.

[16] Peng Fu, Danny Pudjianto, Xi Zhang, and Goran Strbac. Integration of Hydrogen into Multi-Energy Systems Optimisation. *Energies*, 13(7):1606, January 2020. ISSN 1996-1073. doi: 10.3390/en13071606.

[17] Hans Christian Gils, Hedda Gardian, and Jens Schmugge. Interaction of hydrogen infrastructures with other sector coupling options towards a zero-emission energy system in Germany. *Renewable Energy*, 180:140–156, December 2021. ISSN 0960-1481. doi: 10.1016/j.renene.2021.08.016.

[18] Pedro Vargas-Ferrer, Eduardo Álvarez Miranda, Claudio Tenreiro, and Francisca Jalil-Vega. Integration of high levels of electrolytic hydrogen production: Impact on power systems planning. *Journal of Cleaner Production*, 409:137110, July 2023. ISSN 0959-6526. doi: 10.1016/j.jclepro.2023.137110.

[19] G. Matute, J. M. Yusta, J. Beyza, and L. C. Correas. Multi-state techno-economic model for optimal dispatch of grid connected hydrogen electrolysis systems operating under dynamic conditions. *International Journal of Hydrogen Energy*, 46(2):1449–1460, January 2021. ISSN 0360-3199.

[20] Can Wang, Haipeng Xie, Zhaohong Bie, Gengfeng Li, and Chao Yan. Fast supply reliability evaluation of integrated power-gas system based on stochastic capacity network model and importance sampling. *Reliability Engineering & System Safety*, 208:107452, April 2021. ISSN 0951-8320. doi: 10.1016/j.ress.2021.107452.

[21] Andrea Antenucci and Giovanni Sansavini. Adequacy and security analysis of interdependent electric and gas networks. *Proceedings of the Institution of Mechanical Engineers, Part O: Journal of Risk and Reliability*, 232(2):121–139, April 2018. ISSN 1748-006X. doi: 10.1177/1748006X17715953.

[22] Osama Aslam Ansari, C. Y. Chung, and Enrico Zio. A Novel Framework for the Operational Reliability Evaluation of Integrated Electric Power–Gas Networks. *IEEE Transactions on Smart Grid*, 12(5):3901–3913, September 2021. ISSN 1949-3061. doi: 10.1109/TSG.2021.3075918.

[23] Sheng Wang, Yi Ding, Chengjin Ye, Can Wan, and Yuchang Mo. Reliability evaluation of integrated electricity–gas system utilizing network equivalent and integrated optimal power flow techniques. *Journal of Modern Power Systems and Clean Energy*, 7(6):1523–1535, November 2019. ISSN 2196-5420. doi: 10.1007/s40565-019-0566-x.

[24] Mohammad Amin Mirzaei, Ahmad Sadeghi Yazdankhah, Behnam Mohammadi-Ivatloo, Mousa Marzband, Miadreza Shafie-khah, and João P. S. Catalão. Stochastic network-constrained co-optimization of energy and reserve products in renewable energy integrated power and gas networks with energy storage system. *Journal of Cleaner Production*, 223:747–758, June 2019. ISSN 0959-6526. doi: 10.1016/j.jclepro.2019.03.021.

[25] Chen Juanwei, Yu Tao, Xu Yue, Cheng Xiaohua, Yang Bo, and Zhen Baomin. Fast analytical method for reliability evaluation of electricity-gas integrated energy system considering dispatch strategies. *Applied Energy*, 242:260–272, May 2019. ISSN 0306-2619. doi: 10.1016/j.apenergy.2019.03.106.

[26] C. M. Correa-Posada and P. Sánchez-Martín. Integrated Power and Natural Gas Model for Energy Adequacy in Short-Term Operation. *IEEE Transactions on Power Systems*, 30(6):3347–3355, November 2015. ISSN 1558-0679. doi: 10.1109/TPWRS.2014.2372013.

[27] Modassar Chaudry, Jianzhong Wu, and Nick Jenkins. A sequential Monte Carlo model of the combined GB gas and electricity network. *Energy Policy*, 62:473–483, November 2013. ISSN 0301-4215. doi: 10.1016/j.enpol.2013.08.011.

[28] Zihan Meng, Shouxiang Wang, Qianyu Zhao, Zhijie Zheng, and Liang Feng. Reliability evaluation of electricity-gas-heat multi-energy consumption based on user experience. *International Journal of Electrical Power & Energy Systems*, 130:106926, September 2021. ISSN 0142-0615. doi: 10.1016/j.ijepes.2021.106926.

[29] Hejun Yang, Yeyu Zhang, Yinghao Ma, Dabo Zhang, Lei Sun, and Shiwei Xia. Reliability assessment of integrated energy system considering the uncertainty of natural gas pipeline network system. *IET Generation, Transmission & Distribution*, 13(22):5033–5041, 2019. ISSN 1751-8695. doi: 10.1049/iet-gtd.2019.0323.

[30] Xiaping Zhang, Liang Che, Mohammad Shahidehpour, Ahmed S. Alabdulwahab, and Abdullah Abusorrah. Reliability-Based Optimal Planning of Electricity and Natural Gas Interconnections for Multiple Energy Hubs. *IEEE Transactions on Smart Grid*, 8(4):1658–1667, July 2017. ISSN 1949-3061. doi: 10.1109/TSG.2015.2498166.

[31] Chuan He, Lei Wu, Tianqi Liu, and Zhaohong Bie. Robust Co-Optimization Planning of Interdependent Electricity and Natural Gas Systems With a Joint N-1 and Probabilistic Reliability Criterion. *IEEE Transactions on Power Systems*, 33(2):2140–2154, March 2018. ISSN 1558-0679. doi: 10.1109/TPWRS.2017.2727859.

[32] Paolo Pelacchi and Davide Poli. The influence of wind generation on power system reliability and the possible use of hydrogen storages. *Electric Power Systems Research*, 80(3):249–255, March 2010. ISSN 0378-7796. doi: 10.1016/j.epsr.2009.09.007.

[33] Tao Wu and Jianhui Wang. Reliability Evaluation for Integrated Electricity-Gas Systems Considering Hydrogen. *IEEE Transactions on Sustainable Energy*, pages 1–14, 2022. ISSN 1949-3037. doi: 10.1109/TSTE.2022.3229896. in press.

[34] Li Li, Ziyu Zeng, Xinran He, Kang Wang, Fangde Chi, and Tao Ding. Risk Assessment for Renewable Energy Penetrated Power Systems Considering Battery and Hydrogen Storage Systems. In *2021 Power System and Green Energy Conference (PSGEC)*, pages 379–384, August 2021. doi: 10.1109/PSGEC51302.2021.9542445.

[35] Vicki Bennett, Kate Bowman, and Sarah Wright. Wasatch Solar Project final report. Technical Report DOE-SLC-6903-1, Salt Lake City Corporation, Salt Lake City, UT, September 2018.

[36] Bart W Tuinema, JL Rueda Torres, Alexandru I Stefanov, Francisco M Gonzalez-Longatt, and MA van der Meijden. *Probabilistic reliability analysis of power systems*. Springer, 2020.

[37] Wenyuan Li. *Risk assessment of power systems: models, methods, and applications*. John Wiley & Sons, 2014.

[38] Roy Billinton and Ronald N Allan. *Reliability evaluation of power systems*. Plenum Press, second edition, 1996.

[39] Roy Billinton and Wenyuan Li. *Reliability Assessment of Electric Power Systems Using Monte Carlo Methods*. Springer US, Boston, MA, 1994. ISBN 978-1-4899-1348-7 978-1-4899-1346-3. doi: 10.1007/978-1-4899-1346-3.

[40] Gord Stephen, Simon Tindemans, John Fazio, Chris Dent, Armando Figueroa Acevedo, Bagen Bagen, Alex Crawford, Andreas Klaube, Douglas Logan, and

Daniel Burke. Clarifying The Interpretation and Use of The Lole Resource Adequacy Metric, June 2022.

[41] Methodology for calculating the value of lost load, the cost of new entry and the reliability standard- annex i. Technical report.

[42] Avis du conseil d'État précédant l'arrêté royal du 31 août 2021 relatif à la détermination de la norme de fiabilité et à l'approbation des valeurs du coût de l'énergie non distribuée et du coût d'un nouvel entrant., . URL `https://www.ejustice.just.fgov.be/eli/arrete/2021/08/31/2021021813/justel`.

[43] Elia. CRM Design Notes - Derating factors. Technical report, 2019.

[44] SPF Economy. Note: Détermination du coût d'un nouvel entrant (CONE) - Juin 2022. Technical report, June 2022.

[45] SPF Economy. Avis de la DG Energie du SPF Economie sur la proposition de la CREG (C)2425 d'une norme de fiabilité pour le territoire belge, June 2022.

[46] SPF Economy and Bureau Fédéral du Plan. Note: Estimation unique du coût de l'énergie non distribuée pour le territoire belge (VoLL) - Avril 2021. Technical report, April 2021.

[47] SPF Economy and Bureau Fédéral du Plan. Note: Estimation unique du coût de l'énergie non distribuée pour le territoire belge (VoLL) - Juin 2022. Technical report, June 2022.

[48] Loi relative à l'organisation du marché de l'électricité, . URL `https://www.ejustice.just.fgov.be/eli/loi/1999/04/29/1999011160/justel#LNK0002`.

[49] CREG : Commission de Régulation de l'Électricité et du Gaz. Proposition de norme de fiabilité révisée pour le territoire belge. Technical report, June 2022. URL `https://www.creg.be/fr/publications/proposition-c2425`.

[50] Elia. Formeel advies Elia inzake het CREG ontwerpvoorstel (C)2425 over de herziening van de betrouwbaarheidsnorm voor het Belgisch grondgebied. Technical report, July 2022.

[51] Direction générale de l'Energie. Advies van de AD Energie van de FOD Economie over het voorstel van de CREG (C)2425 van een betrouwbaarheidsnorm voor het Belgisch grondgebied. Technical report, June 2022.

[52] Antares Simulator. URL `https://antares-simulator.org/pages/modele/2/`.

[53] ACER. Decision No 06/2024 of the European Union Agency for the Cooperation of Energy Regulators. Technical report, May 2024.

[54] T. Smolinka, E. Ojong, and T. Lickert. Fundamentals of PEM Water Electrolysis: Principles and Applications. In *PEM Electrolysis for Hydrogen Production : Principles and Applications*, pages 11–33. October 2015. ISBN 978-1-4822-5229-3. doi: 10.1201/b19096-3.

[55] P. Ayivor, J. Rueda Torres, M. van der Meijden, R. van der Pluijm, and B. Stouwie. Modelling of Large Size Electrolyzer for Electrical Grid Stability Studies in Real Time Digital Simulation. *3rd International Hybrid Power Systems Workshop*, 2018.

[56] P. Ayivor. *Feasibility Of Demand Side Response From Electrolyzers To Support Power System Stability*. PhD thesis, 2018.

[57] Elia Belgian TSO. Donnees de production eolienne.

[58] Elia. Open Data Portal, . URL `https://opendata.elia.be/pages/home/`.

[59] Hydrogen Demand | European Hydrogen Observatory. URL `https://observatory.clean-hydrogen.europa.eu/hydrogen-landscape/end-use/hydrogen-demand`.

[60] N-SIDE. Study on the outage parameters of generation units and DC links. Technical report, October 2022.

[61] Antonio Gómez-Expósito, editor. *Electric energy systems: analysis and operation*. The electric power engineering series. CRC Press, Boca Raton, Fla., 2009. ISBN 978-0-8493-7365-7.

[62] R. Billinton, S. Kumar, N. Chowdhury, K. Chu, K. Debnath, L. Goel, E. Khan, P. Kos, G. Nourbakhsh, and J. Oteng-Adjei. A reliability test system for educational purposes-basic data. *IEEE Transactions on Power Systems*, 4(3):1238–1244, August 1989. ISSN 1558-0679. doi: 10.1109/59.32623.

[63] ClusterTweed. Roadmap h2 pour la wallonie. `https://fr.slideshare.net/cluster_tweed/roadmap-hydrogne-pour-la-wallonie-cluster-tweed`, June 2018 (accessed 01/01/23).

[64] Belgian Offshore Platform. Map of offshore wind farms. https://www.belgianoffshoreplatform.be/en/projects/, 2024. Accessed: 2024-03-25.

[65] SPF Economy. Belgian offshore wind energy - extra capacity. URL https://economie.fgov.be/en/belgian-offshore-wind-energy.

[66] Thuy-hai Nguyen, Jean-François Toubeau, Emmanuel De Jaeger, and François Vallée. Fast and Reliable Modeling of Offshore Wind Generation for Adequacy Studies. *IEEE Transactions on Industry Applications*, 59(6):7116–7125, November 2023. ISSN 1939-9367. doi: 10.1109/TIA.2023.3307076.

[67] Elia. Adequacy and flexiblity study for belgium 2024-2034. https://www.elia.be/en/electricity-market-and-system/adequacy/adequacy-studies, 2023. Accessed: 2023-06-29.

[68] Elia. Belgian electricity system blueprint for 2035-2050. Technical report, September 2024.

[69] Solar-PV power generation data from Elia, . URL https://www.elia.be/en/grid-data/generation-data/solar-pv-power-generation-data. Accessed: 2024-10-15.

[70] Elia. Net transfer capacities [.xlsx] - input data of eraa 2023, 2023. URL https://www.entsoe.eu/outlooks/eraa/2023/eraa-downloads/.

[71] Elia. Physical flow - by border, . URL https://opendata.elia.be/explore/dataset/ods026/information/.

[72] Solar-PV power generation data from Elia, . URL https://www.elia.be/en/grid-data/generation-data/solar-pv-power-generation-data. Accessed: 2022-07-02.

[73] The Wind Power Database. URL https://www.thewindpower.net/country_zones_en_21_belgium.php.

[74] Rik van Rossum, Jaro Jens, Gemma La Guardia, Anthony Wang, Luis Kuhnen, and Martijn Overgaag. European Hydrogen Backbone - A European Hydrogen Infrastructure vision covering 28 countries. Technical report, April 2022.

[75] Elia. Forced unavailability of grid components (380/220kV), 2024. URL https://opendata.elia.be/explore/dataset/ods030/?flg=fr.

[76] F. Anderson, R. Dawid, D. García Cava, and D. McMillan. Operational Metrics for an Offshore Wind Farm & Their Relation to Turbine Access Restrictions and Position in the Array. *Journal of Physics: Conference Series*, 2018(1):012002, September 2021. ISSN 1742-6596. doi: 10.1088/1742-6596/2018/1/012002. Publisher: IOP Publishing.

[77] Elia. Static grid data. https://www.elia.be, 2018. Accessed: 2021-03-25.

[78] Elia. Map of the high voltage grid 2022. https://www.elia.be/en/infrastructure-and-projects/our-infrastructure, 2022. Accessed: 2024-03-25.

[79] Ember. Wholesale day-ahead electricity price data for European countries, sourced from ENTSO-e and cleaned by Ember, 2024. URL https://ember-climate.org/data-catalogue/european-wholesale-electricity-price-data/.

[80] Elia. Input data for the adequacy and flexiblity study 2024-2034. https://www.elia.be/fr/consultations-publiques/20221028_public-consultation-adequacy-study-2022-2032, 2022. Accessed: 2024-03-25.

[81] Kristina Juhrich. CO2 Emission Factors for Fossil Fuels - Update 2022 - German Environment Agency (UBA). Technical report, German Environment Agency (UBA). URL https://www.umweltbundesamt.de/en/publikationen/co2-emission-factors-for-fossil-fuels-0.

[82] Engie. Coo pumped storage power station. https://corporate.engie.be/en/energy/water/coo-pumped-storage-power-station, 2024. Accessed: 2024-03-30.

[83] Sofco, and SPW. Appel d'offres en vue de la concession de l'usage d'une centrale hydroelectrique de pompage-turbinage sur le complexe des lacs de la plate-taille et de l'eau d'heure à silenrieux (cerfontaine) - annexes 1 à 5. https://sofico.org/app/uploads/2021/09/sof-22-plate-taille-annexe-2-annexes-1-a-5-def.pdf, 2024. Accessed: 2024-03-30.

[84] Fluxys (Belgian Gas Operator). Indicative Investment Plan Fluxys Belgium & Fluxys LNG 2022-2031. Technical report, February 2022.

[85] Davide Tonelli, Lorenzo Rosa, Paolo Gabrielli, Ken Caldeira, Alessandro Parente, and Francesco Contino. Global land and water limits to electrolytic hydrogen production using wind and solar resources, June 2023.

[86] International Energy Agency (IEA). Net zero by 2050. `https://www.iea.org/reports/net-zero-by-2050`, 2021. License: CC BY 4.0.

Appendix A

Convergence criteria of Monte Carlo simulations

The value of interest when simulating one Monte Carlo year is the energy-not-served (ENS) which is minimized in the objective function of the economic dispatch. However, in adequacy computations, the value of interest is the expected value, i.e. the expected energy-not-served.

In probabilistic adequacy studies using Monte Carlo simulations, the relative standard deviation (RSD), also called the coefficient of variation (CV) of the interest value Z is usually the criteria of convergence, i.e. when RSD(Z) reaches a certain threshold (e.g. 1 or 0.1 %), the number of samples are considered sufficient to evaluate the expected value with a certain confidence interval. However, this criterion can be highly dependent on the magnitude of Z. Therefore, we examine the relative difference of RSD(Z) as a convergence criterion [1].

Six convergence indicators are considered and will be compared.

[1] The concept of relative difference of the RSD is inspired by the methodology defined by the European Resource Adequacy Assessment (ERAA).

$$\alpha = \frac{\sigma(X)}{\mu(X)} = \frac{\sigma(\text{ENS})}{\mu(\text{ENS})} = RSD(\text{ENS}) \qquad \alpha' = \frac{\mid \alpha_n - \alpha_{n-1} \mid}{\alpha_{n-1}}$$
$$\beta = \frac{\sigma(Y)}{\mu(Y)} = \frac{\sigma(\text{EENS})}{\mu(\text{EENS})} = RSD(\text{EENS}) \qquad \beta' = \frac{\mid \beta_n - \beta_{n-1} \mid}{\beta_{n-1}}$$
$$\gamma = \frac{\sigma(X)}{\sqrt{n}\mu(Y)} = \frac{\sigma(\text{ENS})}{\sqrt{n}\mu(\text{EENS})} \sim RSD(\text{ENS}) \qquad \gamma' = \frac{\mid \gamma_n - \gamma_{n-1} \mid}{\gamma_{n-1}}$$

where X is the observed value (ENS) and $Y = \bar{X}$ is the average of the observed value (EENS).

Among these indicators, α, β, γ represent RSD and α', β', γ' represent the relative differences of these RSD. While α, and β represent the RSD of the ENS, and the EENS respctively, γ represents the RSD of EENS (after a certain number of samples), similarly to β but considering the Central Limit Theorem, i.e. $\sigma(\bar{X}) = \sigma(X)/n$ when $n \to \infty$.

A.1 Illustration with example

A.1.1 Data set

The data set consists of the ENS value of 1000 Monte Carlo years. Two variants of this data set are also analyzed: one with an offset = 2, and another with an offset = 100. The three data set are presented in Fig. A.1.

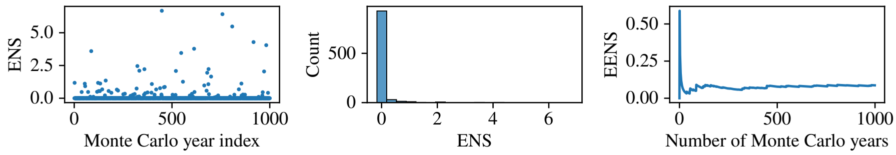

(a) Original data set

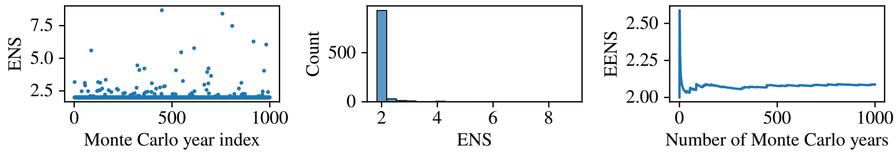

(b) Data set with offset = 2

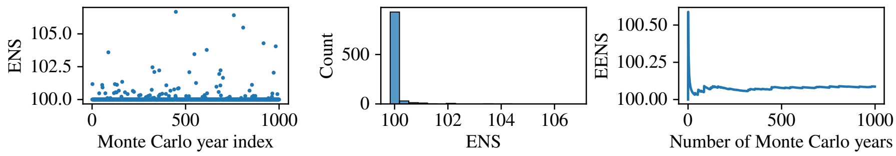

(c) Data set with offset = 100

Figure A.1: Variants of the data set for a 1000 year Monte Carlo simulation.

A.1.2 RSD vs. relative difference of RSD: convergence comparison

In Fig. A.2, the evolution of the different indicators is plotted for the original data set, as well as the variants with the offsets. In Fig. A.2a, the different indicators based on the RSD (α, β, γ) evolve rapidly at the beginning, and then very slowly for the rest of the simulation. However, they do not drop similarly at the start. Indeed, with an offset of 100, the threshold of 0.001 is reached very rapidly, while the others never reach that threshold. This graph clearly shows that depending on the data set, the indicators cannot all reach the same threshold.

In Fig. A.2a, the different indicators based on the relative difference of the RSD (α', β', γ') evolve in a similar way. Their evolutions seem independent of the offset, and they can all reach the threshold of 0.001.

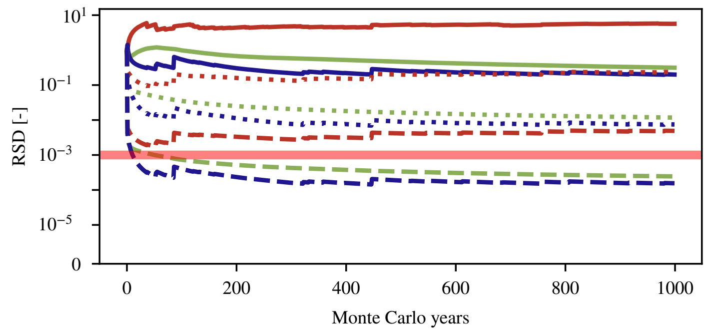

(a) Evolution of the different RSD [-]: α, β, γ.

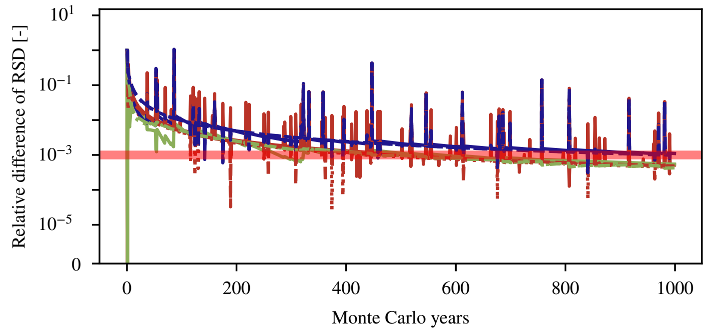

(b) Evolution of the relative difference of the different RSD [-]: α', β', γ'.

Figure A.2: Convergence evolution based on different values. Legend: α/α' (▬) - β/β' (▬) - γ/γ' (▬) - Original data set (——) - Data set with offset = 2 (- - -) - Data set with offset = 100 (⋯⋯)

Because the relative difference of the RSD is independent of the absolute value of observed value, convergence based on that criteria is chosen. However, spikes occur in the evolution of the relative difference of the RSD. Negative spikes are problematic because they reach the threshold suddenly while the criterion is not converging globally. In the following section, different smoothing techniques are applied.

A.1.3 Relative difference of the RSD

A detailed overview of the α', β', and γ' indicators is illustrated in Fig. A.3 with different smoothing filters. Two methods are applied: rolling mean and rolling median, both with a window of 30 samples. It can be observed that the rolling median smoothes better the spikes than the rolling mean for α' and *gamma*'. The γ' indicator has a somewhat different behavior than the others: while α' and γ' have sudden spikes which are relatively easy to smooth, the β' indicator exhibits broader fluctuations making it harder to smooth with a similar window.

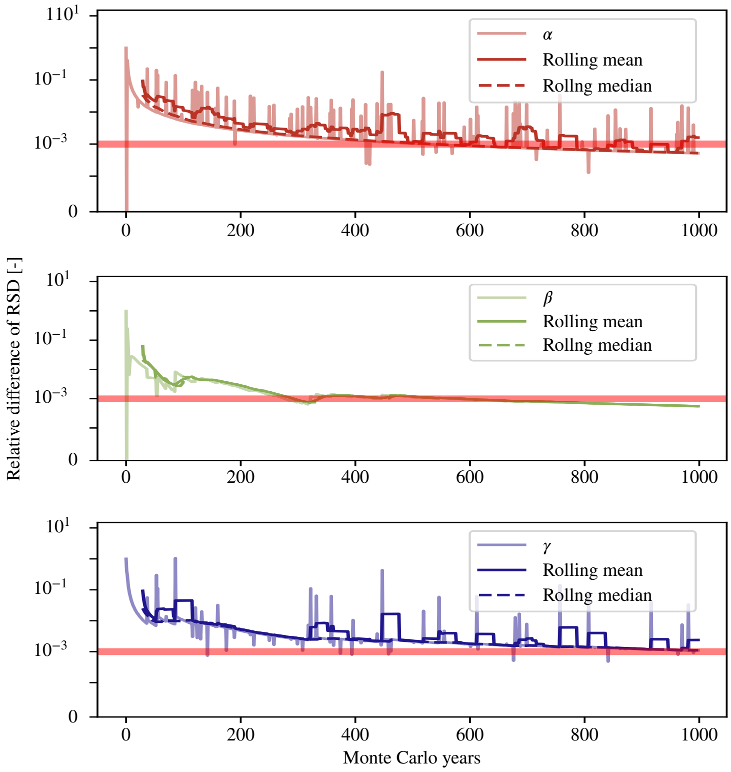

Figure A.3: Relative difference of the RSD [-] with smoothing filters.

A.1.4 Choice of the convergence indicator

Because the average observations are the values of interest in adequacy studies, the α' is dropped. Additionally, since γ' is a good approximation of β' when $n \to \infty$ but may not be at the beginning, we choose β' as our convergence indicator with a rolling median smoothing on a 30-sample window. Moreover, as a precaution to avoid an premature convergence, a minimum number of Monte Carlo years can be set. In our study, it will be set to 400.

APPENDIX B

Data for Belgium 2030 case

B.1 Construction of the transmission grid topology: buses, branches, and interconnections on 220/380 kV voltage level.

The Belgian high voltage transmission grid is composed of 380 and 220 kV lines. Historically, the high voltage network was composed of 150 kV lines, except for lines connecting the south of the country and covering long distances, which were of 220 kV. When nuclear power plants were built, the 380 kV network begun to be deployed. This is why, in Belgium two level of high voltage lines coexist: 220 and 380 kV.

B.1.1 Database used

- **[77]: 20181231-grid-statc-data-.xslx** The grid topology can be found on Elia website. The excel file gives information about lines, interconnections with neighboring countries, and transformers. Hereunder are listed the parameters given in this excel file:
  - Lines parameters: Voltage U [kV], length [km], nominal current Inom [A], line resistance R [ohm], line reactance X [ohm], shunt admittance wC [µC].
  - Interconnections parameters: Voltage U [kV], length [km], nominal current Inom [A], line resistance R [ohm], line reactance X [ohm], shunt admittance wC [µC].
  - Transformers parameters: Voltage U [kV], primary voltage V1 [kV], secondary voltage V2 [kV], tertiary voltage V3 [kV] (optionnal), primary

nominal power P1 [MVA], secondary nominal power P2 [MVA], tertiary nominal power P3 [MVA] (optional), primary short-circuit impedance Zcc1 [%], secondary short-circuit impedance Zcc2 [%], tertiary short-circuit impedance Zcc3 [%] (optional), minimum tap [#], nominal tap [#], max tap [#].

This database enumerates 93 lines, 12 interconnections, and 67 transformers.

- **[78]: The Elia High Voltage Grid Map 2022** This map allows to visualize the existing lines, substations, and generators.

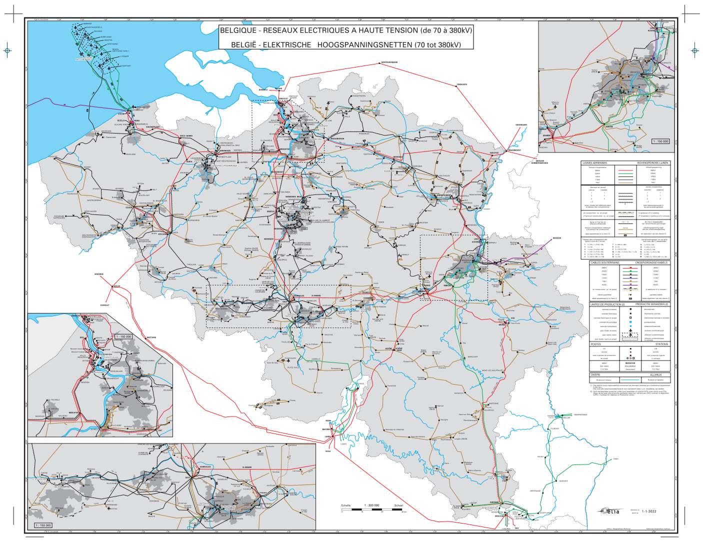

Figure B.1: The Elia High Voltage Grid Map 2022

From the databases listed above, a realistic Belgian transmission network was built.

B.1.2 Buses of the network

The buses have been defined from the lines data [77]: *from* buses and *to* buses. Moreover, the following modifications have been brought:

- Duplicate the nodes that are at the 220/380 kV networks interface :
  - *Aubange (AUBAN)* has been split into *Aubange 220 kV (AUBAN220)*, and *Aubange 380 kV (AUBAN380)*.

  - *Lixhe (LIXHE)* has been split in *Lixhe 220 kV (LIXHE220)*, and *Lixhe 380 kV (LIXHE380).*
  - *Rimière (RIMIE)* has been split in *Rimière 220 kV (RIMIE220)*, and *Rimière 380 kV (RIMIE380).*
- Merge nodes
  - All Tihange substations (*TIBIS, TIHA1, TIHA2, TIHA3*) have been merged into one bus: *TIHA1*
  - *Achene SNCB (ACHES)* has been aggregated to *Achène (ACHEN)*
  - *André Dumont* has been aggregated to the *Zutendaal (ZUTE+)* station.
  - *Drogenbos (DROGE)* has been aggregated to *Mekingen (MEKI+).*
  - *RODEN* substation has been merged with to *RODE+*
  - *Tergnée (TERGN)* has been aggregated to *St-Amand STAM+*
  - *Heinsh (HEINS)* aggregated to *Aubange (AUBAN220)*
  - *Houffalize (HOUFF, and HOUF+)* substations to *Brume (BRUME).*
  - *Latour (LATOU, LATO+)* to *Aubange 220 (AUBAN220).*
  - *Marcourt (MARCO, and MARC+)* to *Aubange 220 (AUBAN220)*
  - *Romssée SNCB (ROMSS)* to *Romsée (ROMSE)*
  - *Rouvroy (ROUVR)* to *Aubange 220 (AUBAN220)*
  - *St mard (SMARD, SMARS)* to *Aubange 220 (AUBAN220).*
  - *La Troque (ATRO)* to *Seraing (SERAI)*
  - *Le Val (LEVAL)* to *Seraing (SERAI).*
- Add nodes:
  - The 220 kV node *BERNEAU (BERN)* is not in the database [77] but is present on the grid if we look at the Elia Grid Map [78]. It has thus been added.

The resulting buses are listed in Table B.1 and B.2.

Table B.1: Buses 1/2

Node	Name	Full Name	Province	Type	V [kV]	Transfo [MVA]	Load [%]	PV [%]	WT_o [%]	Hydro [%]	DistGen [%]	Hp [%]	Ev [%]	H2 [%]
1	ACHEN	Achène	Namur	Load	380	270	1.54	1.75	5.80	0.00	1.54	1.75	1.75	0.00
2	ALVERINGEM	Alveringem	WV	H2	-	0	0.00	0.00	0.00	0.00	0.00	0.00	0.00	0.00
3	AUBAN220	Aubange 220kV	Lux	Load	220	240	1.37	0.56	0.86	2.20	1.37	0.56	0.56	0.00
4	AUBAN380	Aubange 380 kV	Lux	Load	380	30	0.17	0.00	0.00	0.00	0.17	0.00	0.00	0.00
5	AVLGM	Avelgem	WV	Load	380	1035	5.91	8.11	4.37	0.00	5.91	8.11	8.11	0.00
6	AWIRS	Awirs	Liege	Load	220	560	3.20	0.65	0.89	11.00	3.20	0.65	0.65	0.00
7	BERN	Berneau	Liege	Transfer	220	0	0.00	0.00	0.00	0.00	0.00	0.00	0.00	0.00
8	BRUEG	Bruegel	VB	Load	380	1260	7.19	5.22	1.72	0.00	7.19	5.22	5.22	20.00
9	BRUME	Brume	Liege	Load	380	297	1.70	0.65	0.89	21.10	1.70	0.65	0.65	0.00
10	BUGG+	Buggenhout	OV	Transfer	380	0	0.00	0.00	0.00	0.00	0.00	0.00	0.00	0.00
11	CHAMP	Champion	Namur	Load	380	492	2.81	1.75	5.80	6.30	2.81	1.75	1.75	0.00
12	COO	Coo	Liege	Transfer	380	0	0.00	0.00	0.00	0.00	0.00	0.00	0.00	0.00
13	COURC	Courcelles	Hainaut	Transfer	380	0	0.00	0.00	0.00	0.00	0.00	0.00	0.00	0.00
14	DOEL	Doel	OV	Load	380	155	0.88	4.40	4.56	0.00	0.88	4.40	4.40	0.00
15	EEKLN	Eeklo Noord	OV	Load	380	465	2.65	4.40	4.56	0.00	2.65	4.40	4.40	0.00
16	GEZEL	Gezelle	WV	Transfer	380	0	0.00	0.00	0.00	0.00	0.00	0.00	0.00	0.00
17	GOUY	Houy	Hainaut	Load	380	930	5.31	3.87	8.89	0.00	5.31	3.87	3.87	20.00
18	GRAMM	Gramme	Liege	Load	380	600	3.43	0.65	0.89	7.70	3.43	0.65	0.65	0.00
19	HORTA	Horta	OV	Transfer	380	0	0.00	0.00	0.00	0.00	0.00	0.00	0.00	0.00
20	IZGEM	Izegem	WV	Load	380	980	5.59	8.11	4.37	0.00	5.59	8.11	8.11	0.00
21	JUPIL	Jupille	Liege	Load	220	860	4.91	0.65	0.89	23.30	4.91	0.65	0.65	0.00
22	LINT	Lint	Antw	Load	380	930	5.31	4.06	3.71	0.00	5.31	4.06	4.06	0.00
23	LIXHE220	Lixhe 220 kV	Liege	Load	220	350	2.00	0.65	0.89	17.50	2.00	0.65	0.65	0.00
24	LIXHE380	Lixhe 380 kV	Liege	Load	380	30	0.17	0.65	0.89	0.00	0.17	0.65	0.65	0.00
25	MAERL	Maerlant	WV	Transfer	380	0	0.00	0.00	0.00	0.00	0.00	0.00	0.00	0.00
26	MARC+	Marcourt	Lux	Load	220	105	0.60	0.56	0.86	0.00	0.60	0.56	0.56	0.00
27	MASSE	Massenhoven	Antw	Load	380	465	2.65	4.06	3.71	0.00	2.65	4.06	4.06	0.00
28	MEERH	Meerhout	Antw	Load	380	1138	6.50	4.06	3.71	0.00	6.50	4.06	4.06	0.00
29	MEKI+	Mekingen	VB	Load	380	515	2.94	5.22	1.72	0.00	2.94	5.22	5.22	0.00
30	MERCA	Mercator	OV	Load	380	1170	6.68	4.40	4.56	0.00	6.68	4.40	4.40	20.00
31	NEMO	Nemo	WV	Transfer	380	0	0.00	0.00	0.00	0.00	0.00	0.00	0.00	0.00
32	RIMIE220	Rimière 220 kV	Liege	Load	220	160	0.91	0.65	0.89	0.00	0.91	0.65	0.65	20.00
33	RIMIE380	Rimière 380 kV	Liege	Load	380	80	0.46	0.65	0.89	0.00	0.46	0.65	0.65	0.00
34	RODE+	Rodenhuize	OV	Load	380	465	2.65	4.40	4.56	0.00	2.65	4.40	4.40	20.00
35	ROMSE	Romsée	Liege	Load	220	120	0.69	0.65	0.89	0.00	0.69	0.65	0.65	0.00
36	SENO+	Senochamp	Lux	Load	220	0	0.00	0.56	0.86	0.00	0.00	0.56	0.56	0.00
37	SERAI	Seraing	Liege	Load	220	280	1.60	0.65	0.89	0.00	1.60	0.65	0.65	0.00
38	SLIJKENS	Slijkens	WV	Transfer	380	0	0.00	0.00	0.00	0.00	0.00	0.00	0.00	0.00

Table B.2: Buses 2/2

Node	Name	Full Name	Province	Type	V [kV]	Transfo [MVA]	Load [%]	PV [%]	WT_o [%]	Hydro [%]	DistGen [%]	Hp [%]	Ev [%]	H2 [%]
39	STAM+	St-Amand	Hainaut	Load	380	645	3.68	3.87	8.89	0.00	3.68	3.87	3.87	0.00
40	STEVN	Stevin	WV	Transfer	380	0	0.00	0.00	0.00	0.00	0.00	0.00	0.00	0.00
41	TIHA1	Tihange	Liege	Load	380	570	3.25	0.65	0.89	10.90	3.25	0.65	0.65	0.00
42	VANYK	Van Eyck	Limburg	Transfer	380	0	0.00	0.00	0.00	0.00	0.00	0.00	0.00	0.00
43	VERBR	Verbrande Brug	VB	Load	380	1035	5.91	5.22	1.72	0.00	5.91	5.22	5.22	0.00
44	VILLE	Villeroux	Lux	Load	220	200	1.14	0.56	0.86	0.00	1.14	0.56	0.56	0.00
45	ZANDV	Zandvliet	Antw	Load	380	1085	6.19	4.06	3.71	0.00	6.19	4.06	4.06	0.00
46	ZELZATE	Zelzate	OV	H2	-	0	0.00	0.00	0.00	0.00	0.00	0.00	0.00	0.00
47	ZUTE+	Zutendaal	Limburg	Load	380	0	0.00	13.69	10.35	0.00	0.00	13.69	13.69	0.00

B.1.3 Branches of the network

Branches are defined as assets linking two busbars, i.e. transformers and transmission lines. The lines listed in [77] are set as branches. However, the following modifications have been brought.

- Additional lines:
  - The double 220 kV line connecting *Jupille* to *Berneau* is not in the database [77] but is present on the grid if we look at the Elia Grid Map [78]. Supposing, the double line is 30 km long, and has the same per length characteristics than the 220 kV line ROMSE-JUPIL, the following characteristics is set to each line : R = 1.8 [Ω], X = 12 [Ω], Pmax = 381 [MW].
- Removed lines:
  - The lines in between nodes that have been merged together are logically removed.
- Integration of 220/380 kV transformers:
  - All 380/220 step-down transformers are considered as branches as well as they connect 380 and 220 kV lines at one node.

The resulting branches are listed in Table B.3 and B.4.

B.1 Construction of the transmission grid topology: buses, branches, and interconnections on 220/380 kV voltage level.

Table B.3: Lines 1/2

Line	FromNode	ToNode	V [kV]	Length [km]	Inom [A]	R [ohm]	X [ohm]	Pmax [MW]	MTTF [hours]	MTTR [hours]
1	ACHEN	GRAMM	380	36.9	1999	1.14	12.10	1315.70	73397	26
2	AUBAN380	BRUME	380	104.4	2186	3.55	32.88	1438.78	73397	26
3	AVLGM	HORTA	380	39.7	1999	1.23	13.02	1315.70	73397	26
4	AVLGM	HORTA	380	39.7	2186	1.25	13.00	1438.78	73397	26
5	AVLGM	IZGEM	380	22.8	2186	0.71	7.48	1438.78	73397	26
6	AVLGM	IZGEM	380	22.8	2186	0.71	7.48	1438.78	73397	26
7	BRUEG	MEKI+	380	14.0	1999	0.45	4.63	1315.70	73397	26
8	BRUEG	COURC	380	47.3	2186	1.47	15.51	1438.78	73397	26
9	BRUEG	BUGG+	380	15.9	1999	0.61	5.11	1315.70	73397	26
10	BRUEG	BUGG+	380	15.9	2186	0.50	5.25	1438.78	73397	26
11	BRUME	GRAMM	380	44.3	1999	1.37	14.53	1315.70	73397	26
12	BRUME	GRAMM	380	44.3	2322	1.37	14.53	1528.29	73397	26
13	BRUME	COO	380	2.0	1999	0.06	0.66	1315.70	73397	26
14	BRUME	COO	380	2.0	1999	0.06	0.66	1315.70	73397	26
15	BUGG+	MERCA	380	15.5	1999	0.59	5.00	1315.70	73397	26
16	BUGG+	VERBR	380	21.7	2319	0.66	6.91	1526.32	73397	26
17	BUGG+	MERCA	380	15.5	2186	0.48	5.08	1438.78	73397	26
18	BUGG+	VERBR	380	21.7	2186	0.67	7.12	1438.78	73397	26
19	CHAMP	GRAMM	380	32.2	2186	1.00	10.56	1438.78	73397	26
20	CHAMP	COURC	380	44.1	2186	1.37	14.46	1438.78	73397	26
21	COURC	STAM+	380	12.6	1999	0.39	4.13	1315.70	73397	26
22	COURC	MEKI+	380	33.4	1999	1.03	10.95	1315.70	73397	26
23	COURC	GOUY	380	1.7	1999	0.05	0.56	1315.70	73397	26
24	COURC	GOUY	380	1.8	2186	0.06	0.59	1438.78	73397	26
25	DOEL	ZANDV	380	6.8	1999	0.24	2.40	1315.70	73397	26
26	DOEL	ZANDV	380	7.1	1999	0.07	2.57	1315.70	73397	26
27	DOEL	MERCA	380	22.8	1999	0.71	7.48	1315.70	73397	26
28	DOEL	MERCA	380	22.8	1999	0.71	7.48	1315.70	73397	26
29	DOEL	MERCA	380	22.2	2186	0.80	6.84	1438.78	73397	26
30	DOEL	MERCA	380	22.2	2186	0.80	6.84	1438.78	73397	26
31	EEKLN	HORTA	380	13.0	4560	0.40	4.26	3001.30	73397	26
32	EEKLN	MAERL	380	17.3	4689	0.28	4.07	3086.20	73397	26
33	GEZEL	MAERL	380	10.1	1635	0.09	2.24	1076.12	73397	26
34	GEZEL	MAERL	380	10.1	1635	0.09	2.23	1076.12	73397	26
35	GEZEL	MAERL	380	10.1	1635	0.11	2.21	1076.12	73397	26
36	GEZEL	MAERL	380	10.1	1635	0.11	2.21	1076.12	73397	26
37	GEZEL	STEVN	380	8.0	4644	0.13	1.90	3056.58	73397	26
38	GEZEL	STEVN	380	8.0	4644	0.13	1.90	3056.58	73397	26
39	GEZEL	NEMO	380	0.8	1635	0.01	0.07	1076.12	73397	26
40	GRAMM	LIXHE380	380	53.4	2051	3.04	20.03	1349.93	73397	26
41	GRAMM	ZUTE+	380	55.6	2000	1.85	17.45	1316.36	73397	26
42	GRAMM	TIHA1	380	2.6	2186	0.08	0.85	1438.78	73397	26
43	GRAMM	TIHA1	380	3.3	2186	0.10	1.08	1438.78	73397	26
44	GRAMM	STAM+	380	56.4	1999	1.75	18.50	1315.70	73397	26
45	GRAMM	TIHA1	380	2.9	1999	0.09	0.95	1315.70	73397	26
46	GRAMM	TIHA1	380	2.9	1999	0.09	0.95	1315.70	73397	26
47	GRAMM	RIMIE380	380	14.6	1999	0.45	4.79	1315.70	73397	26
48	HORTA	MAERL	380	29.0	4689	0.43	7.94	3086.20	73397	26
49	HORTA	MERCA	380	48.4	3400	1.58	15.19	2237.81	73397	26
50	HORTA	RODE+	380	14.2	2186	0.44	4.64	1438.78	73397	26
51	LINT	MERCA	380	21.1	2186	0.65	6.92	1438.78	73397	26
52	LINT	MASSE	380	14.1	2188	0.46	4.56	1440.10	73397	26
53	LINT	MERCA	380	21.1	2186	0.65	6.92	1438.78	73397	26
54	LIXHE380	VANYK	380	53.0	1999	2.07	16.53	1315.70	73397	26
55	MASSE	MEERH	380	32.5	2186	1.01	10.66	1438.78	73397	26
56	MASSE	MERCA	380	35.0	2186	1.09	11.54	1438.78	73397	26
57	MEERH	VANYK	380	57.5	2186	1.78	18.86	1438.78	73397	26
58	MERCA	RODE+	380	34.2	1999	1.07	11.21	1315.70	73397	26
59	VANYK	ZUTE+	380	31.1	1999	0.72	9.55	1315.70	73397	26
60	AUBAN220	VILLE	220	47.2	1063	4.01	14.16	405.06	73397	26
61	AWIRS	SERAI	220	6.6	1092	0.33	2.64	416.11	73397	26
62	AWIRS	RIMIE220	220	7.4	976	0.47	3.13	371.91	73397	26
63	JUPIL	RIMIE220	220	20.2	1092	0.61	4.52	416.11	73397	26
64	SERAI	RIMIE220	220	13.4	976	0.77	5.29	371.91	73397	26
65	MARC+	RIMIE220	220	38.0	1063	3.23	11.30	405.06	73397	26
66	MARC+	SENO+	220	26.8	1063	2.28	8.04	405.06	73397	26

Table B.4: Lines 2/2

Line	FromNode	ToNode	V [kV]	Length [km]	Inom [A]	R [ohm]	X [ohm]	Pmax [MW]	MTTF [hours]	MTTR [hours]
67	RIMIE220	SERAI	220	11.4	1037	0.66	4.63	395.15	73397	26
68	ROMSE	SERAI	220	14.3	1037	0.83	5.81	395.15	73397	26
69	SENO+	VILLE	220	2.6	1063	0.63	2.15	405.06	73397	26
70	ROMSE	JUPIL	220	10.0	1000	0.60	4.00	381.05	73397	26
71	JUPIL	BERN	220	30.0	1000	1.80	12.00	381.05	73397	26
72	JUPIL	BERN	220	30.0	1000	1.80	12.00	381.05	73397	26
73	BERN	LIXHE220	220	10.0	1000	0.60	4.00	381.05	73397	26
74	BERN	LIXHE220	220	10.0	1000	0.60	4.00	381.05	73397	26
75	AUBAN380	AUBAN220	380/220	-	-	0.00	82.13	300.00	73397	26
76	AUBAN380	AUBAN220	380/220	-	-	0.00	80.53	300.00	73397	26
77	LIXHE380	LIXHE220	380/220	-	-	0.00	77.87	300.00	73397	26
78	LIXHE380	LIXHE220	380/220	-	-	0.00	77.87	300.00	73397	26
79	RIMIE380	RIMIE220	380/220	-	-	0.00	77.87	300.00	73397	26
80	RIMIE380	RIMIE220	380/220	-	-	0.00	77.87	300.00	73397	26
81	RIMIE380	RIMIE220	380/220	-	-	0.00	77.87	300.00	73397	26
82	GEZEL	SLIJKENS	380	18.0	2186	0.55	5.90	1500.00	73397	26
83	GEZEL	SLIJKENS	380	18.0	2186	0.55	5.90	1500.00	73397	26
84	GEZEL	SLIJKENS	380	18.0	2186	0.55	5.90	1500.00	73397	26
85	GEZEL	SLIJKENS	380	18.0	2186	0.55	5.90	1500.00	73397	26
86	SLIJKENS	IZGEM	380	20.0	2186	0.62	6.56	1500.00	73397	26
87	SLIJKENS	IZGEM	380	20.0	2186	0.62	6.56	1500.00	73397	26
88	SLIJKENS	IZGEM	380	20.0	2186	0.62	6.56	1500.00	73397	26
89	SLIJKENS	IZGEM	380	20.0	2186	0.62	6.56	1500.00	73397	26
90	AVLGM	COURC	380	84.8	2186	2.61	27.81	1500.00	73397	26
91	AVLGM	COURC	380	84.8	2186	2.61	27.81	1500.00	73397	26
92	AVLGM	COURC	380	84.8	2186	2.61	27.81	1500.00	73397	26
93	AVLGM	COURC	380	84.8	2186	2.61	27.81	1500.00	73397	26

B.1.4 Interconnections of the network

Belgium has today, 12 HVAC and 2 HVDC connections with neighboring countries. In the ERAA 2023 study conducted by ENTSOE, the Net Transfer Capacity (NTC) [1] of the belgian interconnections with its neighbouring countries are listed in Table B.5.

Table B.5: Net Transfer Capacities for Belgium in 2024 [70]

Country	Bidding Zone	Imports	Exports	Type
France	FR	4300	2800	HVAC
Netherlands	NL	3400	2400	HVAC
Luxembourg	LUG1+LUB1	180	680	HVAC
Germany	DE	1000	1000	HVDC
United Kingdom	UK	2400	2400	HVDC

Although we have a single NTC between regions, multiple buses in the system can connect Belgium to another region, and several import points exist. To allocate the

[1] defined as NTC = TTC - TRM. Total Transfer Capacty (TTC) is the maximum exchange program between two adjacent control areas that is compatible with operational security standards applied in each system if future network conditions, generation and load patterns are perfectly known in advance. Transmission Reliability Margin (TRM) is a security margin that copes with uncertainties on the computed TTC values.

NTC to the different import points linking a particular region , we can distribute it proportionally based on the line capacities. The parameters of the individual HVAC lines are given in [77]. For each of these interconnections, we have the voltage level [kV] and the nominal current [A]. The theoretical maximum loading of these lines can be obtained by multiplying each nominal current by $\sqrt{3} * U_{nom}$. The parameters of the HVDC lines is not necessary because their nominal power is directly given. The existing HVDC lines are Alegro (Germany - 1 GW), and NemoLink (UK -1 GW). New interconnections are planned to be constructed in 2030, like the subsea hybrid interconnector between Belgium and the UK *Nautilus* which will interconnect on a first segment Belgium and the energy island (1.4 GW - HVDC), and on a second segment, the energy island and the UK (1.4 GW - HVDC). These theoretical maximum loadings will help us distribute the NTC among the different import points.
This sums up to 15 interconnections with neighboring countries which are identified and listed in Table B.7. For each connections, additional data is required [2]: the import price, the maximum yearly energy imported at each connection, the mean-time-to-failure (MTTF), and mean-time-to-repair (MTTR).

Maximum yearly imports

A yearly maximum quantity of electricity is set for each interconnection. By analyzing the physical flows between Belgium and its neighboring bidding zone (France, Germany, Luxembourg, Netherlands, United Kingdom) for the last three years (2021,2022,2023) [71], we can extract the yearly quantity of electricity imported from each region, see Table B.6. We select the maximum value for each region. However, multiple interconnections link the same regions, and thus to allocate a maximum value per interconnection, we can distribute it proportionally based on the line capacities. Concerning the new HVDC line Nautilus, we will authorize the same quantity as NemoLink multiplied by 1.4 (pro rata of the installed capacity).

Table B.6: Yearly Imports [TWh] of Belgium with neighboring countries [71]

	Imports [TWh]		
	2021	**2022**	**2023**
France	4.35	0.85	7.59
Netherlands	5.24	6.23	6.21
United Kingdom	0.14	2.52	0.98
Luxembourg	0.06	0.11	0.04
Germany	2.57	3.23	2.47
Total	12.35	12.94	17.30

[2] which has mainly collected by Thuy-hai Nguyen.

Maximum simultaneous imports

According to the [70] the maximum NTC position for Belgium in 2030 will be 2000 MW for exports and 8272 MW for imports. However, in the study presented in Chapter 6 a value of 7000 MW is considered as a limit of simultaneous imports.

Import price and import availabilities

Thanks to the wholesale day-ahead electricity price data for European countries, sourced from ENTSO-e and cleaned by [79], hourly prices are available for each region between 2015 and today [3]. Two alternatives of considering imports availabilities and prices [4] are proposed:

- Variable price : For each interconnection i, and each hour of the year t, we define a price c_{imp} by averaging the prices of the different years of the considered region:

$$c_{imp}(i,t) = \frac{\sum_{y \in \mathbb{HY}} \text{price}(re(i), y, t)}{n_{hy}} \tag{B.1}$$

  with price(r,y,t) being the price for region re, year y, and hour t, and $\mathbb{HY}$ the set consisting the n_{hy} different historical years. This results in a fixed hourly time series for each interconnection depending on the region of interconnection. For each Monte Carlo year, we add to this time series a white noise. This white noise has a normal $\mathcal{N}(0, \sigma)$ with $\sigma = 6.15$ [€/MWh]. Imports are permitted at all time (price-signal) if the interconnection is available.

- Fixed price: A single price per interconnection (similar for interconnections with the same region) constant all over the year. This price is the mean value of averaged day ahead price:

$$c_{imp}(i,t) = c_{imp}(i) = \frac{1}{8760} \sum_{t=1}^{8760} \frac{\sum_{y \in \mathbb{HY}} \text{price}(re(i), y, t)}{n_{hy}} \tag{B.2}$$

[3]The studied period is 01/01/2015 00:00:00 to 01/03/2023 00:00:00. Moreover, years 2021 and 2022 are excluded because way different than the others.

[4]The prices resulting from both methodologies has been proposed by my collegue Thuy-hai Nguyen.

> In this case, it is supposed that half of the year the interconnection is dedicated for imports, and the other half for exports. This gives a yearly availability of 50%. More over, during the available periods, we consider a uniform distribution of the neighbors available capacity [0,100] %. Thus, it sums to a yearly availability of 25%. To do so, we generate a random time series of 8760 elements between -1 and 1. The negative values are set to zero.

The resulting interconnections are listed in Table B.7.

Table B.7: Imports

Interconnection	Country	FromNode	ToNode	Type	NTC [MW]	Inom [A]	Unom [kV]	Pmax [MW]	MTTF [hours]	MTTR [hours]	Emax,year [TWh]	Price [€/MWh]
1	UK	NEMO	CANTERBURY	HVDC	1000	-	-	1000	31300	14	0.14	51.67
2	Netherlands	ZANDV	BORSSELE	HVAC	653.1	2499	380	1644.8	31300	14	1.31	41.67
3	Netherlands	ZANDV	GEERTRUIDENBERG	HVAC	653.1	2499	380	1644.8	31300	14	1.31	41.67
4	Netherlands	VANYK	MAASTRICHT	HVAC	571.3	2186	380	1438.8	31300	14	1.31	41.67
5	Netherlands	VANYK	MAASTRICHT	HVAC	522.4	1999	380	1315.7	31300	14	1.31	41.67
6	Germany	LIXHE380	ALEGRO	HVDC	1000	-	-	1000.0	31300	14	2.57	36.84
7	Luxembourg	AUBAN220	BELVAL	HVAC	90.0	1037	220	395.2	31300	14	0.03	36.84
8	Luxembourg	AUBAN220	SANEM	HVAC	90.0	1037	220	395.2	31300	14	0.03	36.84
9	France	AUBAN220	MOULAINE 1	HVAC	348.9	1160	220	442.0	31300	14	0.725	42.56
10	France	AUBAN220	MOULAINE 2	HVAC	348.9	1160	220	442.0	31300	14	0.725	42.56
11	France	GOUY	CHOOZ	HVAC	318.3	1058	220	403.2	31300	14	0.725	42.56
12	France	ACHEN	LONNY	HVAC	1038.7	1999	380	1315.7	31300	14	0.725	42.56
13	France	AVLGM	MASTAING	HVAC	1038.7	1999	380	1315.7	31300	14	0.725	42.56
14	France	AVLGM	AVELIN	HVAC	1206.5	2322	380	1528.3	31300	14	0.725	42.56
15	UK	SLIJKENS	UK1	HVDC	1000	-	-	1000	31300	14	0.14	51.67

B.2 Large-scale Conventional Production Units

The units that are taken into account in this study are the units that will be operational in 2030 and listed by Elia in [80].

B.2.1 Database used

- **[80]: 20221028_AssumptionsWorkbook_AdFlex_2023_PublicConsult.xlsx** The generators data can be found on Elia website. This excel file gives informations about the owner, the type of unit (TJ: Turbo-Jet, CCGT: Combined Cycle Gas Turbine, GT: Gas Turbine, T: Steam Turbine, CHP: Combined Heat and Power, IS: incinerator, NU: nuclear), the fuel type (Oil, Gas, Biomass, Waste, Uranium), the net generation capacity [MW], the efficiency [%], the variable operations and maintenance (VOM) costs [€/MWh] and the existence (or not) of the unit for the next ten years.
- **[78]: The Elia High Voltage Grid Map 2022** This map allows to visualize the existing lines, substations, and generators.

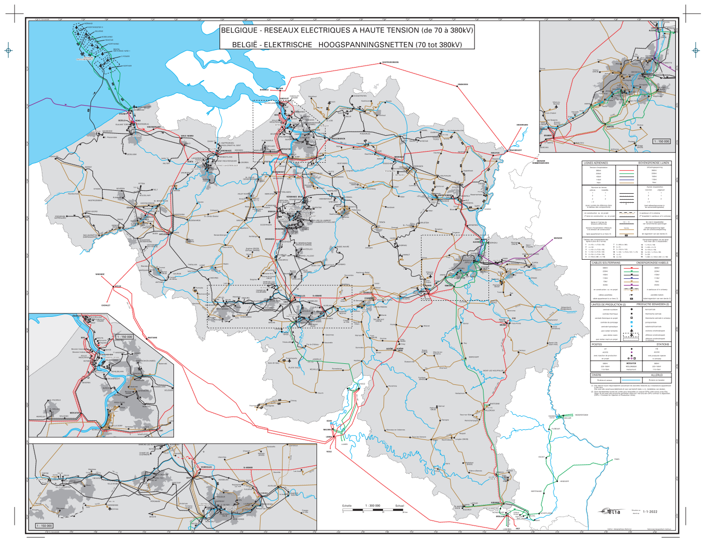

Figure B.2: The Elia High Voltage Grid Map 2022

B.2.2 Spatial distribution

The distribution of the generation units among the different nodes of the system has been done manually thanks to the Elia Grid Map [78].

B.2.3 Variable operational cost

The variable operational costs of the large-scale conventional generators modeled individually is the sum of the fuel cost, the cost of emissions, and the VOM. Although biomass and waste emit CO_2 during combustion, it is supposed that the cost related to their emissions is not considered in their operational costs.

$$\begin{aligned}\text{Variable cost } [€/\text{MWh}_{\text{elec}}] &= \frac{\text{fuel cost } [€/\text{MWh}_{\text{fuel}}]}{\text{efficiency } [\text{MWh}_{\text{elec}}/\text{MWh}_{\text{fuel}}]} \\ &+ \frac{\text{carbon price } [€/\text{t}_{\text{CO}_2}] \times \text{CO}_2 \text{ emission factor } [\text{t}_{\text{CO}_2}/\text{MWh}_{\text{fuel}}]}{\text{efficiency } [\text{MWh}_{\text{elec}}/\text{MWh}_{\text{fuel}}]} \\ &+ \text{VOM } [€/\text{MWh}_{\text{elec}}] \end{aligned} \tag{B.3}$$

The fuel costs are defined in Table B.8, their corresponding emission factors in Table B.9, the VOM of the different units in Table B.10, and the carbon price in Table B.11.

Table B.8: Prediction of fuel costs for 2030.

Fuel	Fuel Cost [€/MWh]	Source
Uranium	1.87	Elia AdeFlex 2024-34 [67]
(Light) Oil	70.67	Elia AdeFlex 2024-34 [67]
Natural Gas	26.95	Elia AdeFlex 2024-34 [67]
Biomass	26.64	-
Waste	26.64	-

Table B.9: Emission factors of fuels.

Fuel	CO_2 Emission Factor [t_{CO_2}/MWh_{fuel}]	Source
Uranium	0	UBA [81]
(Light) Oil	0.2639	UBA [81]
Natural Gas	0.2008	UBA [81]
Biomass	0.3879	UBA [81]
Waste	0.256	UBA [81]

Table B.10: Prediction of different unit types' VOM for 2030.

Unit Type	VOM [€/MWh]	Source
CCGT	2.4	Elia AdeFlex 2024-34 [67]
OCGT & engines	13.2	Elia AdeFlex 2024-34 [67]
Classic (ST, bio fired…)	3.6	Elia AdeFlex 2024-34 [67]
Oil	4	Elia AdeFlex 2024-34 [67]
Nuclear	10.8	Elia AdeFlex 2024-34 [67]

Table B.11: Prediction of CO_2 prices for 2030.

Fuel	Fuel Cost	Source [€/t_{CO_2}]
CO_2	125	Elia AdeFlex 2024-34 [67]

The data concerning these large-scale conventional generators is summarized and listed in Table B.12 and B.13.

Table B.12: Generators 1/2

Gen	Name	Node	Pmax [MW]	Type	Fuel	Efficiency [-]	VOM [€/MWh]	Fuel Cost [€/MWh_{fuel}]	CO_2 Emissions [t_{CO2}/MWh_{fuel}]	MTTF [hours]	MTTR [hours]
1	AALTER TJ	EEKLN	18	TJ	Oil	0.26	4	70.6688	0.2665	2607.5	130
2	AMERCOEUR 1R GT	GOUY	289	CCGT-GT	Gas	0.58	2.4	26.95	0.2008	821.9	110
3	AMERCOEUR 1R ST_cur	GOUY	162	CCGT-ST	Gas	0.58	2.4	26.95	0.2008	821.9	110
4	BEERSE TJ	MASSE	32	TJ	Oil	0.26	4	70.6688	0.2665	2607.5	130
5	Beveren 2 Indaver	MERCA	21	IS	Waste	0.36	3.6	26.64	0.02664	2909.7	111
6	Beveren 3 Indaver	DOEL	24	IS	Waste	0.36	3.6	26.64	0.02664	2909.7	111
7	Beveren Ineos Phenol Chem	MERCA	25.1	OCGT (CHP)	Gas	0.41	13.2	26.95	0.2008	2909.7	111
8	Beveren Sleco	MERCA	41	IS	Waste	0.36	3.6	26.64	0.02664	2909.7	111
9	Biomassa Oostende	GEZEL	18	IS	Biomasse	0.36	3.6	26.64	0.0118	2909.7	111
10	Biostoom Oostende	GEZEL	19.4	IS	Waste	0.36	3.6	26.64	0.02664	2909.7	111
11	Borealis Kallo Cogen GT_ST	MERCA	32	CCGT (CHP)	Gas	0.45	2.4	26.95	0.2008	2909.7	111
12	CIERREUX TJ	BRUME	18	TJ	Oil	0.26	4	70.6688	0.2665	2607.5	130
13	DROGENBOS GT1	MEKI+	150	CCGT-GT	Gas	0.52	2.4	26.95	0.2008	821.9	110
14	DROGENBOS GT2	MEKI+	150	CCGT-GT	Gas	0.52	2.4	26.95	0.2008	821.9	110
15	DROGENBOS ST	MEKI+	160	CCGT-ST	Gas	0.52	2.4	26.95	0.2008	821.9	110
16	EDF Luminus Angleur GT31	SERAI	25	OCGT	Gas	0.3	13.2	26.95	0.2008	731.2	221
17	EDF Luminus Angleur GT32	SERAI	25	OCGT	Gas	0.3	13.2	26.95	0.2008	731.2	221
18	EDF Luminus Angleur GT41	SERAI	64	OCGT	Gas	0.42	13.2	26.95	0.2008	731.2	221
19	EDF Luminus Angleur GT42	SERAI	64	OCGT	Gas	0.42	13.2	26.95	0.2008	731.2	221
20	EDF Luminus Ham GT31	RODE+	58	OCGT	Gas	0.42	13.2	26.95	0.2008	731.2	221
21	EDF Luminus Ham GT32	RODE+	58	OCGT	Gas	0.42	13.2	26.95	0.2008	731.2	221
22	EDF Luminus Ham STEG	RODE+	39	CCGT	Gas	0.45	2.4	26.95	0.2008	821.9	110
23	EDF Luminus Ringvaart STEG	RODE+	385	CCGT	Gas	0.55	2.4	26.95	0.2008	821.9	110
24	EDF Luminus Seraing GT1	SERAI	150	CCGT-GT	Gas	0.52	2.4	26.95	0.2008	821.9	110
25	EDF Luminus Seraing GT2	SERAI	150	CCGT-GT	Gas	0.52	2.4	26.95	0.2008	821.9	110
26	EDF Luminus Seraing NEW	SERAI	885	CCGT	Gas	0.61	2.4	26.95	0.2008	821.9	110
27	Euro-Silo	RODE+	12.9	CCGT (CHP)	Gas	0.45	2.4	26.95	0.2008	2909.7	111
28	E-wood	MERCA	22	IS	Waste	0.36	3.6	26.64	0.02664	2909.7	111
29	Flémalle NEW	AWIRS	890	CCGT	Gas	0.61	2.4	26.95	0.2008	821.9	110
30	Fluxys LNG Zeebrugge WKK	GEZEL	40	OCGT (CHP)	Gas	0.41	13.2	26.95	0.2008	2909.7	111
31	Greenpower Oostende	GEZEL	20	IS (CHP)	Waste	0.36	3.6	26.64	0.02664	2909.7	111
32	HERDERSBRUG GT1	GEZEL	157	CCGT-GT	Gas	0.51	2.4	26.95	0.2008	821.9	110
33	HERDERSBRUG GT2	GEZEL	156.3	CCGT-GT	Gas	0.51	2.4	26.95	0.2008	821.9	110
34	HERDERSBRUG ST	GEZEL	167	CCGT-ST	Gas	0.51	2.4	26.95	0.2008	821.9	110
35	INESCO GT1	MERCA	44.8	CCGT-GT (CHP)	Gas	0.58	2.4	26.95	0.2008	2909.7	111
36	INESCO GT2	MERCA	44.8	CCGT-GT (CHP)	Gas	0.58	2.4	26.95	0.2008	2909.7	111
37	INESCO ST	MERCA	48.5	CCGT-ST (CHP)	Gas	0.58	2.4	26.95	0.2008	2909.7	111

Table B.13: Generators 2/2

Gen	Name	Node	Pmax [MW]	Type	Fuel	Efficiency [-]	VOM [€/MWh]	Fuel Cost [€/MWh_{fuel}]	CO_2 Emissions [t_{CO2}/MWh_{fuel}]	MTTF [hours]	MTTR [hours]
38	Intradel Herstal IS	JUPIL	32	IS	Waste	0.36	3.6	26.64	0.02664	2909.7	111
39	Ipalle Thumaide	GOUY	34	IS	Waste	0.36	3.6	26.64	0.02664	2909.7	111
40	ISVAG	MERCA	12	IS	Waste	0.36	3.6	26.64	0.02664	2909.7	111
41	IVBO	GEZEL	16	IS	Waste	0.36	3.6	26.64	0.02664	2909.7	111
42	IZEGEM	IZGEM	20	CCGT (CHP)	Gas	0.45	2.4	26.95	0.2008	2909.7	111
43	Jemeppe-sur-Sambre GT1	STAM+	48	CCGT-GT (CHP)	Gas	0.45	2.4	26.95	0.2008	2909.7	111
44	Jemeppe-sur-Sambre GT2	STAM+	48	CCGT-GT (CHP)	Gas	0.45	2.4	26.95	0.2008	2909.7	111
45	Jemeppe-sur-Sambre ST	STAM+	10	CCGT-ST (CHP)	Gas	0.45	2.4	26.95	0.2008	2909.7	111
46	Lillo Degussa GT1	MERCA	43	CCGT-GT (CHP)	Gas	0.45	2.4	26.95	0.2008	2909.7	111
47	Lillo Degussa GT2	MERCA	32	CCGT-GT (CHP)	Gas	0.45	2.4	26.95	0.2008	2909.7	111
48	Lillo Degussa ST	MERCA	10	CCGT-ST (CHP)	Gas	0.45	2.4	26.95	0.2008	2909.7	111
49	Marcinelle Energie TGV	GOUY	413	CCGT	Gas	0.52	2.4	26.95	0.2008	821.9	110
50	Monsanto Lillo WKK EBL	MERCA	43	OCGT (CHP)	Gas	0.41	13.2	26.95	0.2008	2909.7	111
51	NOORDSCHOTE TJ	IZGEM	18	TJ	Oil	0.26	4	70.6688	0.2665	2607.5	130
52	Oorderen Bayer	MERCA	43	OCGT (CHP)	Gas	0.41	13.2	26.95	0.2008	2909.7	111
53	SAINT-GHISLAIN STEG	GOUY	378	CCGT	Gas	0.51	2.4	26.95	0.2008	821.9	110
54	Sappi Lanaken GT	ZUTE+	43	OCGT (CHP)	Gas	0.41	13.2	26.95	0.2008	2909.7	111
55	SCHAERBEEK SIOMAB ST1	VERBR	15	IS	Waste	0.36	3.6	26.64	0.02664	2909.7	111
56	SCHAERBEEK SIOMAB ST2	VERBR	15	IS	Waste	0.36	3.6	26.64	0.02664	2909.7	111
57	SCHAERBEEK SIOMAB ST3	VERBR	15	IS	Waste	0.36	3.6	26.64	0.02664	2909.7	111
58	Scheldelaan Exxonmobil	MERCA	140	CCGT (CHP)	Gas	0.45	2.4	26.95	0.2008	2909.7	111
59	STORA LANGERBRUGGE WKK1	RODE+	10	CL (CHP)	Biomasse	0.38	3.6	26.64	0.0118	2909.7	111
60	STORA LANGERBRUGGE WKK2	RODE+	40	CL (CHP)	Biomasse	0.38	3.6	26.64	0.0118	2909.7	111
61	Syral Aalst GT	BRUEG	43	CCGT-GT (CHP)	Gas	0.45	2.4	26.95	0.2008	2909.7	111
62	Syral Aalst ST	BRUEG	5	CCGT-ST (CHP)	Gas	0.45	2.4	26.95	0.2008	2909.7	111
63	TAMINCO Gent WKK	RODE+	6.3	OCGT (CHP)	Gas	0.41	13.2	26.95	0.2008	2909.7	111
64	T-Power	MEERH	425	CCGT	Gas	0.58	2.4	26.95	0.2008	821.9	110
65	Wilmarsdonk Total GT1	MERCA	43	OCGT (CHP)	Gas	0.41	13.2	26.95	0.2008	2909.7	111
66	Wilmarsdonk Total GT2	MERCA	43	OCGT (CHP)	Gas	0.41	13.2	26.95	0.2008	2909.7	111
67	Wilmarsdonk Total GT3	MERCA	43	OCGT (CHP)	Gas	0.41	13.2	26.95	0.2008	2909.7	111
68	Zandvliet Power	ZANDV	419	CCGT (CHP)	Gas	0.57	2.4	26.95	0.2008	821.9	110
69	Zedelgem TJ	GEZEL	18	TJ	Oil	0.26	4	70.6688	0.2665	2607.5	130
70	Zeebrugge TJ	GEZEL	18	TJ	Oil	0.26	4	70.6688	0.2665	2607.5	130
71	Zelzate 2 Knippegroen	RODE+	305	CL	Gas	0.42	3.6	26.95	0.2008	2909.7	111
72	Zelzate TJ	RODE+	18	TJ	Oil	0.26	4	70.6688	0.2665	2607.5	130
73	Zwijndrecht Lanxess GT	MERCA	43	CCGT-GT (CHP)	Gas	0.45	2.4	26.95	0.2008	2909.7	111
74	Zwijndrecht Lanxess ST	MERCA	15	CCGT-ST (CHP)	Gas	0.45	2.4	26.95	0.2008	2909.7	111

B.3 Distributed conventional units

Small distributed conventional units are also considered in this study, but in an aggregated manner. Their total installed capacity is defined by [67] and totals 1.9 GW. Following the same hypothesis as Elia, three types of units are considered: small gas CHPs (1379 MW), biomass units (503 MW), and waste units (46 MW). They are forced to operate at a constant load factor of 60 % throughout the year. This corresponds to a constant production of 1.14 GW in every hour of the year. It is supposed that its nodal distribution is similar to the load one (see Section B.6.2), and is listed in Table B.1 and B.2.

B.4 Renewable Energy Sources

B.4.1 Offshore Wind Farms

In the Belgian waters, 9 wind farms next to one another (see Fig. B.3b) are present today, with a total amount of 2262 MW of installed capacity [64]. They are all connected to the Stevin substation.

(a) Zone A: existing - Zone B: Princess Elisabeth Zone (PEZ), to be constructed.

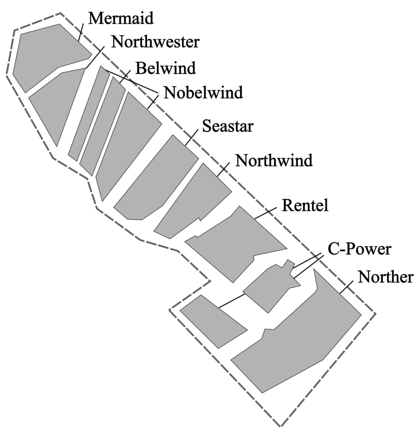

(b) Zoom on existing wind farms (Zone A)

Figure B.3: The planned belgian offshore wind farms for 2030.

New wind farms are planned for installation in a new area called Princess Elisabeth Zone (PEZ), as shown in Fig. B.3a [65]. It is assumed that this new zone will consist of 15 MW wind turbines, totaling 3500 MW: a first zone with 728 MW (49 turbines), and a second and third zone with a combined total of 2782 MW (185 turbines). These are detailed and listed in Table B.14.

Table B.14: Offshore wind farms

Name	Node	Pmax [MW]	Nb WT [#]	MTTF [hours]	MTTR [hours]
Belwind	STEVN	171	56	1059	272
C-Power	STEVN	325	54	1059	272
Mermaid	STEVN	235	28	1059	272
Nobelwind	STEVN	165	50	1059	272
Norther	STEVN	370	44	1059	272
Northwester2	STEVN	219	23	1059	272
Northwind	STEVN	216	72	1059	272
Rentel	STEVN	309	42	1059	272
Seastar	STEVN	252	30	1059	272
P1_3500_15	SLIJKENS	728	49	1059	272
P23_3500_15	SLIJKENS	2782	185	1059	272

Distributed Onshore Wind Turbines and Photovoltaic Panels

The forecast installed capacities for 2030 are 14.1 GW for photovoltaic and 5.3 GW for onshore wind turbines according to Elia [67].

It is assumed that the geographic distribution of future onshore wind turbines and photovoltaic capacities will be similar to the situation in mid-year 2022. The existing capacities of onshore wind turbines and photovoltaic are provided by province in [73] and [72] respectively and summarized in Table B.15. To convert this provincial distribution to a nodal distribution, we follow this method: the installed capacity of a province is evenly distributed among each node of the system located within that province, provided the node is connected to a distribution network (excluding transfer nodes). For example, if x % of onshore wind turbines are installed in the province of Antwerp, and there are 4 distribution-connected nodes in that province, each node will be assigned x/4 % of the wind capacity. The nodal distribution is referenced in Table B.1 and B.2.

Table B.15: Distribution of PV [72] and onshore wind power [73] at mid-year of 2022

Region	Abbreviation	Onshore Wind Turbines Installed Power [MW]	[%]	Photovoltaics Installed Power [MW]	[%]
Antwerpen	Antw	324.91	10.76	1402	19.51
Brabant wallon	BW	95.9	3.18	136	1.89
Hainaut	Hain	537.95	17.82	508	7.07
Liège	Liège	297.705	9.86	746	10.38
Limburg	Limb	313.6	10.39	759	10.56
Luxembourg	Lux	104.8	3.47	162	2.25
Namur	Nam	345.05	11.43	212	2.95
Oost-Vlaanderen	OV	674.05	22.33	1421	19.77
Vlaams-Brabant	VB	60.3	2.00	665	9.25
West-Vlaanderen	WV	264.86	8.77	1175	16.35
Total		3019.125	100.00	7186	100.00

The spatial distribution of onshore wind turbines, and photovoltaic panels are listed in Table B.1 and B.2.

B.4.2 Distributed Run-of-River Hydroelectric Generation Plant

The forecast installed capacities for 2030 is 0.151 GW for run-of-river hydroelectric generation plants according to Elia [67]. Its spatial distribution is listed in Table B.1 and B.2.

B.5 Storage units

B.5.1 Pumped-Hydro-Storage

Two pumped-hydro storage are considered for Belgium:

- Coo power station can provide 1080 MW for six hours, with a start-up time of under two minutes [82]. So a storage capacity of 6*1080 = 6480 MWh. The round-trip efficency of the power station is 75% meaning that the input/output efficiency is of 86.6%.
- Plate-Taille power station can provide 144 MW and has a hydro reservoir capacity of 67.8 million m³. [Trouver sources et données pour le potential energie] [83]. Ces deux données viennet de adequacy fx elia :

The data is grouped in Table B.16.

Table B.16: Pumped-hydro storages

Name	Node	Pmax [MW]	Emax [MWh]	eff_pump [-]	eff_turb [-]
Coo	COO	1161	5600	0.866	0.866
Plate-Taille	GOUY	144	700	0.866	0.866

B.5.2 Batteries

In [67], batteries are divided in two categories: 1) Large-scale batteries (industrial projects) whose charging/discharging profile is optimised within the formulation and 2) Small-scale batteries, also called residential batteries, which have can either have a predefined charging/discharging profile depending on the PV production, or an optimized operation just like large-scale batteries. It is assumed that in 2030, all residential batteries will have a market dispatch. The installed power and energy capacity of these two categories are referenced in Table B.17. Also, all of the batteries are considered to have a round-trip efficiency of 85% which means an input/output efficiency of $\sqrt{85} = 92.19\%$

	Large-scale			Small-scalle	Total
	In service	Potential New Capacities	All	All	All
Total Power [MW]	330	2140	2470	511.5	2981.5
% of 2-hours duration	66.4	0	8.9	100	24.5
% of 4-hours duration	33.6	100	91.1	0	75.5
Energy [MWh]	881.4	8560.0	9441.4	1023	10464.4

Table B.17: Large-scale and small-scale batteries for Belgium in 2030 - Elia estimation [67]

It has been assumed that their locations is distributed among all the industrial hubs (Gent, Antwerpen, Brussels, Hainaut, Liège) and at the shore (Zebrugge) equally. The details ar provided in Table B.18.

Table B.18: Batteries

Batt	Node	Pmax [MW]	Emax [MWh]	eff_batt_in [-]	eff_batt_out [-]
1	STEVN	497	1744	0.9219	0.9219
2	RODE+	497	1744	0.9219	0.9219
3	MERCA	497	1744	0.9219	0.9219
4	BRUEG	497	1744	0.9219	0.9219
5	GOUY	497	1744	0.9219	0.9219
6	RIMIE220	497	1744	0.9219	0.9219

B.6 Traditional Electrical demand

According to [67], the annual electrical demand in 2030 reaches 112.8 TWh. This "englobes" the traditional electrical usage supposing to increase, the additional demand for industry heat, electric vehicles, heat-pumps, and electrolyzers. Because in the model used in this work, electric vehicles, heat pumps, and electrolyzers are treated as a different type of demand, they can be substracted from the total annual demand: 112.8 [TWh] - 5.13 [TWh] (EVs) - 2.9 [TWh] (HPS) - 0.6 [TWh] (electrolyzers) = 104.17 [TWh]. This annual electrical demand has to be distributed in the time (among the hours of the year) and space (among the different nodes of the system) dimensions.

B.6.1 Time distribution methodology

The hourly distribution of the annual demand is based on the total load time series of 2018 available online on Elia's data platform.

B.6.2 Space distribution methodology

Three types of transformers [5] connected to the VHV grid are identified and categorized as follows:

i) Phase shifters: when the high voltage side (380 or 220 kV) is equal to the low voltage side of the transformer.
ii) Step-down 380/220 transformers: when the high voltage side is 380 kV and the lower side is 220 kV, the transformer permits the connection of 380 and 220 kV lines.
iii) Load feeders: when the high voltage side is 380 or 220 kV and the lower side 150 kV or lower, then the transformer is a step-down transformer used to feed a load.

The load is then distributed to the pro-rata of the installed capacities of load feeders transformers (iii) at each node. An exception is made for the node Stevin where a consequent capacity (1260 MW) of <150 kV transformer are installed which are not load feeders per se. The spatial load distribution is available in Table B.1 and B.2.

B.7 Electric Vehicles

Electric vehicles are taken into account in this study. A total of 1.9 millions of EVS are planned to be in circulation by 2030 according to [67]. The annual demand from the EVs is calculated with the following assumptions [67]: cars travel 15000 [km/year], with a consumption of 18 [kWh/100 km]: 1.9 M x 15000 [km/year] x 0.18 [kWh/km] = 5.13 [TWh/year]. This annual demand is distributed equally among the days of the year (∼14 GWh/day).

B.7.1 Time distribution

The distribution among the hours of the day is not uniform, and depends on the EV type.

Four types of electric vehicles can co-exist depending on their charging behavior :

1. V0: natural charging profile (pre-defined time series) with a peak in the evening (plain line in Fig. B.4)
2. V1H: delayed charging profile (pre-defined time series) with a peak in the middle of the night (dashed line in Fig. B.4)

[5] Transformers can be constituted of 2 or 3 windings. If three windings, the HV side is unique, and there exist two LV sides.

3. V2H: bi-directional charging profile (pre-defined time series) where the EV has a battery behavior, charging during the night and restituting during the evening (dashdotted line in Fig. B.4)
4. V1M: smart charging profile (result of the optimisation) concerning EVs that are flexible and produce optimally during the day. The share of the smart EV fleet connected to a flexible charger during the day is not constant and represented in Fig. B.5.

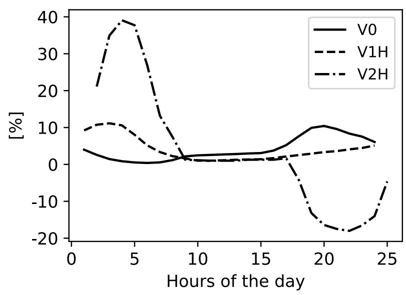

Figure B.4: V0 (classical) and V1H (smart) charging profiles [67].

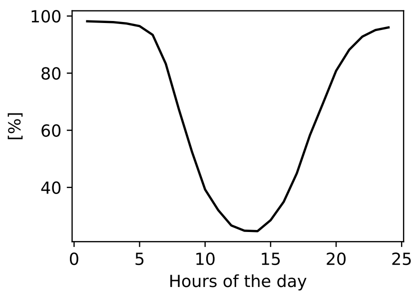

Figure B.5: Share of the flexible EV fleet connected to a flexible charger during the day [67].

The following share is considered in 2030 according to [67] - V0: 30 % - V1H: 45 % - V2H: 4% - V1M: 21% [6]. Also, flexible chargers are supposed to have a power of 7 kW.

B.7.2 Spatial distribution

Their nodal distribution is considered to be similar to the photovoltaic distribution and is referenced in Table B.1 and B.2.

B.8 Heat-Pumps

Heat-pumps are taken into account in this study. A total of of 1.2 million heat-pumps are considered to be in operation by 2030 according to [67]. An annual demand of 2.9 [TWh/year] for the HPs operation is taken from [67].

[6] In the study [67], smart vehicule-to-grid is also considered (V2M). However, the model used in this work does not permit V2G. Thus the share of V2M (1%) is given to the V2H category(3% $\longrightarrow$ 4%).

B.8.1 Time distribution

This annual demand is distributed among the different months as shown in Fig. B.6 and the distribution among the hours of the day depends on the HP type.
They are splitted into 3 categories depending on their behaviors:

1. HP0: natural profile (pre-defined time series) with a peak in the morning, and in the evening (plain line in Fig. B.7)
2. HP1H: pre-heated profile (pre-defined time series) with an additional peak (compare to HP0) during the day, which reduces the evening peak (dashed line in Fig. B.7)
3. HP1M: smart profile (result of optimisation) concerning HPs that are flexible and produce optimally during the day.

The following share is considered in 2030 according to [67] - HP0: 59 % - HP1H: 31 % - HP1M: 10%. Also, flexible HPs are supposed to have a thermal power 10 [kW_{th}], and a COP of 3 which amounts to an electrical power of 3.33 [kW].The repartition among the nodes is set identical to the PV distribution.

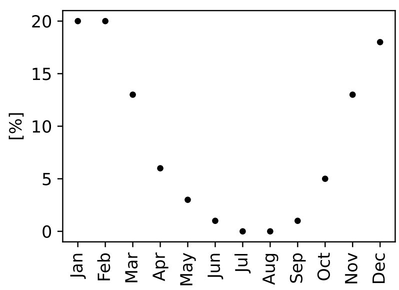

Figure B.6: Monthly distribution of annual heat-pump demand inspired by [67] (simplification applied)

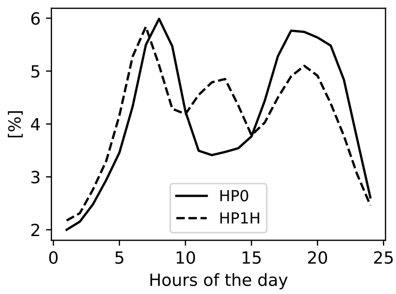

Figure B.7: HP0 (classical) and HP1H (smart) charging profiles [67].

B.8.2 Spatial distribution

Their nodal distribution is considered to be similar to the photovoltaic distribution and is referenced in Table B.1 and B.2.

B.9 Hydrogen Network Topology

B.9.1 Hydrogen Pipelines

The construction of the future hydrogen system is designed based on a document published by Fluxys [84] where they propose a first short-term (2030) network deployment for constructing the European Hydrogen Backbone, as illustrated in Fig. B.8a. This network has been simplified using the following assumptions:

- Clusters are grouped in one node
- Pipelines joining elsewhere a node location are deviated towards a node
- Eynatten considered in Liège cluster
- Blaregnies considered in Hainaut cluster

and can be visualized in Fig. B.8b.

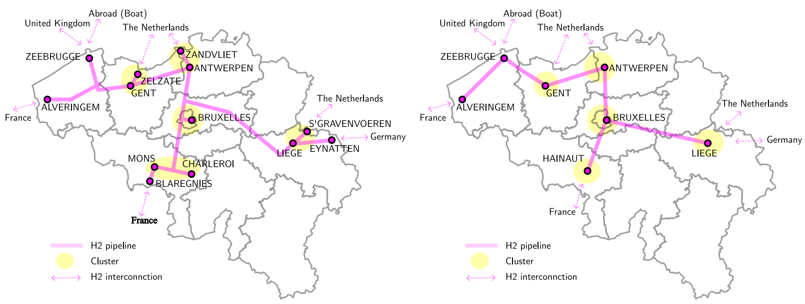

(a) Short-term option fo the deployment of the hydrogen backbone from Fluxys [84]

(b) Simplified hydrogen backbone considered for this work

Figure B.8: Hydrogen network topology.

The nodes of the hydrogen network are assigned to an existing node of the electrical system if there is:

- Alveringem: no corresponding node in area thus creation of a new node
- Zeebrugge: connected to Stevin (STEVN) node
- Gent: connected to Rodenhuize (RODE+) node
- Antwerpen: connected to Meractor (MERCA) node
- Bruxelles: connected to Bruegel (BRUEG) node
- Hainaut: connected to Gouy (GOUY) node
- Liège connected to Rimière 220 (RIMIE220) node.

Moreover, based on the hydrogen pipelines specifications in [74] and summarized in Table B.19, it assumed that the short-term hydrogen network deployment will consist in medium repurposed pipelines with a capacity of 3.6 GW.

Table B.19: Hydrogen pipelines specifications for the European Hydrogen Backbone [74]

Type		Capacity [GW]	Pressure operation [bar]
Small	new	1.2	50
	repurposed	1.2	50
Medium	new	4.7	50
	repurposed	3.6	50
Large	new	13	80
	repurposed	13	80

The hydrogen pipelines can be found in Table B.20.

Table B.20: Hydrogen pipelines

Pipeline	FromNode	ToNode	Qmax [MW_{H_2}]
1	ALVERINGEM	STEVN	3600
2	STEVN	RODE+	3600
3	RODE+	MERCA	3600
4	MERCA	BRUEG	3600
5	BRUEG	RIMIE220	3600
6	BRUEG	GOUY	3600

B.9.2 Hydrogen interconnections

The yearly quantity of imported hydrogen is not limited. However, the hourly quantity is limited at each interconnection by the pipeline capacity of 3.6 GW. This is detailed in Table B.21.

Table B.21: Hydrogen imports

H2Imp	Name	Node	Qmax [MW]	PriceH2Imports [€/MWh]
1	Alveringem	ALVERINGEM	3600	150
2	Zeebrugge	STEVN	3600	150
3	Zelzate	RODE+	3600	150
4	Zandvliet	MERCA	3600	150
5	S-Gravenvoeren	RIMIE220	3600	150
6	Eynatten	RIMIE220	3600	150
7	Blaregnies	GOUY	3600	150

Hydrogen Import price

The price is set to 150 [€/MWh_{H_2}], which is equivalent to 5[€/kg_{H_2}]. The price is considered similar at all interconnections and is referenced in B.21.

B.10 Electrolyzers

Their installed capacity sum up to 447 MW according to Elia's study [67]. The efficiency of electrolyzers is considered to be 70 %, and the energy necessary to compress the hydrogen is set to 9 % of the electrical consumption of the electrolyzer. These specificities can be found in Table B.22.

Table B.22: Electrolyzers

Electrolyzer	Location	Node	Pmax [MW]	Efficiency [-]	Compression share [-]	MTTF [hours]	MTTR [hours]
1	Zeebrugge	STEVN	74.5	0.7	0.09	2000	50
2	Gent	RODE+	74.5	0.7	0.09	2000	50
3	Antwerpen	MERCA	74.5	0.7	0.09	2000	50
4	Bruxelles	BRUEG	74.5	0.7	0.09	2000	50
5	Hainaut	GOUY	74.5	0.7	0.09	2000	50
6	Liège	RIMIE220	74.5	0.7	0.09	2000	50

B.10.1 Spatial distribution

We suppose that they are installed at shore (Zeebrugge), and at industrial hubs (hydrogen clusters): Gent, Antwerpen, Brussels, Hainaut, Liège with an even distribution.

B.11 Hydrogen-to-power units

Hydrogen-to-power units: no projects of this type is planned for Belgium in 2030.

B.12 Hydrogen storage units

Hydrogen storage units are located nearby each electrolyzers unit, with the same installed power, and a storage capacity of 10 hours, i.e. 10*P. The specificities are detailed in Table B.23.

Table B.23: Hydrogen storage

H2Sto	Location	Node	Pmax [MW_H2]	Emax [MWh_H2]	eff_in [-]	eff_out [-]
1	Zeebrugge	STEVN	74.5	745	1	1
2	Gent	RODE+	74.5	745	1	1
3	Antwerpen	MERCA	74.5	745	1	1
4	Bruxelles	BRUEG	74.5	745	1	1
5	Hainaut	GOUY	74.5	745	1	1
6	Liège	RIMIE220	74.5	745	1	1

B.13 Hydrogen demand

Hydrogen demand for 2030 can be derived in multiple ways:

1. End-use demand method: Today, hydrogen is used as a primary feedstock in the industry sector for the production of end-use demands such as: the high-value chemicals (HVC), methanol, and ammonia. To derive the hydrogen demand from these end-use demands, various assumptions about the processes involved and their efficiencies has to be made.

2. Models method: Future hydrogen demands are derived by several studies for 2050, this including the industrial demands, but also other end-use demands from the electricity, heat, or mobility sectors that could be satisfied by hydrogen in the future. Usually, these reports define a demand for 2050, so a linear interpolation shall be made for the 2030 demand.

3. Up-bottom approach: In 2022, the Belgian hydrogen consumption was 378.2 [kt_{H_2}] [59] and a scaling factor can be applied to it for 2030.

4. The hydrogen demand has been estimated for very country in the world for 2050 in [85] based on the *Net Zero scenario of IEA in 2050* [86]. Among all the countries, the predictions for Belgium is 48.2 [TWh_{H_2}/year] (vs. 16 [TWh_{H_2}/year] in 2020). If we consider a lower-heating value of hydrogen of LHV_{H_2}= 33.33 [MWh/t], this demand is of 1.44 Mt_{H_2}/year. To define the demand for 2030, we can interpolate, and suggest that the consumption will be of 1/3*(48.2-16) [TWh_{H_2}/year] = 26.7 [TWh_{H_2}/year] = 0.8 [Mt_{H_2}/year].

In this study, the fourth manner is used, and the yearly demand is set to 800 [kt/year] = 26.6 [TWh_{H2}/year].

B.13.1 Time distribution

The yearly demand is evenly distributed among the days of the year, i.e. 73 [GWh_{H_2}/day]. Then, we can define a fixed and a flexible share. The fixed share distributes this daily demand evenly among the hours of the day. The flexible share does not impose any hourly demand, the hourly production is optimized, and only the daily demand is constraining. In this study, the hydrogen demand is set 100 % flexible.

B.13.2 Spatial distribution

The yearly demand is evenly distributed among the industrial hubs, i.e. Antwerpen, Ghent, Bruxelles, Hainaut, and Liège, and the nodal distribution is referenced in Table B.1 and B.2.

B.14 Outages of different components

B.14.1 Branches and interconnections

The outages of branches (transformers and internal lines) and interconnections (tielines) are considered in this study. Their MTTR and MTTF are defined thanks to data from Elia [75] and are summarized in Table B.24. The transformers MTTR/MTTF are based on only 3 components that have failed with a very large spread of outage durations (2 outages of ∼ 3 months): the fact that few data is available and that some seem extreme, the MTTR/MTTF of the transformers will be based on internal lines instead.

Table B.24: Outages of 220/380 kV components from Elia database [75] that studies a period of ∼ 9 years (77344 hours).

[a]220/380 kV components	[a]Existing comp. [77]	[a]Failed comp.	Total outages	MTTR [hours]	[b]$MTTF_{failed}$ [hours]	[c]$MTTF_{no\ failed}$ [hours]	[d]MTTF [hours]
Internal lines	90	18	27	26	57606	77344	73397
Transformers	67	3	9	547	27838	77344	75128
Tielines (HVAC)	12	6	9	84	44807	77344	61076
Tielines (HVDC)	2	2	18	24	3287	77344	3287

[a] excludes the lines going from Stévin towards the offshore wind farms.
[b] the mean duration between two failures of an asset (concerns the assets that have failed on the studied period). If an asset fails only once, the MTTF = studied period.
[c] it is assumed that the assets that haven't failed have a MTTF = studied period.
[d] The MTTF is a weighted sum of both $MTTF_{failed}$, and $MTTF_{no\ failed}$.

B.14.2 Generators

From the average forced outage rates (FOR) and the average repair time (MTTR) of the different units defined by Elia in [67] and detailed in Table B.25, the mean-time-to-failure (MTTF) can be derived with the following relation: $\text{FOR} = \frac{\text{MTTR}}{\text{MTTR+MTTF}}$.

Table B.25: Forced outage rate (FOR), mean-time-to-repair (MTTR) and mean-time-to-failure (MTTF) of different units.

Unit Type	Average FOR [67] [%]	MTTR [67] [hours]	MTTF [hours]
Nuclear	4*-20.5**	199	4776-771.73
CCGT	5.5	110	1890
OCGT	8.2	221	2474.12
TJ	9.8	130	1196.53
CHP, waste, biomass	6.4	111	1623.37

*Only considering technical forced outages.
**Also considering long-lasting forced outage..

B.14.3 Offshore Wind Turbines

Offshore wind farms can fail to supply the foreseen production because wind turbines or another component linking the turbine to the transmission grid (e.g. submarine cables, transformers) may undergo failures. In this study, only failures concerning wind turbines are considered. Indeed, it has been supposed that the wind farms are directly connected to the onshore nodes, neglecting cables and transformers in between.

The MTTF and MTTR values for each single wind turbine is taken from a study [76].

Table B.26: Failures rates, and mean time-to-repair for offshore wind turbines [76].

	Minor Repair	Major Repair	Major Replacement	All
Share	-	-	-	
Lambda [/turbine/year]	5.73	0.89	0.13	6.75
Repair time [hours]	16.11	82.16	498.58	34.21
MTTF [hours]	1528.8	9842.7	67384.62	1297.78

The number of failures per year regardless the severity is $\lambda = 5.73+0.89+0.13 = 6.75$ [failures/turbine/year]. The average repair time, considering the occurrence of each severity, is MTTR = 34.21 [hours]. From this, can be derived the MTTF = $\frac{8760}{\lambda}$ = 1297.78 [hours].

B.14.4 Electrolyzers

The MTTF is set to 2000 hours and MTTR to 50 hours.